TAMPERE UNIVERSITY OF TECHNOLOGY

KAHO

BRAM ROTTHIER

EFFECTS OF TEMPERATURE AND HUMIDITY ON THE DIELECTRIC PROPERTIES OF THERMALLY SPRAYED CERAMIC COATINGS

Master of Science Thesis

Examiners: Dr. Tech. Kari Lahti,
Assoc. Prof. Kari Kannus
The examiners and the topic were approved in the Faculty of Computing and Electrical Engineering Council meeting on 4.4.2012

ABSTRACT

TAMPERE UNIVERSITY OF TECHNOLOGY
Master's Degree in Electrical Energy Engineering
ROTTHIER, BRAM: Effects of temperature and humidity on the dielectric properties of thermally sprayed ceramic coatings
Master of Science Thesis, 83 pages, 16 Appendix pages
May 2012
Major: Electrical Energy Engineering
Examiners: Dr. Tech. Kari Lahti, Associate Professor Kari Kannus
Keywords: Dielectric properties, Insulation, Al_2O_3, Thermal spray, Coating, HVOF, APS, Flexicord

Electrical insulation is indispensable in electrical equipment. Thermally sprayed ceramic coatings are promising materials, offering insulating capabilities in areas where other materials do not fulfil the requirements. For instance their chemical stability, a high wear resistance and an ability to withstand high temperatures are significant advantages.

This thesis is a part of the HICC project (Highly Insulating Ceramic Coatings), in which a new class of thermally sprayed ceramic coatings, with significantly improved dielectric properties, will be developed. It contributes to that project in two ways. First by the development of a measurement program to measure the relative permittivity and the loss index in thermally sprayed coatings. Secondly by the analysis of the dielectric properties of three Al_2O_3 coatings, coated by respectively ethylene high velocity oxygen fuel (HVOF) spraying, atmospheric plasma spraying (APS) and flexicord spraying.

In the theoretical part of this thesis, a thorough literature study regarding general insulator behaviour and thermally sprayed ceramic coatings is performed. In the empirical part, the dielectric properties of the coatings were studied using dielectric spectroscopy measurements. It was found that at temperatures below 100°C the permittivity and the losses are strongly dependent on the frequency, the temperature and the humidity. Regarding permittivity and dielectric losses, the flexicord sprayed sample showed the most promising results. On the other hand, the plasma sprayed sample showed the highest values for those quantities. These variations are found to be related to differences in microstructure and phase composition, due to the distinctions between the various spraying techniques. At temperatures above 100°C, an unexpected permanent decrease in relative permittivity and loss index was observed during heat treatments.

The outcome of this thesis provides a good base for the continuation of the HICC-project. More recommendations for further research and the advice to use stainless steel substrates for future samples, are provided as well.

PREFACE

This Master of Science thesis was written at the Department Electrical Energy Engineering at Tampere University of Technology as a part of the HICC-project. My examiners were Dr. Tech. Kari Lahti and Associate Professor Kari Kannus.

First, I would like to show my thanks to Kari Lahti. Four months ago, I made my first and totally unexpected appearance in the high voltage lab, seeking for a topic for a M.Sc. Thesis. One day later, he offered me this highly interesting thesis subject. Without his guidance, advice and support, it would have been impossible for me to write this thesis. I also owe a large debt of gratitude to M.Sc. Minna Niittymäki and M.Sc. Ilkka Rytöluoto for their highly esteemed help and feedback during the writing process.

I also want to thank my family and friends for their endless support, even at the more difficult moments. I am also very grateful to the companies involved in this project for providing me with the needed information and to the people of the Department Electrical Energy Engineering for the pleasant work atmosphere.

Last but not least, for all those from Tampere University of Technology and from my home university KaHo Sint-Lieven, who made it possible to write my thesis here, in Tampere: Kiitos!

Tampere, May 17th 2012.

Bram Rotthier
bram.rotthier@gmail.com

TABLE OF CONTENTS

ABBREVIATIONS AND NOTATION

NOTATION

A	Cross-sectional area
A_c	Surface area of electrodes
A_k	Pre-exponential constant
c	Correlation coefficient
C	Capacitance
C_a	Capacitance in the equivalent circuit of a real dielectric
C_e	Correction factor for edge capacitance
C_0	Capacitance of a vacuum capacitor
d	Thickness of test sample
d_0	Thickness of standard sample
d_1	Diameter of the smallest electrode
d_c	Distance between electrodes of a capacitor
$\overline{D}$	Flux of electric displacement
D_0	Maximum flux of electric displacement
δ	Phase retardation
$\tan\delta$	Dissipation factor
E	Electric field strength
E_0	Maximum electric field strength
E_A	Activation energy
E_b	Breakdown field strength
$E_{b,0}$	Breakdown field strength of standard sample
ε	Absolute permittivity
ε_0	Permittivity of free space
ε_s	Static relative permittivity
ε_r	Relative permittivity
ε^*	Complex permittivity
ε'	Real part of the complex permittivity
ε''	Imaginary part of the complex permittivity, loss index
ε_1	Approximate value of the relative permittivity
ε_∞	Instantaneous relative permittivity
h	Coating thickness
I	Current
I_c	Displacement current
I_r	Resistive or lossy current
J	Current density
l	Length of the material

m	Mass of an electron
μ	Mobility of an electron
n	Free carrier concentration
n_i	Free carrier concentration due to field injection
n_t	Free carrier concentration due to thermal activity
ω	Angular frequency
$\bar{P}$	Polarization
P_{loss}	Power loss
q	Electric charge of an electron
Q	Total charge
Q_0	Total charge on a vacuum capacitor
R	Resistance
R_a	Resistance in the equivalent circuit of a real dielectric
R_g	Gas constant
ρ	Resistivity
σ	Conductivity
T	Absolute temperature
τ	Relaxation time
τ_c	Average time between collisions of an electron and the atoms of the material
U	Voltage
U_0	Maximum voltage
v_d	Drift velocity of an electron
χ	Dielectric susceptibility
ω	Angular frequency
Z	Impedance

ABBREVIATIONS

Al_2O_3	Aluminium oxide
AlOH	Aluminium hydroxide
APS	Atmospheric plasma spraying
CVD	Chemical vapour deposition
HICC	Highly insulating ceramic coatings
HVOF	High velocity oxygen fuel
PVD	Physical vapour deposition
RH	Relative humidity
TEKES	The Finnish funding agency for technology and innovation
TUT	Tampere University of Technology
XRD	X-ray diffraction
VPS	Vacuum plasma spraying
VTT	Technical research centre of Finland

SAMPLE CODES

653_14	Sample with ethylene-HVOF sprayed Al_2O_3 coating
TS_EXT_123	Sample with flexicord sprayed Al_2O_3 coating
#184 alu	Sample with atmospheric plasma sprayed Al_2O_3 coating

1 INTRODUCTION

Electrically insulating materials are used to separate objects with a difference in electric potential. They are essential for a proper and safe operation of electrical equipment. Traditionally, ceramic materials were very often used as electric insulators. A good example is porcelain, in former times commonly applied as an insulator in high voltage networks. Nowadays, ceramic insulators are often substituted by insulators made of synthetic polymer materials, which are mostly better insulating and less brittle. Nevertheless, there is still a wide range of application for ceramic insulating materials in areas where polymer based insulators do not fulfil the requirements. In applications, for example at very high temperatures or with a need for wear resistant insulators, ceramic materials can be a good alternative.

This thesis is a part of the HICC project at Tampere University of Technology, a research project on Highly Insulating Ceramic Coatings. This project is a co-operation between TUT and VTT, supported and funded by ABB, Kuopion Konepaja, Millidyne, Saint-Gobain, Wärtsilä and TEKES, the Finnish funding agency for technology and innovation. The main objective of the HICC project is to develop a new class of thermally sprayed coating materials with significantly improved dielectric properties. Therefore it is important to understand the main parameters affecting the electrical performance of thermally sprayed coatings. The differences between the standard thermal spraying methods, regarding the insulating capability of the coatings, are not fully known and only little information is available in the literature. Thereby the study of those differences is an important part of the project.

The contribution of this thesis to the HICC project is twofold. The first contribution is the development of a preliminary test procedure to measure the dielectric losses and the permittivity of the coatings by dielectric spectroscopy. The second contribution is the measurement of those properties for three ceramic coatings, coated by three different standard thermal spraying processes. The dielectric properties will be measured at different ambient temperatures and humidities. The results of these measurements can be used in the HICC project as basic knowledge of the relation between the spraying process and the electrical performance of the sprayed coating.

The theoretical background of the thesis is thoroughly discussed in Chapters 2 and 3. Chapter 2 discusses general electrical insulator behaviour and focuses on conductivity, dielectric losses and dielectric breakdown. The emphasis in Chapter 3 is on ceramic materials. First, ceramic materials and coatings are discussed in general, after which the different thermal spraying processes are introduced and compared.

Chapter 3 concludes with a discussion on earlier research on the dielectric properties of two relevant spraying processes.

The measurement setup used in this thesis and the measurement procedure developed to perform the measurements, are described in detail in Chapter 4. The results of the measurements are presented and extensively analysed in Chapter 5. The first section of Chapter 6 is dedicated to a summary of the measurement results, with an emphasis on the observed tendencies. In the rest of the chapter, the measurement results are discussed. The thesis as a whole is summarized in Chapter 7.

2 ELECTRICAL INSULATORS

A good electrical insulator has to measure up to various requirements. The most important requirements are its electric properties, such as resistivity, dielectric strength and dielectric losses. Those properties will be discussed in this chapter. It should be noted that these are not the only important parameters regarding insulation. Properties such as heat conductance and resistance to mechanical stress are also considerable discussing the appropriate behaviour of insulation. [1]

In electrical power engineering, an insulator is intended as a device, separating objects with a difference in potential. It mostly consists of several different insulating materials. In this chapter, the term insulator is used for electrical insulating materials in general.

2.1 Conductivity

The main difference between insulators and conductors is their *conductivity* σ. Regarding conductors, the main goal is to facilitate the migration of free charge carriers through a material. Consequently conductors have a high conductivity. Regarding insulators, the main goal is to prevent charge carriers from migrating through the material, therefore the conductivity of insulators has to be very low. An ideal insulator would not involve any motion of charge carriers, but those insulators do not exist. Accordingly, all insulators have at least some conductivity. [2]

2.1.1 Band theory of solids

For a more profound discussion about the difference between conductors and insulators, the band theory of solids should be considered. In solids, atoms are positioned very close to each other. Due to the small distance, the wave functions associated with the electrons in the outer shells of the atoms will interact. They will cluster into broad energy bands. Each material has both allowed and forbidden energy bands. The allowed energy bands correspond with the ranges of energy a certain electron in a material can have. The forbidden energy bands correspond with the ranges of energy that are impossible for an electron in a certain material. [3,4**]**

Discussing the difference between conductors and insulators, the valence band, conduction band and band gap are important concepts. The *valence band* is the range of energy whereby electrons are bound to their atoms. Therefore the migration of electrons is impossible, which describes an ideal insulator. The *conduction band* is the range of energy whereby electrons have enough energy to migrate freely through the lattice,

which describes an ideal conductor. The energy range between the highest energy level of the valence band and the lowest energy level of the conduction band is called the *band gap* or the *forbidden band*. [3,4]

Conductors often have an overlap between the valence band and the conduction band. On the other hand, in insulators there is a very large band gap between the valence band and the conduction band, as shown in Figure 2.1 (a). This large band gap makes it very difficult for electrons to jump from the valence band to the conduction band. In semiconductors the size of the band gap is such that some carriers can make the leap, as shown in Figure 2.1(b). [3,5]

In insulators *tunnelling* is an important mechanism. It causes charge transport at high electric field strengths [6,7]. Tunnelling is a quantum mechanical property that states that there is a finite probability that an electron can cross a border wherefore the needed energy is larger than the energy of the electron. For more detailed information about the tunnelling phenomenon, the reader is advised to consult [3], p18-20 or more specialized literature. [3]

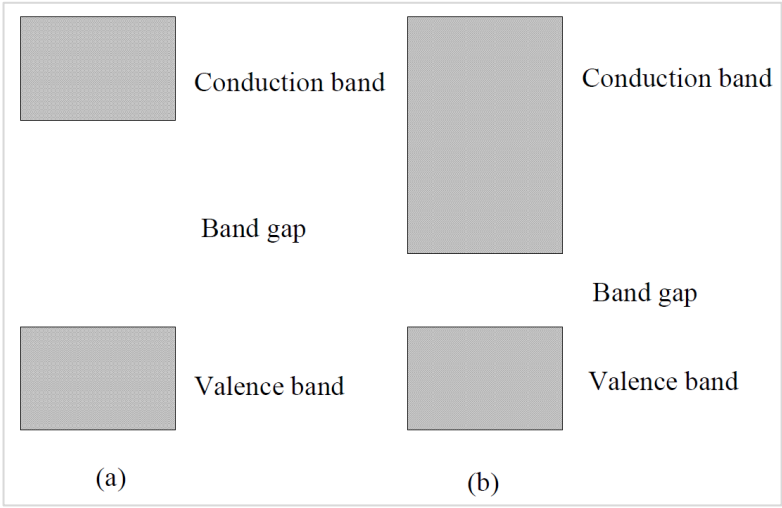

Figure 2.1. Band theory of solids for (a) insulators and (b) semiconductors.

The band theory of solids is based on an ideal crystal lattice structure without impurities or structural defects. The presence of impurities or structural defects causes localized states in the forbidden band, called *electron traps*. These electron traps make it more difficult for electrons to jump to the conduction band and may therefore improve the insulating properties. In amorphous materials the band theory has to be adapted. The different wave functions will still cluster into energy bands, but the edges of the energy bands will become rather foggy and electron traps will appear. [3,4]

Electrons can jump from the valence band to the conduction band due to an increase in energy. An important energy form is thermal energy, this partially explains the dependence of conductivity on the temperature. [3,4]

2.1.2 Microscopic view at conductivity

The band theory of solids explains the main difference between both insulators and conductors. It also gives an explanation for the amount of free charge carriers in a material. This section will take a closer look at the behaviour of free migrating electrons in materials.

Electric current can be described as charge carriers, typically electrons, migrating through a material forced by an applied electric field. The electrons that are not bound with atoms will still encounter friction while migrating through the lattice. This friction is caused by collisions with atoms that are bound in the lattice structure. Those collisions are slowing down the migrating electrons and are causing a decrease in conductivity. The *conductivity* σ of a material can be formulated as

$$\sigma = \frac{nq^2\tau_c}{m}, \tag{2-1}$$

whereby n is the *free carrier concentration*, q the *electric charge of an electron*, m the *mass of an electron* and τ_c the *average time between collisions* of an electron and the atoms of the material. With an increase in temperature, the vibrations of the atoms in the lattice will increase, which increases the amount of collisions and therefore the conductivity decreases. [8]

2.1.3 Influences on conductivity

As mentioned above, temperature has a large influence on conductivity. In Section 2.1.1, it was concluded that an increase in temperature will cause an increase in conductivity. This was explained by the fact that an increase in temperature will increase the energy of the electrons, making it possible for more electrons to jump to the conduction band. In Section 2.1.2, it was stated that an increase in temperature will cause a decrease in conductivity, due to the increase of collisions. At first sight these two conclusions look contradictory. In reality these phenomena will occur at the same time, which causes the different temperature behaviour of several materials. For example the conduction of semi-conductors will increase with an increase in temperature, this is due to a rather small band gap. This small band gap makes it possible for electrons to jump to the conduction band, even with a small increase in energy. In this scenario, the increase of free charge carriers is more important than the decrease in energy of the free charge carriers due to the increasing amount of collisions. On the other hand, in most insulating materials an increase in temperature will cause a decrease in conductivity. Due to the very large band gap, there are still not many electrons that have sufficient energy to jump to the conduction band. Due to the increase in temperature, the free charge carriers will encounter more friction, causing the decrease in conductivity with increasing temperature. [3,4,8]

Crystalline defects and impurities have also two different influences on conductivity. On the one hand, they are sources of free electrons causing an increase in conductivity with an increasing amount of impurities and defects. On the other hand, they are a cause of electron traps, resulting in a decrease in conductivity. These contrary influences induce a different behaviour of several materials to an increasing amount of crystalline defects and impurities. [3,5,9]

2.1.4 Macroscopic view at conductivity

An often used material property, inversely proportional with conductivity, is the *electrical resistivity* ρ.

$$\rho = \frac{1}{\sigma} \tag{2-2}$$

The electrical resistivity of a material can be defined as a measure for the resistance of a material against the migration of charge carriers when the material is exposed to an electric field. [8]

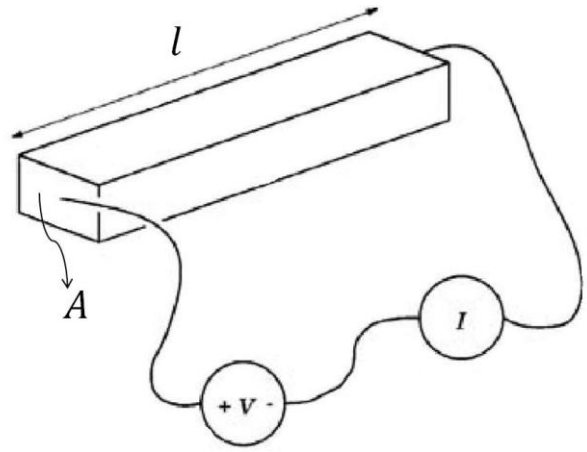

Figure 2.2. Resistive bar of material. [8]

Ohm's law states that the electrical resistivity equals the ratio of the *electric field strength E* to the *current density J*.

$$\rho = \frac{E}{J} \tag{2-3}$$

The electric field strength and the current density can be expressed by following equations:

$$E = \frac{U}{l}, \tag{2-4}$$

$$J = \frac{I}{A}, \tag{2-5}$$

whereby *U* is the *voltage* over the material, *l* the *length* of the material, *I* the *current* through the material and *A* the *cross-sectional area* of the material, as shown in Figure 2.2. The combination of Equations (2-3), (2-4) and (2-5) yields

$$\frac{U}{I} = \frac{E}{J}\frac{l}{A} = \rho\frac{l}{A} \triangleq R. \tag{2-6}$$

Equation (2-6), known as Pouillet's law, shows that the *resistance R* of a material depends, oppositely up to the resistivity, on the size and the shape of the material. [8]

Ohm's law can also be written by

$$\sigma = \frac{J}{E}, \tag{2-7}$$

with

$$J = nqv_d, \tag{2-8}$$

$$v_d = \mu E, \tag{2-9}$$

where v_d is the *drift velocity* and μ is the *mobility* of an electron. Substitution of Equation (2-9) into Equation (2-8) yields

$$J = nq\mu E. \tag{2-10}$$

The free carrier concentration can be expressed by

$$n = n_t + n_i, \tag{2-11}$$

where n_t is the *free carrier concentration due to thermal activity* and n_t is the *free carrier concentration* due to field injection. The latter can be expressed by

$$n_i = \varepsilon E. \tag{2-12}$$

The *absolute permittivity* ε will be thoroughly discussed in the next subchapter. Substituting last two equations into Equation (2-10) yields

$$J = n_t q\mu E + \varepsilon E^2 q\mu. \tag{2-13}$$

For conductors, where $n_t >> n_i$, there is a linear relation between the voltage and the current. This is also what Ohm's law implies. On the other hand, for insulators applies that $n_t << n_i$, whereby the relation between voltage and current is expressed by the following square law

$$J = \mu q \varepsilon E^2. \tag{2-14}$$

Increasing temperature will cause an increase in the concentration of free charge carriers due to thermal activity, which will lead to a more linear relation. [10]

2.2 Capacitor fundamentals

An insulator can roughly be described as a medium that separates two conductors with a difference in potential. A property of conductors in such a system is that they have the ability to attract and store electric charge [10]. Therefore it is important to understand the basic capacitor operation principle in order to discuss the insulating properties of materials.

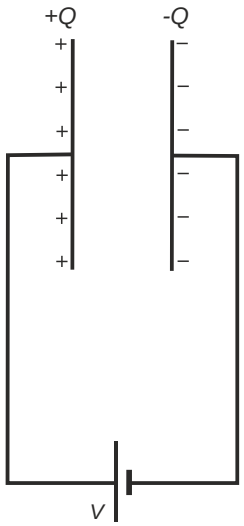

Figure 2.3. Parallel plate capacitor. [11]

Consider a vacuum parallel plate capacitor consisting of two electrodes, as shown in Figure 2.3. The variable A_c denotes the *surface area of the electrodes, the* variable d_c the *electrode distance* . The *vacuum capacitance* C_0 of a capacitor is defined as the ratio of the *stored charge* Q_0 to the *potential difference* U between the two electrodes.

$$C_0 = \frac{Q_0}{U} \tag{2-15}$$

Neglecting the edge effects, a homogeneous electric field will be formed between the two electrodes. The *electric field strength* $|\bar{E}|$ between the capacitor electrodes is determined by:

$$|\bar{E}| = \frac{U}{d_c}. \tag{2-16}$$

The *permittivity of free space* ε_0 is the ratio of the stored charge per unit area to the electric field strength.

$$\varepsilon_0 = \frac{Q_0}{|\bar{E}|A_c} = 8.8542 * 10^{-12}\frac{F}{m} \tag{2-17}$$

Therefore the stored charge on the electrodes of a vacuum parallel plate capacitor can be written as:

$$Q_0 = \varepsilon_0 A_c \frac{U}{d_c}. \tag{2-18}$$

If a dielectric is introduced between the electrodes, the ability of the capacitor to store charge will increase. This is due to the polarizability of the dielectric. This phenomenon will be thoroughly discussed in Section 2.3. The amount of charge that can be stored on the electrodes of the capacitor will increase with a proportionality constant ε_r, the *relative permittivity* of the dielectric.

$$Q = \varepsilon_r Q_0 = \varepsilon_0 \varepsilon_r A_c |\bar{E}| = \varepsilon A_c |\bar{E}|, \tag{2-19}$$

whereby ε is the *absolute permittivity* of the dielectric. [3,11,12]

2.3 Polarization

In Section 2.2, it was stated that the ability of a capacitor to store charge increases when a dielectric is placed between the electrodes. This phenomenon will be further elaborated in this subchapter.

An externally applied electric field will result in an accumulation of charge on the surface of the electrodes of a capacitor. This collection of charges produces an electric field which is equal to the summation of the individual fields produced by each charge. Thus an electric field exists between the two electrodes of the capacitor. That electric field is a measure of the force acting on charges between the electrodes. [5]

A dielectric is an insulating material, in which there are few free charge carriers. However, there is a large amount of bound charge carriers, that will be influenced by the existing electric field, thus the dielectric material will become polarized. There are

four different mechanisms of polarization, each with its own specific properties and its own frequency range. [5,6]

2.3.1 Interfacial polarization

Interfacial polarization is the slowest polarization mechanism and thus only significant at low frequencies. This mechanism involves the motion of free charges, in contrast to the other mechanisms where bound charges are involved. Free charges in the dielectric, caused by contaminants or irregularities, will drift through the dielectric and accumulate at interfaces. These interfaces can be boundaries between different materials, but they can also be, for example, voids or crystal defects in the lattice structure of the dielectric. An important interface where interfacial polarization often occurs, is the contact between the electrodes and the dielectric. [6,11,13]

A considerable contribution to interface polarization is given by *hopping charge carriers*. Hopping charge carriers are charge carriers that migrate between localized states, such as electron traps. The hopping itself is caused by thermal vibrations of the lattice. If an electric field is applied over the dielectric, it will be easier for the charge carriers to jump in a certain direction, leading to polarization of the dielectric. [3,10,14]

Interfacial polarization always results in a distortion of the macroscopic electric field. Since this master thesis is about insulating coatings, interfacial polarization will be of great importance. [3,15]

2.3.2 Orientational polarization

Orientational polarization, also called *dipole polarization*, occurs in dielectrics with permanent dipoles, so called *polar dielectrics* [3]. This phenomenon is noticeable at frequencies up to 10^6 Hz in solids [9]. In the presence of an external electric field, the dipoles will rotate and become partially aligned with the electric field. This process is very dependent of the temperature. Orientational polarization is an important mechanism in polar dielectrics, such as most polymers, but it does not occur to a great extent in ceramics. [1,10,13,15]

2.3.3 Ionic polarization

Ionic polarization, also called *atomic polarization*, takes place in ionically bounded materials. The external electric field causes a relative displacement of the negative and positive ions. This mechanism is nearly temperature independent and is very important in ceramic materials. The effect of ionic polarization is the most significant in the frequency range around 10^{12} - 10^{13} Hz. Ionic polarization still occurs at higher frequencies than orientational polarization because the displacement of ions is a faster process than the rotation of dipoles. [1,9,10,15]

2.3.4 Electronic or optical polarization

Electronic polarization is the fastest polarization mechanism and thereby occurs up to the highest frequencies. This polarization mechanism is noticeable up to frequencies of 10^{17} Hz. This mechanism arises from the displacement of the electron cloud relative to the positive nucleus of the atom. Electronic polarization occurs in all materials and is not influenced by any temperature differences. [1,10]

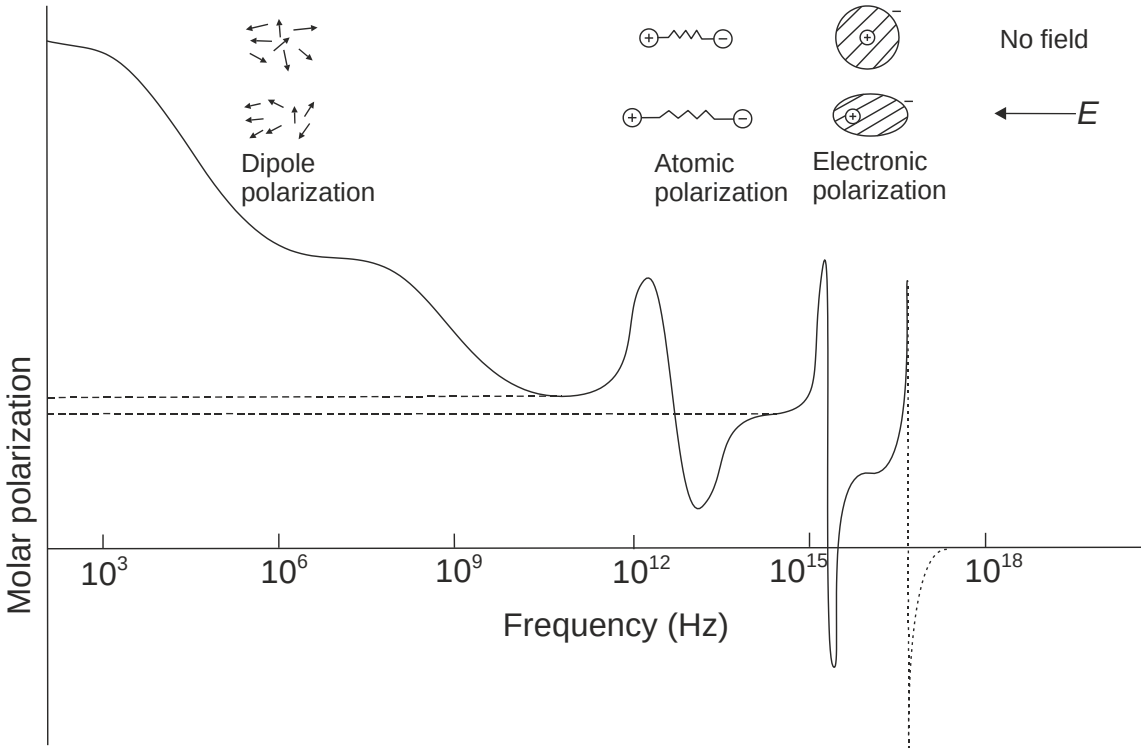

Figure 2.4. Contribution of the polarization mechanisms to the total polarization. [11]

The total polarization of a dielectric is the summation of these four polarization mechanisms. Consider a frequency increase in the changing electric field to a frequency higher than the frequency range of a certain polarization mechanism. The system will not be able to follow the changing electric field anymore and the total polarization will decrease. For example at a frequency of 10^9 Hz, the electric field is changing too quickly for the orientational polarization mechanism. Thus the total polarization at 10^4 Hz will be higher than the total polarization at 10^9 Hz. Generally speaking, polarization decreases with increasing frequency as shown in Figure 2.4. [3,6]

2.3.5 Effect of polarization on permittivity

When a dielectric is polarized, the induced dipoles on the surface of the dielectric attract more electric charge. This enhances the charge accumulation of the system. Based on Equation (2-19), the *relative permittivity* ε_r can be defined as

$$\varepsilon_r = \frac{Q}{Q_0}. \tag{2-20}$$

Thus the relative permittivity of a dielectric is proportional to the polarization of that dielectric. This means that the relative permittivity is frequency dependent and will generally decrease with increasing frequency. This frequency dependence will be discussed more thoroughly in Section 2.4.3. [10]

In order to discuss the electric breakdown mechanisms of dielectrics, it is important to define the *flux of electric displacement* $\bar{D}$*:*

$$\bar{D} = \varepsilon_0 \varepsilon_r \bar{E} = \varepsilon_0 \bar{E} + \bar{P}. \tag{2-21}$$

With $\bar{P}$ the *polarization* of the dielectric material

$$\bar{P} = \bar{D} - \varepsilon_0 \bar{E} = \varepsilon_0 \varepsilon_r \bar{E} - \varepsilon_0 \bar{E} = \varepsilon_0 (\varepsilon_r - 1)\bar{E}. \tag{2-22}$$

The *electric susceptibility* χ of a dielectric is defined as

$$\chi = \varepsilon_r - 1. \tag{2-23}$$

Since introducing a dielectric between the electrodes of a capacitor enhances the charge storage capacity of that capacitor, the relative permittivity is greater than one and thus the electric susceptibility is a positive number. Substitution of Equation (2-23) into Equation (2-22) shows that the polarization of the dielectric material can be written as:

$$\bar{P} = \varepsilon_0 \chi \bar{E}. \tag{2-24}$$

The electric displacement flux $\bar{D}$ is continuous through a dielectric. This has an important consequence in dielectrics composed of materials with different permittivities, as shown in Figure 2.5. This can be presented as two dielectrics in series: a first dielectric with a permittivity ε_A and an electric field strength $\overline{E_A}$, a second dielectric with ε_B and $\overline{E_B}$. The electric displacement flux is continuous so:

$$\bar{D} = \varepsilon_A \overline{E_A} = \varepsilon_B \overline{E_B}, \tag{2-25}$$

hence

$$\frac{\varepsilon_{rA}}{\varepsilon_{rB}} = \frac{\overline{E_B}}{\overline{E_A}}. \tag{2-26}$$

This is an important insight regarding dielectric breakdown strength. Equation (2-26) shows that in a non-homogeneous dielectric, the electric field strength will increase with decreasing relative permittivity. [3,5,11,12,15]

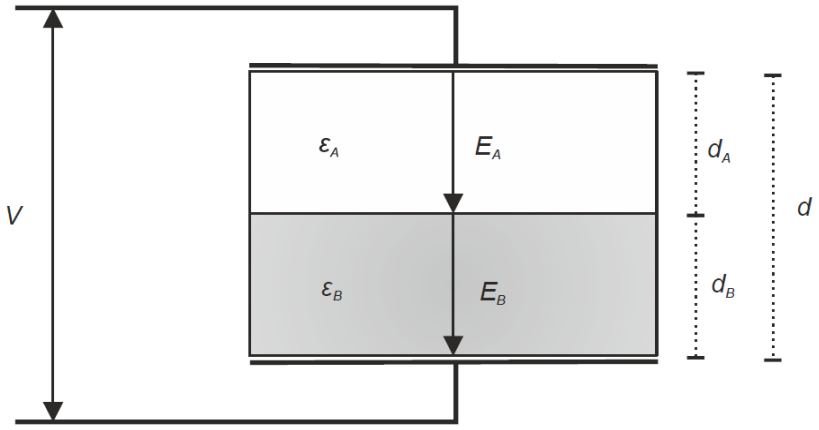

Figure 2.5. A dielectric composed of materials with different permittivities. [11]

2.4 Dielectric losses

2.4.1 Complex permittivity

In order to discuss dielectric losses, it is necessary to introduce the concept of *complex permittivity*. An ideal dielectric would be represented by only a capacitor and would cause a current that is 90° out of phase with the voltage. However, real dielectrics also have a resistive component, due to power losses. There exist various models for a real dielectric. They are all applied in different situations, thus it is difficult to define which model is the most accurate. In this thesis, a real dielectric is modeled as a parallel circuit, consisting of a resistor R_a and a capacitor C_a, as shown in Figure 2.6. [5]

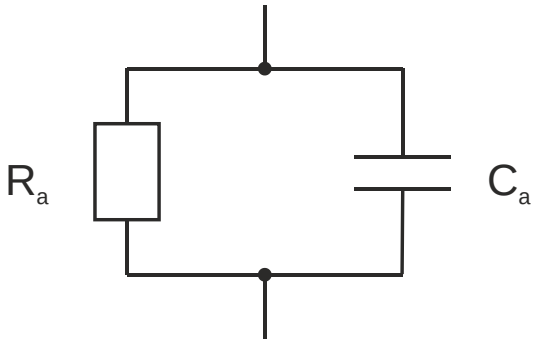

Figure 2.6. The equivalent electric circuit used to model a real dielectric. [11]

Because of Equation (2-21) the *complex permittivity* ε^* can be written as

$$\varepsilon^* = \frac{\bar{D}}{\bar{E}}, \tag{2-27}$$

with $\bar{E}$ is the sinusoidally changing electric field

$$\bar{E} = E_0 e^{j\omega t}, \tag{2-28}$$

where E_0 is the *maximum electric field strength* and ω is the *angular frequency*. Taking into account the *phase retardation* δ of the charging current and thus of the electric displacement flux yields

$$\bar{D} = D_0 e^{j(\omega t - \delta)}, \tag{2-29}$$

whereby D_0 is the *maximum flux of electric displacement*. Substituting Equations (2-28) and (2-29) into Equation (2-27) yields

$$\varepsilon^* = \frac{D_0}{E_0} e^{-j\delta} = \frac{D_0}{E_0}(\cos\delta - j\sin\delta). \tag{2-30}$$

Hence,

$$\varepsilon' = \frac{D_0}{E_0}\cos\delta, \tag{2-31}$$

$$\varepsilon'' = \frac{D_0}{E_0}\sin\delta, \tag{2-32}$$

whereby ε' is the *real part* of the complex permittivity and ε'' is the *imaginary part*, the *loss index*. The real part of the complex permittivity is out of phase with the applied voltage and is a measure for the capacitance of the dielectric. The imaginary part of the complex permittivity is in phase with the applied voltage and depicts the resistive losses. The quality of a dielectric is often described by the *dissipation factor tan δ:*

$$\tan\delta = \frac{\varepsilon''}{\varepsilon'}. \tag{2-33}$$

The relation between the different components of the complex permittivity is shown in Figure 2.7. [3,5,13]

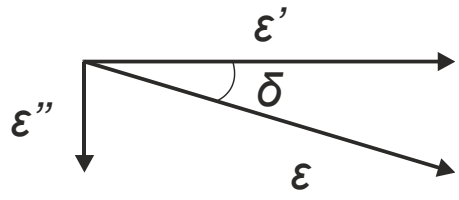

Figure 2.7. The components of the complex permittivity. [11]

2.4.2 Power loss

Regarding the equivalent circuit of a dielectric, the current through a dielectric can be split in two different currents: the *resistive* or *lossy current* I_r and the *displacement current* I_c, illustrated in Equations (2-34) and (2-35). [5]

$$I_r = \omega \varepsilon'' E \tag{2-34}$$

$$I_c = j\omega \varepsilon' E \tag{2-35}$$

The resistive current is caused by the conductivity of the dielectric and by losses due to the movement of charges, caused by polarization. The resistive losses caused by polarization are for example losses due to interfacial polarization or due to the friction between molecules involved in orientational polarization. For a vacuum parallel plate capacitor applies that: [5]

$$\varepsilon_0 = \frac{Q_0}{E}, \tag{2-36}$$

$$C_0 = \frac{Q_0}{U}. \tag{2-37}$$

Substitution of Equation (2-37) into Equation (2-36) yields

$$E = \frac{C_0}{\varepsilon_0} U, \tag{2-38}$$

hence [5]

$$I = I_r + I_c = (\omega\varepsilon'' + j\omega\varepsilon')\frac{C_0}{\varepsilon_0}U = j\omega\frac{\varepsilon^*}{\varepsilon_0}C_0U. \tag{2-39}$$

The corresponding *power loss* P_{loss} is defined by following equation:

$$P_{loss} = \omega\frac{\varepsilon''}{\varepsilon_0}C_0U_{rms}^2. \tag{2-40}$$

Equation (2-40) shows that the power loss is proportional to the loss index at a constant frequency and voltage. [16]

2.4.3 Frequency dependence

Polarization is a process that takes a finite time to attain its maximum. Each polarization mechanism has its own time constant τ and therefore its own frequency range. Every polarization phenomenon exhibits its own characteristic ε''-loss peak at a particular absorption frequency ω_0 in the frequency range as shown in Figure 2.8. The dielectric loss behaviour as a function of the frequency is described by the *Pellat-Debye equations*. Equation (2-41) provides a link between the *complex permittivity* ε^*, *the relaxation time* τ and the *angular frequency* ω.

$$\varepsilon^*(\omega) = \varepsilon_\infty + \frac{\varepsilon_s - \varepsilon_\infty}{1 + j\omega\tau} \tag{2-41}$$

Hence

$$\varepsilon'(\omega) = \varepsilon_\infty + \frac{\varepsilon_s - \varepsilon_\infty}{1 + \omega^2\tau^2}, \tag{2-42}$$

$$\varepsilon''(\omega) = \frac{(\varepsilon_s - \varepsilon_\infty)\omega\tau}{1 + \omega^2\tau^2}, \tag{2-43}$$

whereby ε_∞ is the *instantaneous relative permittivity,* measured immediately after the application of the electric field, and ε_s is the *static relative permittivity*, measured after a time period after which all the polarization processes have taken place. The frequency at which each polarization mechanism reaches its maximum value for the loss index can be determined by:

$$\frac{\partial\varepsilon''}{\partial(\omega\tau)} = (\varepsilon_s - \varepsilon_\infty)\frac{1 - \omega^2\tau^2}{(1 + \omega^2\tau^2)^2} = 0. \tag{2-44}$$

Hence,

$$\omega\tau = 1. \tag{2-45}$$

The evolution of ε' and ε'' as a function of the frequency are shown in Figure 2.8. The dielectric relaxation time will decrease with an increase in temperature. This can be modeled by the *Arrhenius equation:*

$$\tau = A_k e^{\frac{E_A}{R_g T}}, \tag{2-46}$$

whereby A_k is a *pre-exponential constant*, E_A is the *activation energy*, R_g is the *gas constant* and *T* is the *absolute temperature*. As demonstrated in Equation (2-45), the dielectric loss reaches its maximum at ωτ = 1, thus the loss peaks will shift to higher frequencies with increasing temperatures. When the voltage applied to the dielectric is removed, the polarization degree is not suddenly zero, but it also takes a finite time. This phenomenon is known as *dielectric relaxation*. [3,5,11,13]

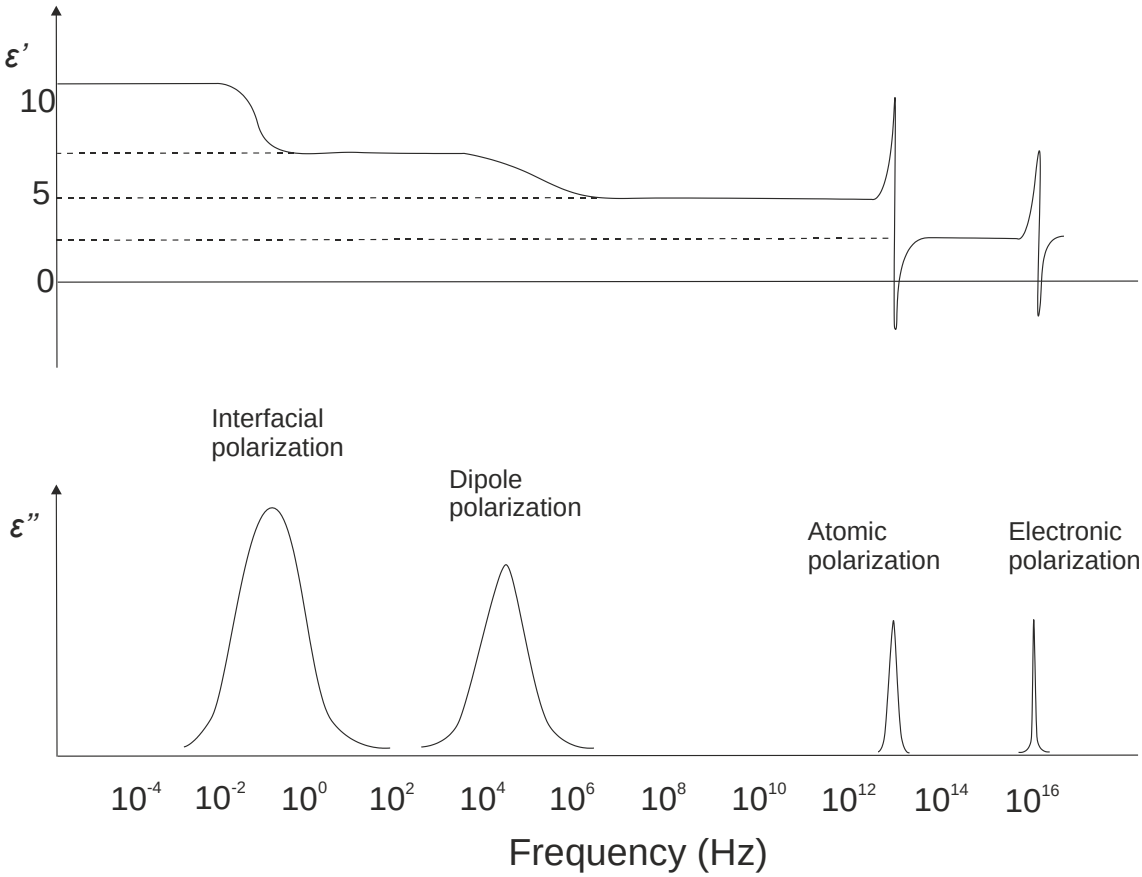

Figure 2.8. Frequency behaviour of the components of the complex permittivity. [11]

2.5 Breakdown in dielectrics

The breakdown voltage of a dielectric is the voltage at which the dielectric loses its insulating capabilities and causes a short circuit between the electrodes. Gaseous and liquid dielectrics are self-healing, therefore the breakdown is not destructive. In solids, the breakdown is destructive, causing a permanent conductive channel through the dielectric. In this subchapter, different breakdown mechanisms are discussed. [13]

2.5.1 Intrinsic breakdown

Intrinsic breakdown is a form of *electronic breakdown*. It is caused by electrons that gain enough energy to cause a collapse of the molecular structure. This breakdown voltage can only be achieved under ideal conditions, thus it can be considered as an upper limit for the real breakdown voltage. [5,11,13]

Electrons gain energy by the existing electric field. In crystalline structures, they lose it in collisions with the lattice. Increasing temperature is causing more thermal lattice vibration, causing more collisions between electrons and the lattice structure. So, in crystalline structures, the breakdown strength will increase with increasing temperature until a critical temperature where electron-electron interactions become more important. On the other hand, in non-crystalline structures, there are no collisions with the lattice, thereby the breakdown strength will decrease with an increase in temperature. [5,11,13,17]

2.5.2 Avalanche breakdown

Avalanche breakdown is the second electronic breakdown mechanism. In an avalanche breakdown, the electric field provides the electrons at least that amount of energy that is necessary to detach other electrons from the lattice by collisions. This results in an exponential increase of free electrons, causing dielectric breakdown. Avalanche breakdown is also temperature dependent, since an increasing temperature will accelerate the breakdown process by providing more energy to free charges. [10,13]

2.5.3 Thermal breakdown

Thermal breakdown occurs when the heat generation in a dielectric is higher than the heat dissipation of that dielectric. This causes an increasing temperature, which results in a decreasing resistance. Due to Ohm’s law, this will cause an increase in heat generation, thus a *thermal runaway* will occur. The temperature of the dielectric will continue rising until finally breakdown occurs. [11,13]

2.5.4 Partial discharges

All previous breakdown mechanisms are very fast phenomena, caused by a sudden high electric field. Partial discharges are the main reason for *dielectric deterioration* over a

long period of time, causing breakdown at much lower electric field stress. Equation (2-26) shows that cracks and voids cause local higher electric fields. This leads to local discharges, causing physical and chemical degradation of the void surface. Due to consecutive discharges many fine degradation paths of a dendritic character can be formed, this phenomenon is known as *treeing*. Treeing leads to deterioration of the dielectric material and eventually to breakdown. [5,11]

With increasing thickness, the electric field stress at which breakdown occurs will decrease. This is due to the fact that because of partial discharges, breakdown often occurs along faults in the dielectric. The incidence of faults increases with increasing thickness. [11,13]

2.5.5 Space charge

Electronic polarization, ionic polarization and orientational polarization are all uniform within the volume of the material. Space charge is a not-linear mechanism, influencing the local internal field and thus the breakdown behaviour of a dielectric considerably. Generally, space charge occurs whenever the rate of charge accumulation is different from the rate of charge removal [3]. Important causes for this space charge phenomenon are charges injected at the electrodes, charges trapped during the fabrication process of the dielectric and interface polarization, as discussed in Section 2.3.1. In Figure 2.9, the different processes causing space charge are summarized. [3,11]

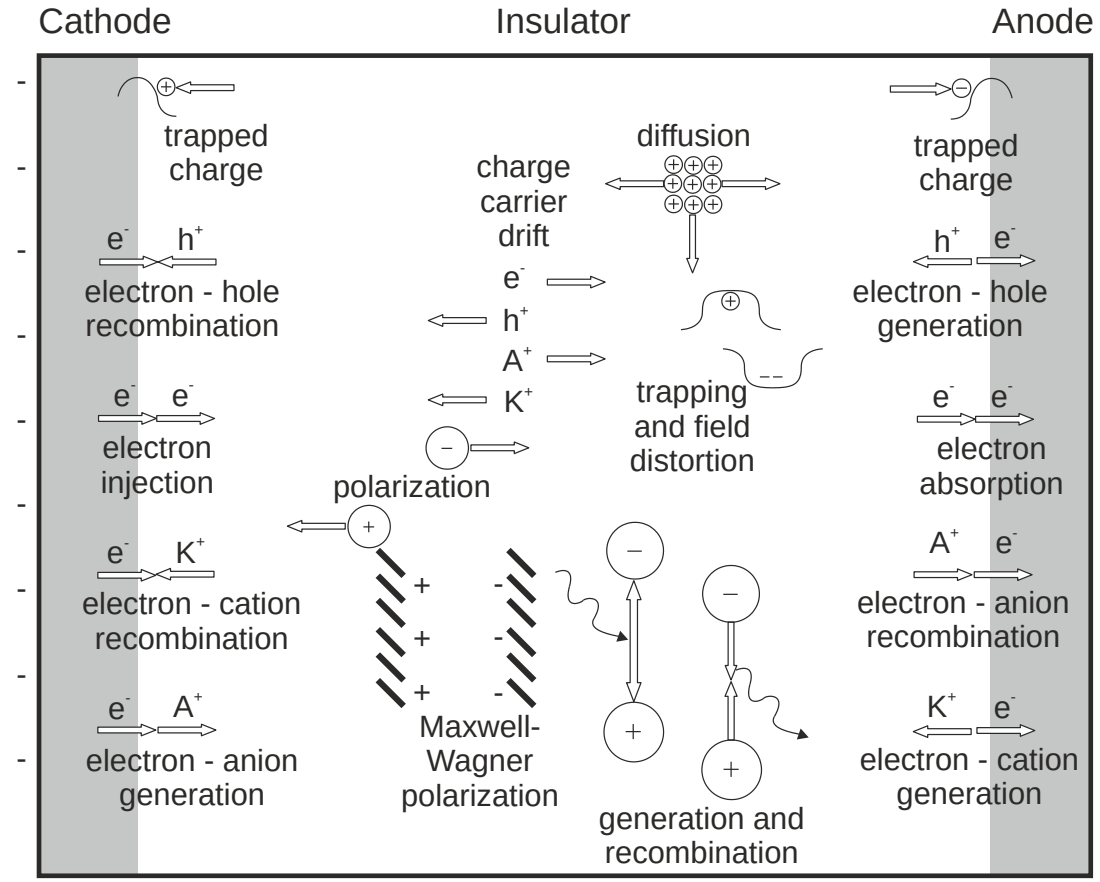

Figure 2.9. Different space charge accumulation processes. [11]

The effect of the injected charges on the local electric field is dependent on the polarity of both the charge and the neighbouring electrode at which the charge is trapped. When trapped charges have the same polarity as the neighbouring electrode, they are called *homo charges*. Thereby the field stress at the electrode will decrease, but in the central region of the dielectric, the field stress will increase. When trapped charges have the opposite polarity as the neighbouring electrode, they are called *hetero charges*. These charges will cause an increased field stress at the electrodes, but a decrease in field stress in the central region of the dielectric. [3,11]

3 CERAMICS

According to Niesz, ceramics can be defined as inorganic, nonmetallic materials processed or consolidated at high temperatures [18]. Traditionally, ceramics were used for utensils such as clay pots and porcelain dinner plates. In the course of history the research field of ceramics has broadened, for example ceramic thermally insulating refractory bricks for ovens and fireplaces have been developed. All these materials belong to the traditional ceramics, ceramics manufactured with inexpensive materials and with relatively large tolerances during the production process.

Recent evolutions in ceramic technology have led to the so-called advanced ceramics. These ceramics are the result of a much more accurate production process in order to optimize certain properties. They have a wide scope: for example heat shields used in space shuttles and a large number of present-day electronic applications are using advanced ceramics. [18,19]

3.1 Ceramic materials

3.1.1 Production process

The beginning of the production process of an advanced ceramic consists of the creation of a ceramic powder with the desired purity and particle size for a certain application. First, the raw material has to be gathered. The raw material is a ceramic powder with a certain purity. There are relatively impure raw materials, for example clays mined from the earth's surface. But if a really pure powder is needed, chemically synthesized ultra-high purity powders are used. The next phase in the production process involves *comminution* (particle size reduction) and *purification* of the mined raw material. The particle size is reduced by crushing, grinding or milling. After comminution, impurities in the raw material are extracted by washing, chemical leaching or magnetic separation. After purification of the powder, the micrometer size particles are agglomerated into larger granules with the right particle size in order to obtain the desired material properties. If a ceramic object is the intended outcome of the production process, the next phase in the manufacturing process is mostly *green forming*. This is the forming of the powders into the desired shape. Green forming is followed by *powder pressing*, which is the densification of the ceramic material by elevated pressure. The last step in the production process is the *sintering* of the material. Sintering is the further densification of the ceramic material by heating it up to temperatures below the melting point, still under elevated pressure. The whole production process is summarized in Figure 3.1. [18,19,20]

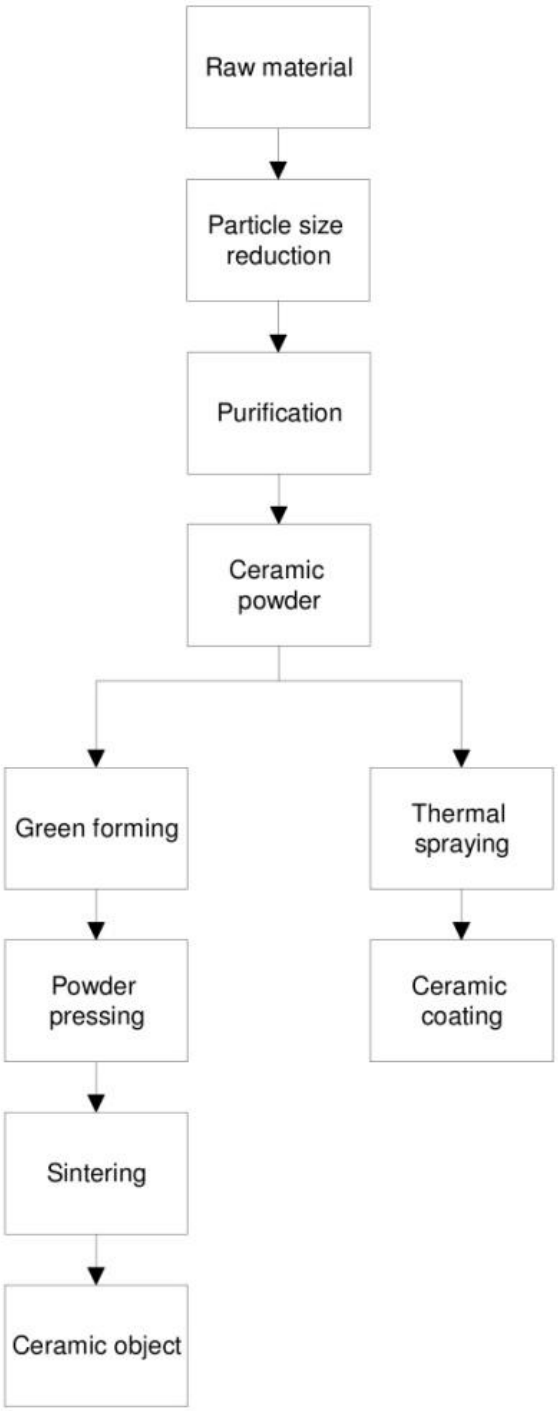

Figure 3.1. Production process of ceramics.

In this master thesis, thermally sprayed ceramic coatings are studied. Thus the powder does not undergo the process of green forming and sintering. Instead the powders are thermally sprayed onto a substrate. This process will be further elaborated in Section 3.3.

3.1.2 Chemical composition

There are various ceramic structure types. Important structure types are nitride ceramics, chalcogenide ceramics and oxide ceramics. Oxide ceramics are the most dominant ceramic structure type, thanks to their chemical stability at high temperatures in an oxygen-containing atmosphere. In oxide ceramics the electron transfer is essentially complete, which leads to strongly ionic bonds. This thesis is focused on alumina ceramics, a subset of the oxide ceramic structure type. [14]

Alumina ceramics is a collective noun for all ceramic bodies prepared from aluminium oxide. Their properties are not always similar because they depend strongly on the manufacturing process and the particle size, but there are some generalities. Corundum (Al_2O_3) has a trigonal structure. This gives corundum an exceptionally high density. There is only one stable modification of corundum, α-Al_2O_3, but also the metastable γ-Al_2O_3 and δ-Al_2O_3 appear. Another important structure in which aluminium oxides appear is the spinel structure, Al_2MgO_4. This structure is based on a cubic closest packing. [14]

3.1.3 Electrical properties

Ceramics are often used because of their mechanical strength, wear resistance, electric behaviour, chemical stability and resistance to thermal shocks. This section focuses on their electric behaviour. [18,19]

In general, ceramics are regarded as materials with a low electrical conductivity over a wide temperature range and a high dielectric strength. There exist ceramic conductors and semiconductors as well, but they will not be discussed in this thesis. As stated in Chapter 2, the electrical properties of insulating materials strongly depend on defects such as porosities, lattice distortions, impurities and interfaces. This strong influence is mainly caused by *trapped charge carriers*. The effect of these trapped charges on the breakdown voltage is strongly dependent on the microstructure of the ceramic. If the microstructure of the material induces a diffused structure of trapped charges, often called stabilized charge, a better breakdown performance will be acquired. This effect can clearly be observed in the relation between breakdown strength and the average grain size of alumina ceramics, as shown in Figure 3.2. The interface density will increase with a decreasing average grain size. This leads to a better diffusion of the trapped charges in the material, resulting in higher breakdown strength. However, if the microstructure is such that trapped charges are locally accumulating, the breakdown voltage decreases significantly. This is because the local accumulation is causing space charge. This effect can be observed by doping the alumina with CaO or MgO, as shown in Figure 3.3. [10,19,21,22]

An increase in temperature leads to a decrease in charge trap depth. This causes an increase in the conductivity of the material, which is a problem for insulating materials. The presence of for example anorthite is causing deeper traps, leading to more favourable dielectric behaviour at increased temperature. [22]

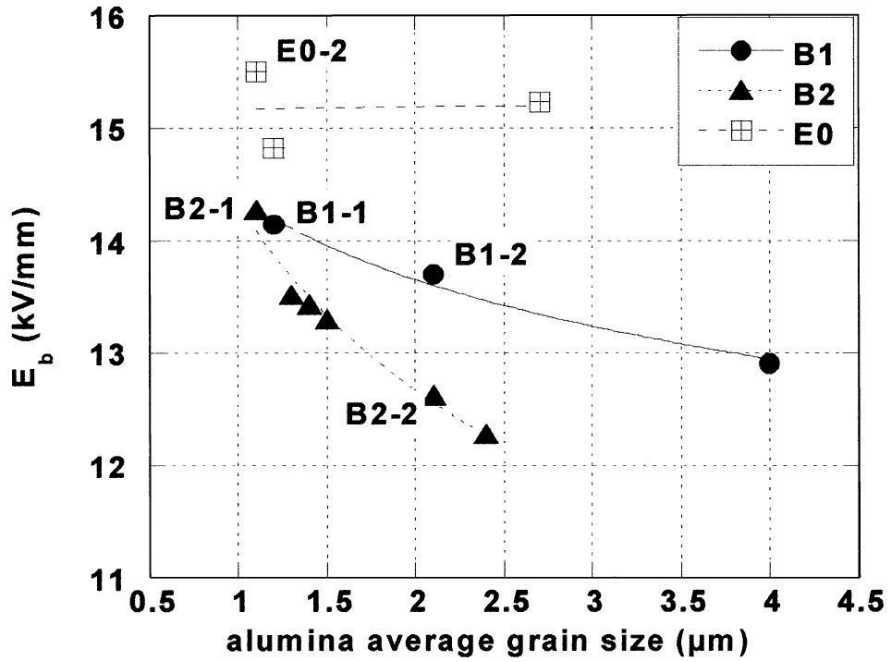

Figure 3.2. Breakdown strength evolution with grain size for 99.8% pure aluminas B1 and B2 compared to 99.99% pure alumina E0. [21]

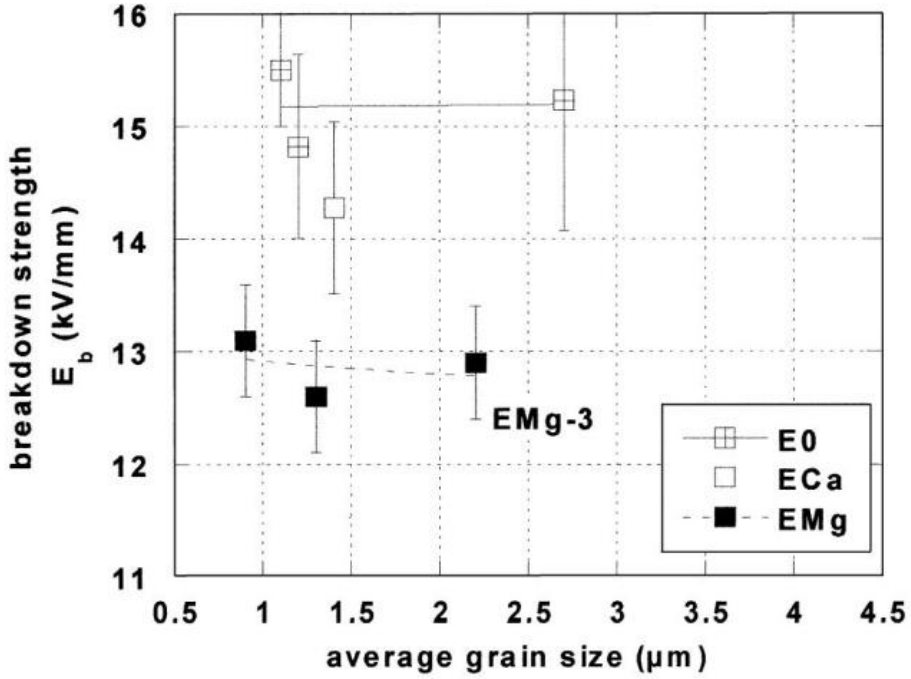

Figure 3.3. Breakdown strength evolution with alumina grain size for pure alumina E0, Ca- and Mg-doped aluminas. [21]

3.2 Coatings

Wierzchon and Burakowski define a coating as a layer of material, formed naturally or synthetically, deposited artificially on the surface of an object made of another material, with the aim of obtaining technical or decorative properties [23]. Coatings are usually known for their decorative properties, in the form of paint. People do not build a wall with green bricks, they build the wall with standard bricks and coat it afterwards with a green paint. But in daily life coatings are also used for their technical properties. For example, varnish is mainly used to protect wood or another substrate against humidity and other ambient influences. In modern technology, coatings are used in an infinite amount of applications. For example anti-corrosion coatings, wear-resistant coatings, hard coatings and waterproof coatings are often used. This thesis focuses on coatings used for another application, on electrically insulating coatings.

The most traditional coating process is painting, which is mainly used for coatings in daily life. Regarding industrial applications, a numerous amount of coating processes has been developed. The various processes differ mostly in the physical way of deposing the coating, the temperature of the coating process and the thickness of the coating layer. *Chemical vapour deposition* (CVD) and *physical vapour deposition* (PVD) are two coating processes often used to deposit ceramic materials. They are based on the same physical phenomenon, evaporation. They differ mainly in the temperature at which the process takes place. In CVD, coatings are deposited at high temperatures, typically in the range from 950°C to 1050°C. In PVD on the other hand coatings are deposited at lower temperatures, typically in the range from 250°C to 500°C. This difference in temperature results in different coating properties. CVD coatings are mostly thicker than PVD coatings, meanwhile the surface of the CVD coatings is mostly rougher than the surface of the PVD coatings. Another process used for depositing ceramic coatings is *electrophoretic deposition*. This technology uses an external electrical field to apply the coating. Only polarized powder particles are eligible for the use of this technique. In this thesis, the investigated ceramic coatings will be thermally sprayed. This coating process will be discussed in the next subchapter. [24,25,26]

An important factor in the deposition of a surface coating is the adhesion between the coating itself and the surface of the substrate. Adhesion is influenced by multiple variables, for example by the thermal coefficient of both materials, dirt, defects on the surface of the substrate and residual stresses. Generally, a high purity of the substrate's surface and a coating material with a lattice structure similar to that of the substrate leads to good adherence. [23,24]

3.3 Thermal spraying

Standard DIN EN 657 defines thermal spraying as "*A process, in which the feedstock is partially or fully melted inside or outside a spraying gun and deposited on a prepared surface."* The principle of the thermal spraying process is illustrated in Figure 3.4. [27]

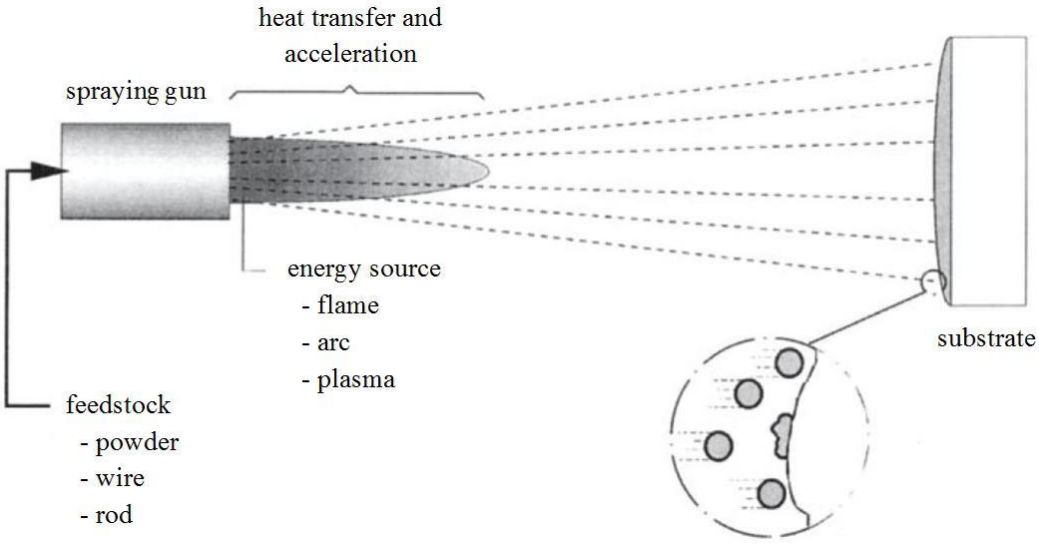

Figure 3.4. Thermal spraying process. [27]

When molten or semi-molten particles of the feedstock strike the surface, they form splats. Splats are the basic building blocks in thermally sprayed coatings. Because of the impact on the surface they have flattened, disk-like structures. Splats will overlap, solidify and adhere to one another, this way they accumulate layer by layer and form a coating with a typical laminar structure. This process is shown in Figure 3.5. [20,27,28]

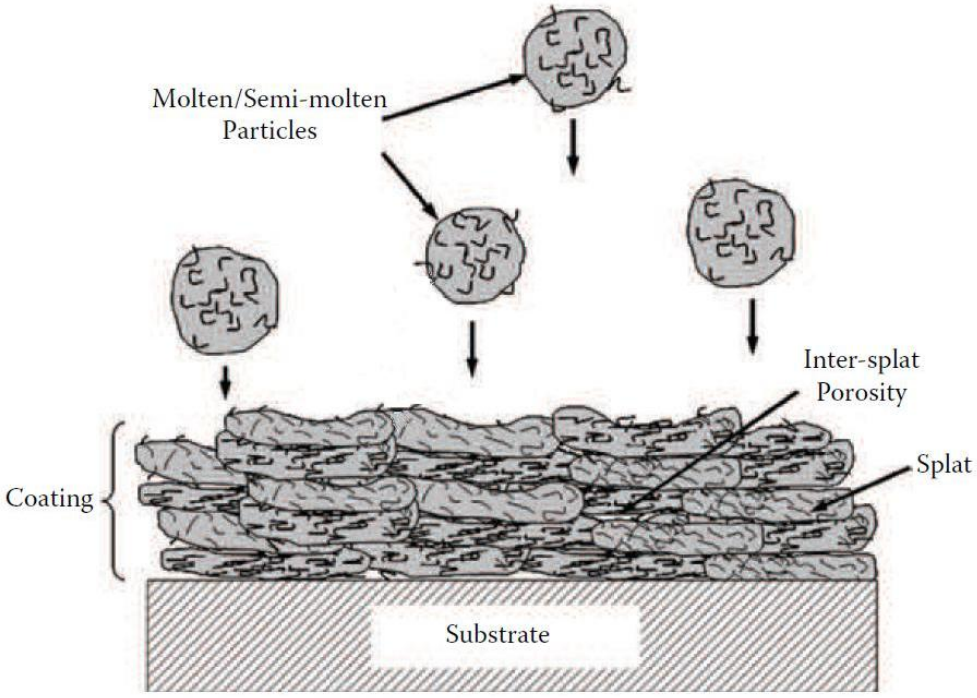

Figure 3.5. Structure of thermally sprayed coatings. [20]

The different thermal spraying techniques differ in particle velocity and particle temperature, as shown in Figure 3.6.

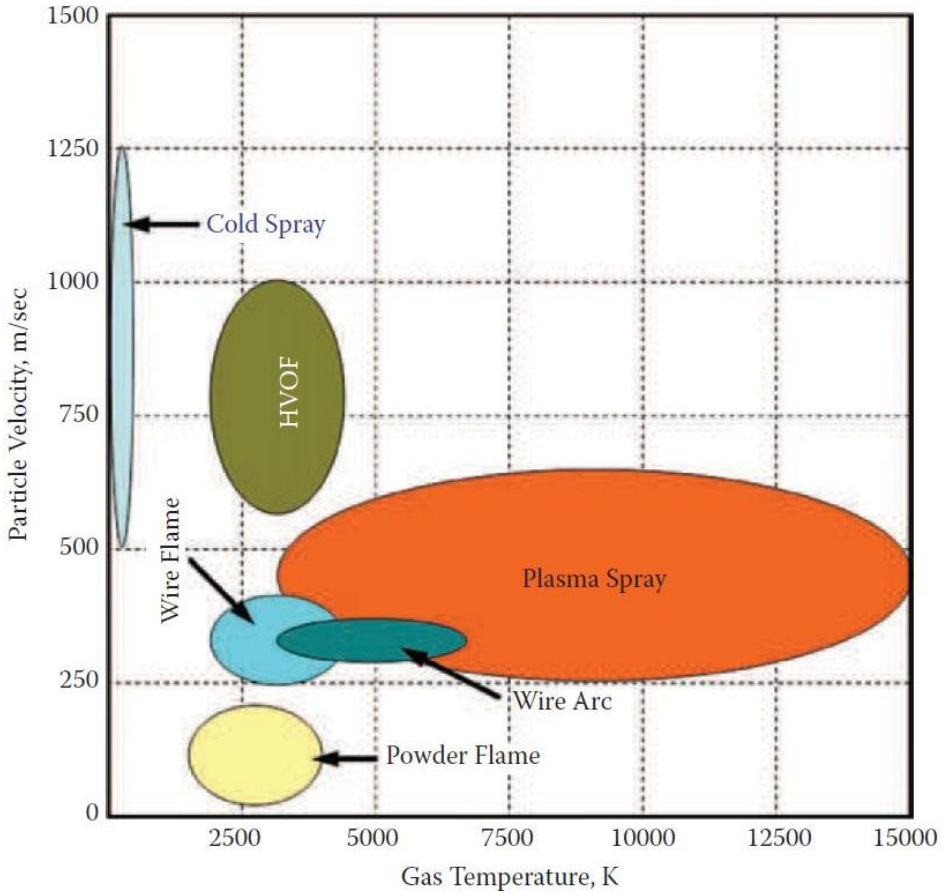

Figure 3.6. Different thermal spraying techniques. [20]

3.3.1 Flame spraying

In the flame spraying process, the coating material is injected into a gaseous oxyfuel flame and subsequently sprayed onto the surface of the substrate. Typical of flame spraying is the moderate particle temperature and the relatively low particle velocity. This results in a more porous and oxidized coating with a lower bond strength compared to other spraying methods. The oxides in the coating provide a wear resistant, hard coating, while the porosity can be advantageous in areas where lubricants are used (for example in bearings). If a high porosity is not desired, a subsequent fusion process is often applied. The feedstock of the flame spraying process can be powders, wires and rods. [25,27,28]

3.3.2 High velocity oxygen fuel spraying

High velocity oxygen fuel spraying (HVOF) is a variant of the flame spraying technique, often used in ceramic insulating coatings. The particle temperature is about

the same but supersonic particle velocities are reached. This high particle velocity results in very dense coatings with high bond strengths. [20]

The oxidation rate of a thermally sprayed coating is mainly determined by in-flight reactions. When the time particles can react with the surroundings or when the amount of ambient oxygen decreases, the oxidation rate will decrease as well. So with a longer flame, and hence more oxygen burning within the flame and shortening the reaction time, the oxidation rate will decrease. A similar result can be obtained by higher particle speeds, and consequently by reducing overheating and shortening the reaction time. New developments in HVOF technology lead to even higher particle velocities and lower particle temperatures and thus resulting in denser coatings with lower oxidation rates. Disadvantages of the HVOF spraying method are the high noise level and the low deposition rate. [20,27,28,29]

3.3.3 Arc spraying

In arc spraying, also called *electric-arc spraying*, the feedstock of the process is a wire of an electrically conductive material. The distance between two oppositely charged wires of the feedstock is gradually reduced until an electric arc between the wires appears. The arc melts the tip of the wires, while a compressed gas atomizes the molten particles and accelerates them to the substrate. Arc spraying is characterized by a relatively low particle velocity, resulting in a decreased coating density and an increased oxidation rate. [25,27,28]

The arc spraying process is economically interesting because of the high deposition rates and the low costs. However, since only electrically conductive materials can undergo this process, it is not suitable for insulating ceramic coatings. [25]

3.3.4 Plasma spraying

Plasma spraying is an important coating technique regarding ceramic coatings. The feedstock particles are heated and accelerated by plasma. Plasma is an ionized gaseous cloud composed of free electrons, positive ions, neutral atoms and molecules [28]. The energy needed to create plasma, thus to ionize a gas, is mostly generated by a DC or an AC arc. The core temperature of the plasma cloud depends on the electrical power, the gas, the pressure and the spraying conditions. The typical temperature range is from 3 500 K to 15 000 K. Because of these extremely high temperatures, any material that has a liquid phase can be melted in plasma. [20,25,27]

The particle velocities involved in the plasma spraying process are typically higher than the particle velocities in the arc and flame spraying processes. This results in denser coatings with a finer coating surface roughness. The most common technique in plasma spraying is the *atmospheric plasma spraying* (APS), where the spraying takes place in ambient air. A more advanced technique is the *vacuum plasma spraying* (VPS), whereby a very homogeneous and oxide-free microstructure can be acquired. [25,27,28]

3.3.5 Cold spraying

Cold spraying is a quite new technique. In this process particle velocities are very high, but the particle temperature is below the melting point of the feedstock material. By impact on the substrate, kinetic energy is transformed into thermal energy and this results in adhering splats. This transformation occurs because of the plastic deformation of the feedstock material. Thereby the sprayed material has to be sufficiently ductile and thus cold spraying is not suitable for brittle, non-deforming ceramic materials. Because of the low temperatures, thermal effects are avoided and the original microstructure of the feedstock material can be preserved. The absence of thermal effects leads to the absence of oxidation while spraying. Other advantages of the cold spraying process are the high deposition rate and the dense coating structure. [20,25,27,28]

3.3.6 Properties of thermally sprayed coatings

An important phenomenon regarding the performance of thermally sprayed coatings is *residual stress*. Residual stress is caused by quenching of coating particles and by differences in thermal expansion coefficients between substrate and coating material. Generally, compressive stresses are advantageous since they have a positive effect on corrosion resistance and fatigue life. On the other hand, tensile stresses are detrimental to coating performance. Residual tensile stress can lead to the formation of cracks, especially in coatings with a porous structure. [23,25,30]

As mentioned earlier, *adhesion* between the coating and the surface of the substrate is important in coating technology. In thermally sprayed coatings, mutual *cohesion* between splats has also a major importance. Cohesion and adhesion are mainly due to physical forces, for instance Van der Waals forces and metallurgical interactions, such as diffusion and chemical reaction between surfaces. The area of contact and thus the level of porosity has a large influence on these phenomena. A reduced level of porosity leads to an increased area of contact, resulting in both stronger adhesion and cohesion. [25]

Defects in thermally sprayed coatings are mostly voids, pores and microcracks. Voids and pores are caused by uneven spreading of splats, incomplete overlap of splats or unmolten particles. Horizontal microcracks can be a sign of bad adhesion, while vertical microcracks are mostly due to quenching stress. A detrimental property of the thermal spraying of Al_2O_3 is the formation of the metastable γ-Al_2O_3 and δ-Al_2O_3. These metastable phases change the properties of the Al_2O_3 coating, which may lead to unexpected behaviour. [25]

3.3.7 Comparison of APS sprayed and HVOF sprayed Al_2O_3

A lower deposition temperature has a limiting effect on the phase transformation of α-Al_2O_3 into the metastable phases. This phenomenon causes a higher α-Al_2O_3 content in HVOF sprayed coatings compared to APS sprayed coatings. [30,31]

The resistivity of both APS and HVOF sprayed coatings are similar at low humidity. At high humidity levels the resistivity of both coating techniques show a significant decrease. The decrease in resistivity due to moisture is more dramatic in APS sprayed coatings than in HVOF sprayed coatings. This is due to the higher hygroscopic γ-Al_2O_3 content in APS-sprayed coatings. The high sensitivity of Al_2O_3-coatings to humidity is due to the capillary condensation of water into voids and to surface conductivity. The latter is a result of the adsorption of water to the surface of the coating. This mechanism consists of water chemisorption, water physisorption and dissociation of water molecules. Dissociation of water molecules results in the release of ions, which increases the surface conductivity. This process is shown in Figure 3.7. [31]

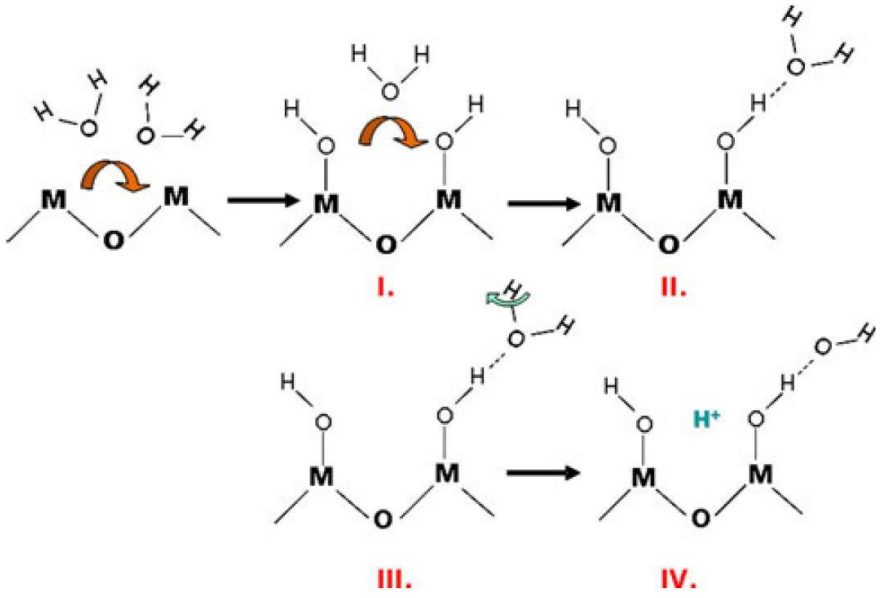

Figure 3.7. (I) Water chemisorption, (II) Water physisorption, (III) Dissociation of physisorbed water, (IV) release of protons. [31]

The more porous microstructure is another disadvantage of APS sprayed coatings regarding their sensitivity to humidity. The interconnected porosities are transverse channels for charge transfers when water is absorbed by capillary condensation. The difference in porosity can clearly be observed in the microstructure shown in Figure 3.8. [30,31]

Electrical resistivity is not dependent on the thickness of the coating. Dielectric breakdown strength on the other hand, is strongly influenced by the thickness of the coating layer. With an increasing thickness, the breakdown voltage increases, but the field stress at which breakdown occurs decreases. The literature consulted mentions two mechanisms that account for this behaviour. First, from the point of view of material science, this phenomenon is often explained by a heat/thermal mechanism. With increasing thickness, the thermal resistance increases faster than the electrical resistance. Hence local thermal instabilities, causing breakdown, will arise at lower field

strengths. This explanation refers to the occurrence of a thermal breakdown. However, in insulators power losses are mostly considered low. That is the reason for the use of a statistical explanation, the so called *power law*, in literature on high voltage. This law is based on the determination that with increasing thickness, the probability of a weak spot causing breakdown at lower voltage, increases as well. The power law is used to predict the breakdown field strength as a function of the coating thickness:

$$E_b = E_{b,0}\left(\frac{d}{d_0}\right)^c, \tag{3-1}$$

where c is a *correlation coefficient*, d_0 is the *thickness of a standard sample* with the corresponding *breakdown field strength* $E_{b,0}$ and d is the *thickness of the test sample* with the corresponding *breakdown field strength* E_b. The dielectric constant generally decreases with an increasing amount of interpass interfaces. [31,32,33,34]

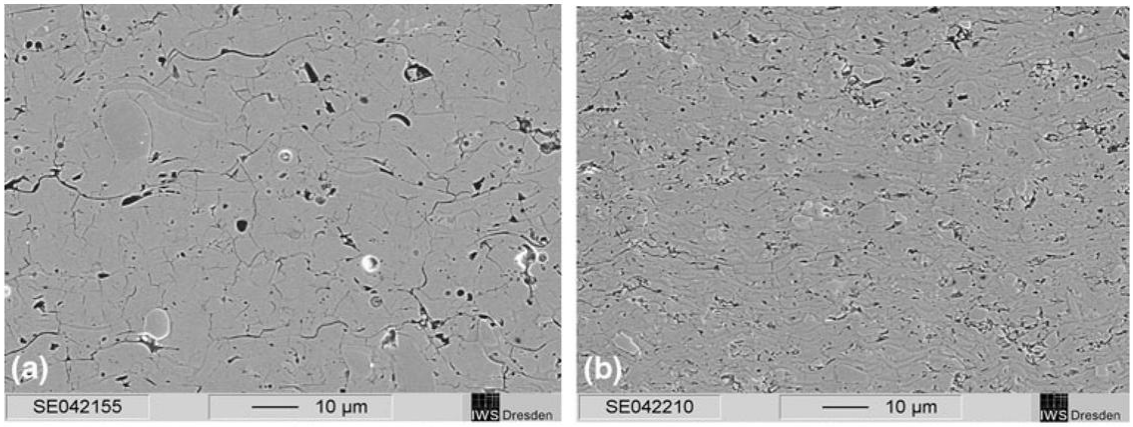

Figure 3.8. Cross-sectional SEM micrographs of (a) APS and (b) HVOF sprayed Al_2O_3 coatings. [31]

Measurements have shown that the breakdown voltage of HVOF sprayed coatings is mostly higher than the breakdown voltage of APS sprayed coatings. This is due to the higher content of interconnected porosities in APS coatings, facilitating the dielectric breakdown. [31]

The general residual stress profile is different for APS and HVOF coatings. For HVOF sprayed coatings the stress evolves generally from compressive at the interface between the coating and the substrate to tensile approaching the surface of the coating. For APS sprayed coatings the stress is generally tensile, lowest at the interface between coating and substrate. [30]

4 MEASUREMENT SETUP

4.1 Preparation of samples

The dielectric properties of Al_2O_3 coatings, coated by three different thermal spraying techniques, are studied in this thesis. The first sample is coded as *653_14*, it has an ethylene-HVOF sprayed Al_2O_3 coating on a carbon steel substrate. For the measurements of this spraying method, different samples were used for the measurements at temperatures below and above 100°C. The code of the second sample is *TS_EXT_123*, which has a flexicord sprayed Al_2O_3 coating on a carbon steel substrate. Flexicord spraying is a modified flame spraying technique. The third sample is coded as *#184 alu*. It has an atmospheric plasma sprayed Al_2O_3 coating on a stainless steel substrate. The specifications of the various samples are summarized in Table 4.1.

Table 4.1. Spraying method, substrate and coating material of the different samples.

Code	Spraying method	Substrate	Coating Material
653_14	Ethylene-HVOF	Carbon steel	Al_2O_3
TS_EXT_123	Flexicord	Carbon steel	Al_2O_3
#184 alu	Atmospheric plasma	Stainless steel	Al_2O_3

The thickness of the coatings was measured by the *Elcometer® 456 – model B.* The coating thickness of each sample was measured on ten different spots. The average thickness and the range of the measured thickness are shown in Table 4.2. The measurement device was always recalibrated before measuring a new sample, except before the measurements of the second sample 653_14. Because of that, the absolute values of the measurements made with that sample should not be compared with other absolute values. However, the aim of the measurements made with that sample was to examine the evolution of the dielectric properties of the sample with an increasing heating time at temperatures above 100°C. The observed evolution is not influenced by any deviations of the measured coating thickness.

Table 4.2. Coating thickness of the different samples.

Code	Average thickness [µm]	Thickness range [µm]
653_14 – sample 1	265.4	254 – 275
653_14 – sample 2	242.8	224 – 253
TS_EXT_123	193.7	180 – 207
#184 alu	303.1	294 – 331

After determining the coating thickness, the samples were prepared in order to avoid any influence by the contact between the electrodes and the surface of the sample. Silver electrodes with a 55 mm diameter were painted on the surface of the coating, using a high purity silver paint. Around the silver electrodes, a guard electrode was painted to avoid surface current. The painted samples are shown in Figure 4.1. Afterwards, the samples were dried at a temperature of 120°C for 2 hours. The preparation of these samples was according to standard IEC 60672-2 [35]. The second 653_14 sample was dried differently, at a temperature of 105°C for 5 hours, as explained in Section 4.3.2.

Figure 4.1. From the left to the right: samples 653_14, TS_EXT_123 and #184 alu.

4.2 Measurement system

The dielectric properties of the samples were studied with the *IDA 200* measurement device. The measuring method used in this device is *dielectric spectroscopy*, in which the dielectric properties of a material are measured as a function of the frequency. The IDA 200 measurement device applies a sinusoidal voltage over the sample, with a varying frequency and a maximum peak voltage of 200 V. The *impedance Z* of the sample at the different frequencies is calculated by measuring the current through the sample and applying the law of Ohm. The measurement scheme is depicted in Figure 4.2. [36]

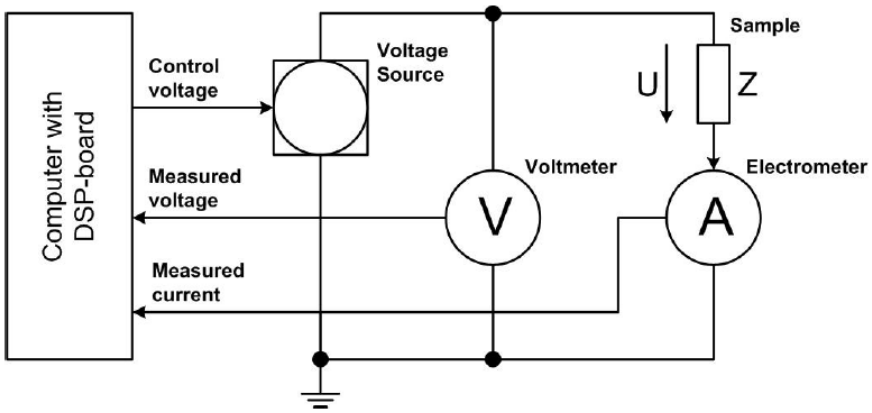

Figure 4.2. The IDA 200 measurement circuit. [36]

The IDA 200 measurement device was connected to the samples by the electrode configuration, shown in Figure 4.3. The sinusoidal voltage is applied between the clamps with the red and the blue wire. The third clamp is the connection between the ground and the guard electrode, painted on the sample.

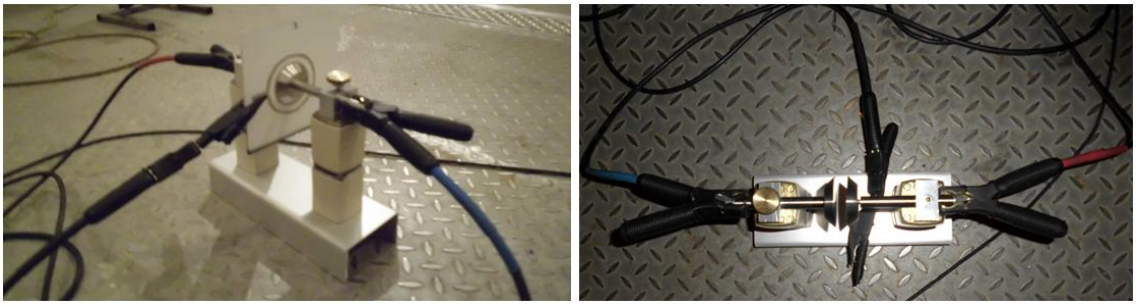

Figure 4.3. The electrode configuration used for the measurements.

4.3 Measurement procedure

Before starting the measurements with the IDA 200, the device was calibrated with the associated calibration box. In every measurement, a sinusoidal voltage with a maximum peak voltage of 200 V was applied over the sample. The followed measurement procedure was different for the measurements below and above 100°C.

4.3.1 Measurements below 100°C

At temperatures below 100°C, the effects of temperature and relative humidity on the samples were examined. The different circumstances whereat the samples were tested, are shown in Table 4.3. Because of the risk of oxidation, there were no measurements at a temperature of 70°C for relative humidities of 60% or higher. For the same reason were at a relative humidity of 90% only measurements made at a temperature of 20°C and 30°C. At every condition, the electric properties of the samples were measured at a frequency of 0.01, 0.05, 0.1, 0.5, 1, 5, 10, 20, 40, 50, 60, 100, 200, 500 and 1000 Hz.

Table 4.3 also shows the sequence of the different measurement conditions. The measurements were performed in this order, to prevent corrosion inside the samples in an early stage of the measurements. Before increasing the relative humidity, the samples were dried at a temperature of 120°C for two hours.

Table 4.3. Measurement sequence for measurements below 100°C.

	20°C	30°C	40°C	50°C	60°C	70°C	Drying
20%	*1*	*2*	*3*	*4*	*5*	*6*	*7*
35%	*8*	*9*	*10*	*11*	*12*	*13*	*14*
45%	*15*	*16*	*17*	*18*	*19*	*20*	*21*
60%	*22*	*23*	*24*	*25*	*26*		*27*
75%	*28*	*29*	*30*	*31*	*32*		*33*
90%	*34*	*35*					*36*

In order to determine the acclimatization time between consequent measurements at different conditions, the stabilization behaviour of the samples had to be examined. The stabilization of the relative permittivity of the samples after drying, at a relative humidity of 40% and a temperature of 25°C, is shown in Figure 4.4, Figure 4.5 and Figure 4.6, for the HVOF, the flexicord and the plasma sprayed sample, respectively. In the measurements made for this thesis, the samples were always measured in this order. Based on the stabilization behaviour, it was decided to let the samples acclimatize for at least four hours before performing the measurements.

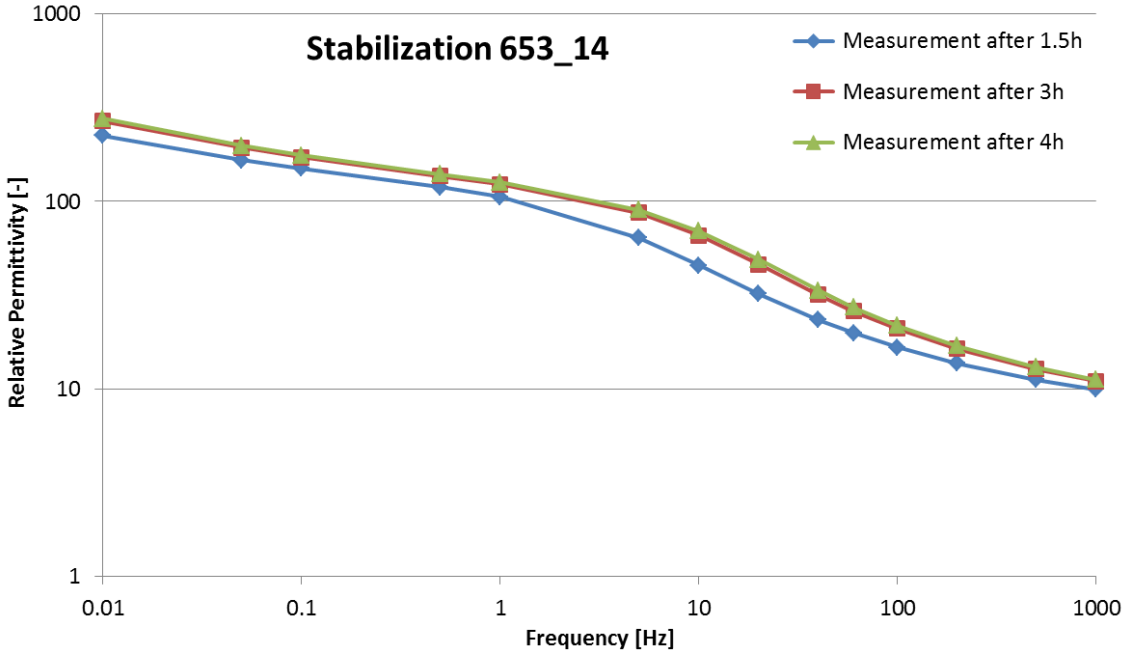

Figure 4.4. Stabilization of the HVOF sprayed sample at T=25°C, RH=40%.

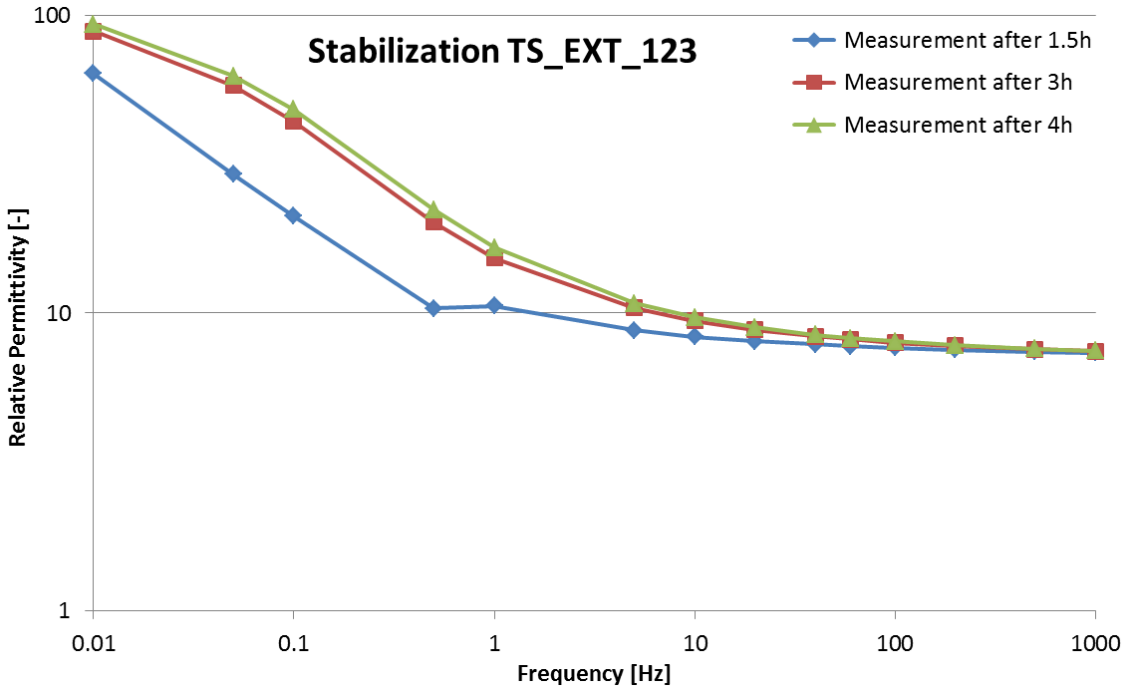

Figure 4.5. Stabilization of the flexicord sprayed sample at T=25°C, RH=40%.

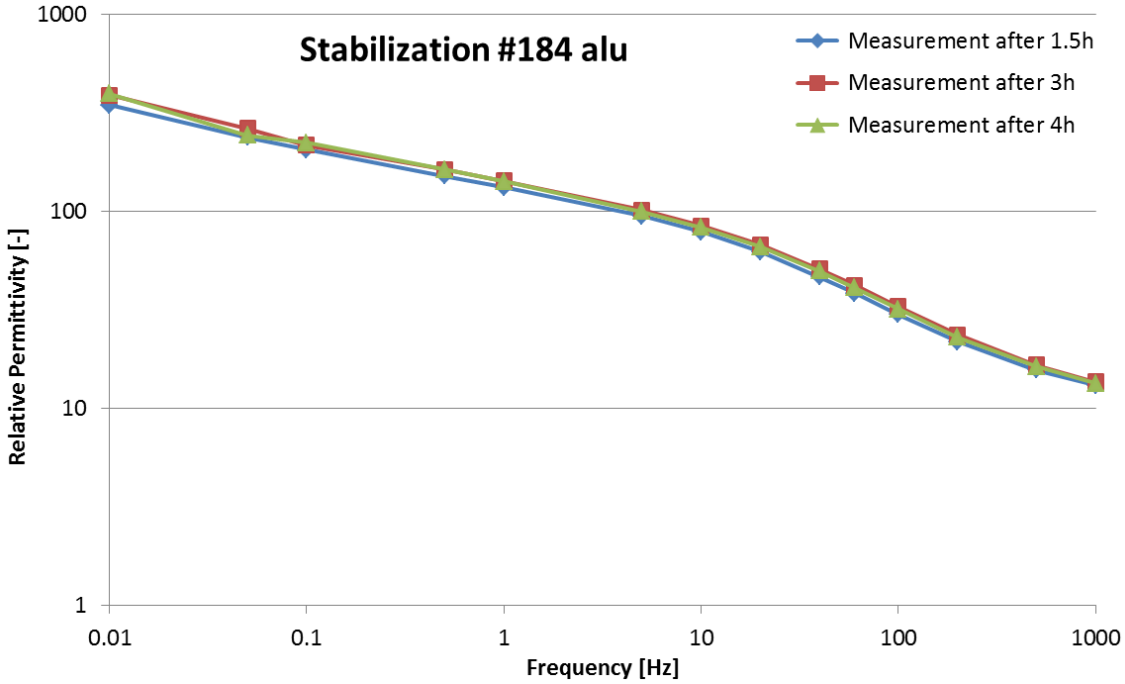

Figure 4.6. Stabilization of the plasma sprayed sample at T=25°C, RH=40%.

Every sample was measured three times at every condition. The electrodes were detached and re-attached before every measurement in order to eliminate coincidences due to the connection between the electrodes and the sample. The results shown in this thesis are the averages of those three measurements.

The measurements at temperatures below 100°C are performed inside the climate room of the high voltage laboratory of TUT. The climate room is designed as a Faraday cage, to prevent any influences of external fields.

4.3.2 Measurements above 100°C

At temperatures above 100°C, the stabilization behaviour of the second HVOF sprayed and the plasma sprayed sample were examined. For the HVOF sprayed sample, measurements were made at a temperature of 120°C, 150°C and 180°C. Because the aim of these measurements was to examine the evolution of the dielectric properties of the samples as a function of the heating time, when heated up to these temperatures for the first time, the HVOF sprayed sample was dried at a temperature of 105°C after the painting of the silver electrode on the coating. Because the plasma sprayed sample was also used in the earlier measurements and thereby heated up to a temperature of 120°C, the stabilization behaviour of the plasma sprayed sample was examined at a temperature of 150°C. These measurements were made at the same frequencies as the measurements below 100°C. The dielectric properties were measured after a heating period of 0, 0.5, 1, 2, 5, 7.5 and 10 hours. For the HVOF sprayed sample at a temperature of 150°C, there were also measurements made after a heating period of 23.5 and 25.5 hours.

The measurements above a temperature of 100°C were performed inside an oven, shown in Figure 4.7, placed inside the climate room of the high voltage laboratory of TUT. During the measurements the temperature of that climate room was 30°C at a relative humidity of 20%. Before placing the sample in the oven, the sample was stabilized in the conditions of the climate room. The measurements were started when the oven, with the sample in it, had reached the relevant temperature.

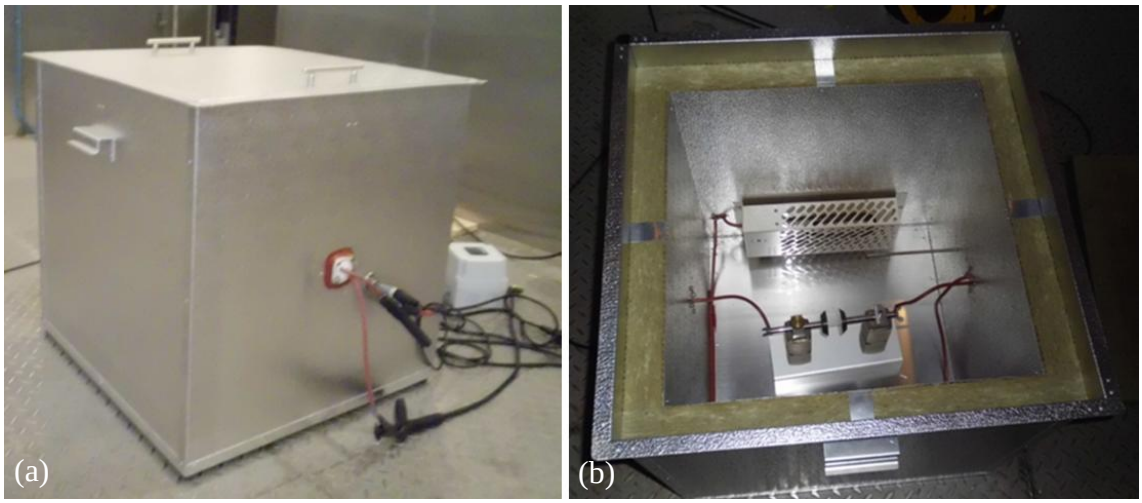

Figure 4.7. (a): the closed oven, (b): the electrode configuration placed in the oven.

4.4 Processing of acquired data

The values for R_a and C_a, the components of the equivalent circuit of a real dielectric as defined in Section 2.4.1, were measured by the IDA 200 measurement device. These values were used to calculate the relative permittivity and the loss index of the samples, according to standard *IEC 60250*. The *vacuum capacitance* C_0 of a sample is calculated by

$$C_0 = 0.06954 \frac{d_1^2}{h}, \tag{4-1}$$

whereby d_1 is the *diameter of the smallest electrode* and h is the *coating thickness*, as shown in Figure 4.8. The *correction factor for edge capacitance* C_e, is calculated by:

$$C_e = (0.041\varepsilon_1 - 0.077 \log h + 0.045)\pi d_1, \tag{4-2}$$

whereby ε_1 is an *approximate value of the relative permittivity* of the coating. The value for the relative permittivity at a frequency of 50 Hz has consistently been chosen as ε_1. The relative permittivity is calculated by:

$$\varepsilon_r = \frac{C_a - C_e}{C_0}. \tag{4-3}$$

The *dissipation factor tan* δ is calculated by:

$$\tan \delta = \frac{1}{R_a C_a \omega}. \tag{4-4}$$

The *loss index* ε'', proportional to the dielectric losses as proved in Section 2.4.2, is calculated by multiplying the relative permittivity and the dissipation factor:

$$\varepsilon'' = \varepsilon_r \tan \delta. \tag{4-5}$$

All the values were calculated using Microsoft Office Excel. [37]

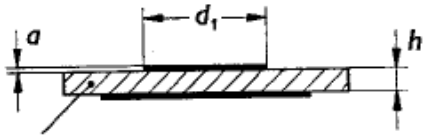

Figure 4.8. Measurement arrangement with unequal electrodes. [37]

5 MEASUREMENT RESULTS

5.1 Introduction

Based on the measurement results, the general observation is that both relative permittivity and loss index increase with decreasing frequency, increasing temperature and increasing relative humidity. The dependency on temperature and relative humidity can be seen in Table 5.1, Table 5.2 and Table 5.3, where the values for the relative permittivity of the different samples at a frequency of 50 Hz are shown for all measured conditions. In Section 5.2, these findings will be thoroughly discussed and the results for the different coating processes will be compared. In Section 5.3, the same observation will be made, but the evolution in function of the heating time at temperatures above 100°C will be studied.

Table 5.1. Relative permittivity of the ethylene-HVOF sprayed sample at 50 Hz.

	20°C	**30°C**	**40°C**	**50°C**	**60°C**	**70°C**
20%	10.4	11.9	13.9	17.0	20.3	25.9
35%	19.3	23.8	31.7	41.5	49.8	57.1
45%	28.8	38.3	48.2	57.1	68.5	92.6
60%	43.9	54.8	69.6	85.6	90.6	
75%	52.5	56.1	63.2	76.9	78.5	
90%	56.8	71.5				

Table 5.2. Relative permittivity of the flexicord sprayed sample at 50 Hz.

	20°C	**30°C**	**40°C**	**50°C**	**60°C**	**70°C**
20%	7.4	7.5	7.5	7.6	7.7	7.9
35%	7.6	7.8	8.0	8.2	8.4	10.0
45%	8.0	8.5	9.3	10.6	13.0	15.6
60%	10.5	13.0	18.2	25.3	31.3	
75%	23.1	27.1	36.5	48.2	54.6	
90%	43.8	43.4				

Table 5.3. Relative permittivity of the atmospheric plasma sprayed sample at 50 Hz.

	20°C	**30°C**	**40°C**	**50°C**	**60°C**	**70°C**
20%	13.4	14.7	18.4	23.6	29.2	36.1
35%	27.3	33.6	45.4	54.7	57.8	77.6
45%	36.2	48.1	59.4	68.5	73.9	92.6
60%	48.4	53.5	68.3	81.0	81.5	
75%	44.1	51.2	61.9	79.6	77.3	
90%	65.1	81.2				

5.2 Measurements below 100°C

5.2.1 Constant temperature, variating relative humidity

HVOF sprayed sample

Figure 5.1 depicts the relative permittivity of sample 653_14, with the ethylene-HVOF sprayed coating, at a temperature of 20°C as a function of the frequency for all measured degrees of relative humidity. It is shown that the relative permittivity generally decreases with increasing frequency and decreasing relative humidity. In Appendix A, figures presenting the relation between the relative permittivity and the relative humidity are shown for all samples at 0.01 Hz, 50 Hz and 1000Hz.

Measurements performed at higher temperatures show higher values for the relative permittivity. This can be seen by comparing Figure 5.1 with the results of the measurements made at 50°C and 70°C, respectively shown in Figure 5.3 and Figure 5.5.

With reference to the results shown in Figure 5.1, it can be noticed that at 20°C, in the relative humidity range from 20% to 60%, the relative permittivity steadily increases with decreasing frequency. At higher humidities, the increase is stronger for frequencies below 5 Hz. At 50°C, the strong increase in relative permittivity at the lower frequencies is also observed at a relative humidity of 60%. The measurements performed at 70°C already show such an increase in relative permittivity at a relative humidity of 45% for frequencies below 0.1 Hz.

In the results of the measurements performed at 20°C and 50°C, it can be observed that the increase in relative permittivity stabilizes at frequencies higher than 10 Hz, even though the relative humidity increases. At 70°C no clear stabilization is noticeable, but it should be noted that the values for the relative permittivity whereat the stabilization occurred at 20°C and 50°C were only reached at a relative humidity of 45% in these measurements.

The loss index of the HVOF sprayed sample at a temperature of 20°C is shown in Figure 5.2. The evolution of the loss index is comparable to the evolution of the relative permittivity. Generally, the loss index decreases with increasing frequency and with decreasing relative humidity. In Appendix A, figures presenting the relation between the loss index and the relative humidity are shown for all samples at 0.01 Hz, 50 Hz and 1000 Hz.

By comparing Figure 5.2 with Figure 5.4 and Figure 5.6, the measurements of the loss index at 50°C and 70°C respectively, an increase in loss index with increasing temperature is observed. There tends to be a linear relation between the relative permittivity and the frequency at higher humidities. At a temperature of 20°C, the measurements at a relative humidity of 75% and 90% show such a behaviour. In the results of the measurements made at a temperature of 50°C, this behaviour is extended to a relative humidity of 60%.

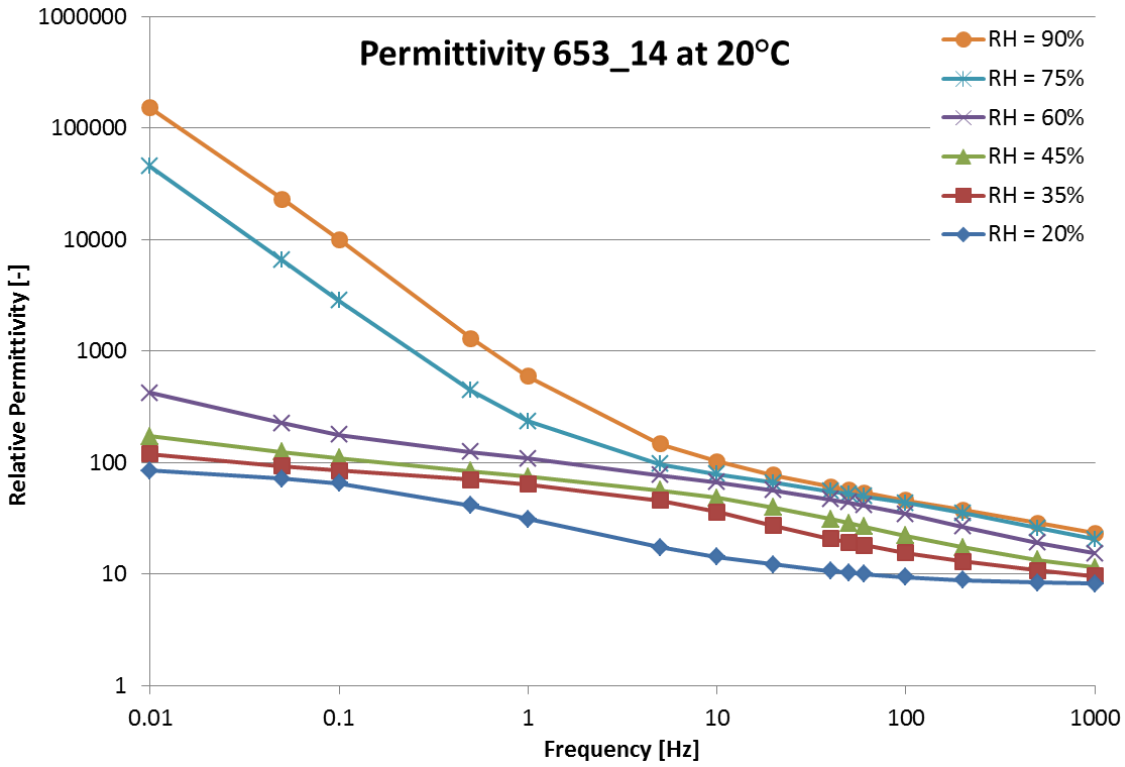

Figure 5.1. Relative permittivity of sample 653_14 at a temperature of 20°C.

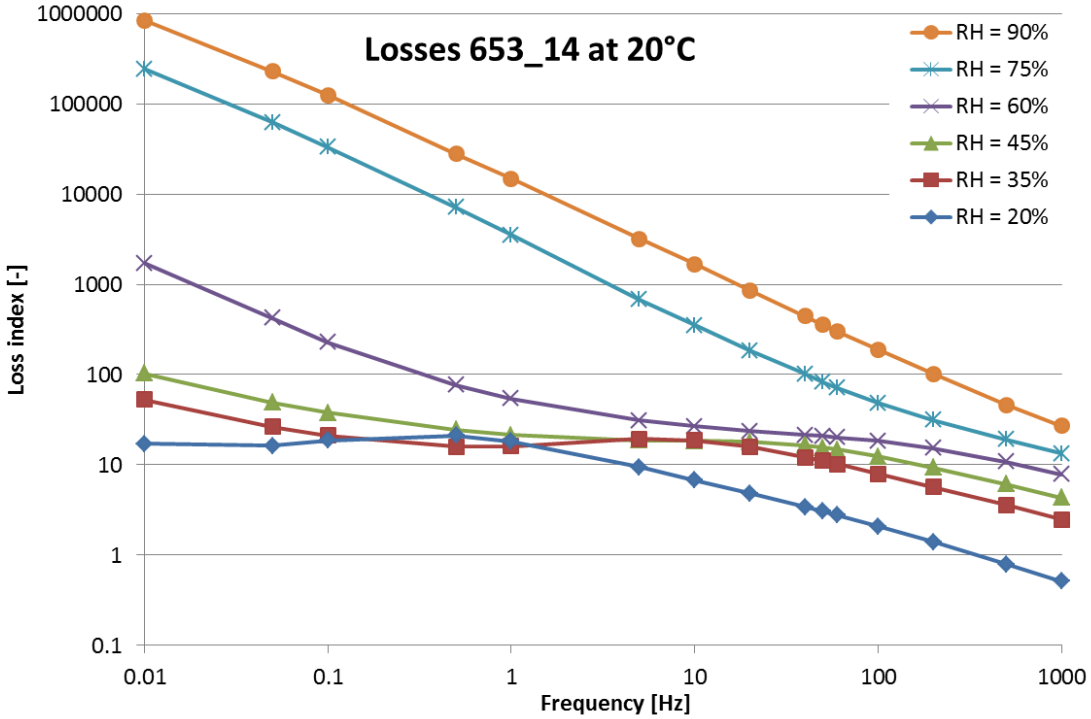

Figure 5.2. Loss index of sample 653_14 at a temperature of 20°C.

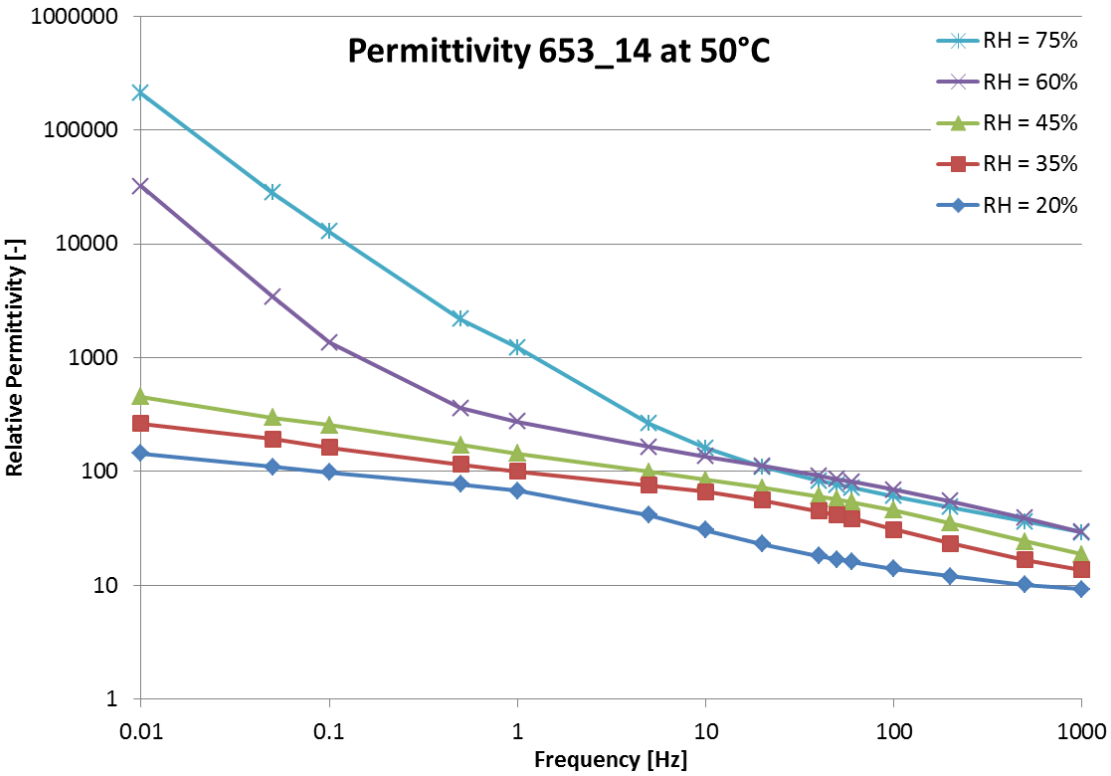

Figure 5.3. Relative permittivity of sample 653_14 at a temperature of 50°C.

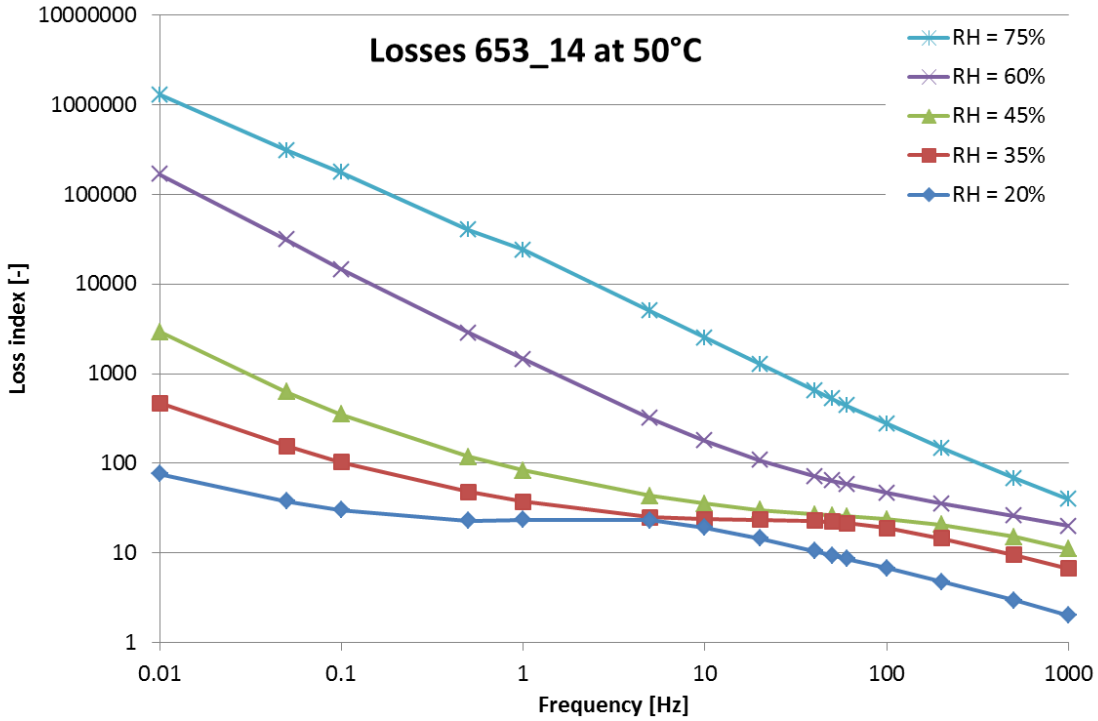

Figure 5.4. Loss index of sample 653_14 at a temperature of 50°C.

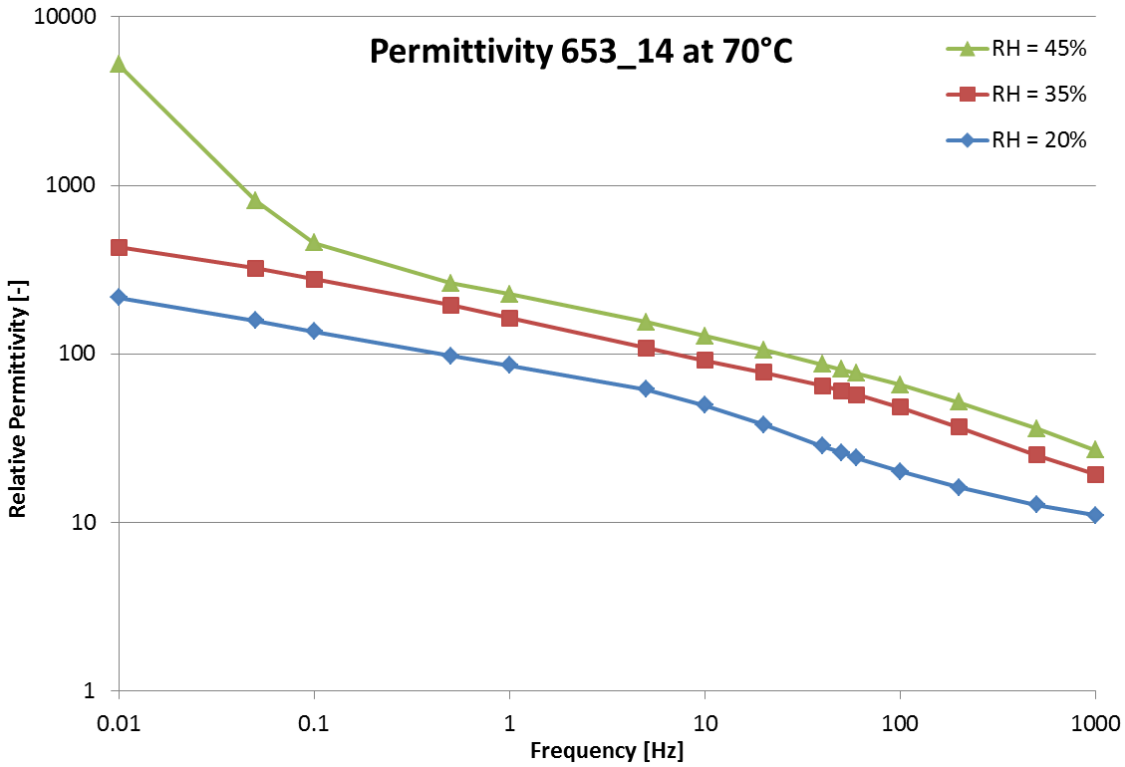

Figure 5.5. Permittivity of sample 653_14 at a temperature of 70°C.

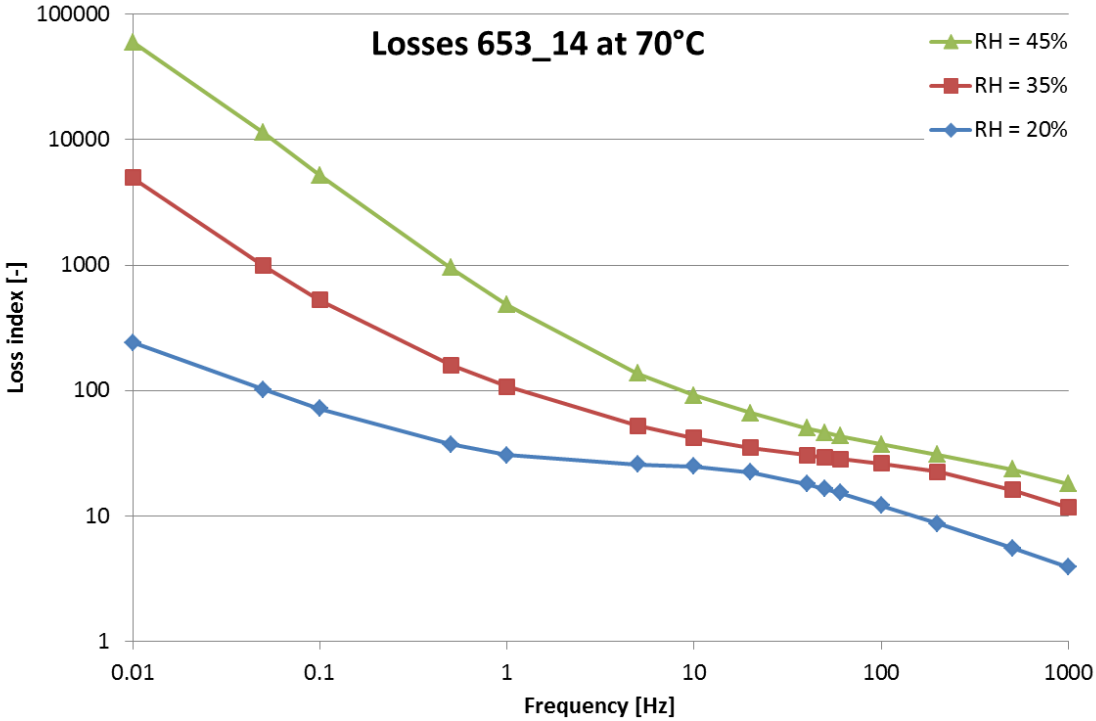

Figure 5.6. Loss index of sample 653_14 at a temperature of 70°C.

Flexicord sprayed sample

In Figure 5.7, the relative permittivity of sample TS_EXT_123, with the flexicord sprayed coating, is shown at a temperature of 50°C. It can be observed that this sample shows a similar behaviour as the HVOF sprayed sample at the same conditions. However, the values for the relative permittivity are notably lower.

There are two differences between both samples regarding the relation between the relative permittivity and the frequency. First, at a relative humidity of 60% the increase in relative permittivity with decreasing frequency is less severe for the flexicord sprayed sample. However, the increase at a relative humidity of 75% is similar. A second difference is the relative permittivity at lower frequencies. In Figure 5.3, a stabilization of the relative permittivity at higher frequencies was noticed for the HVOF sprayed sample. With the flexicord sample there appears to be no such stabilization, but it should be noted that the values whereat the stabilization occurred in the HVOF sprayed sample, were not reached in these measurements.

Figure 5.8 depicts the loss index for the flexicord sprayed sample. It appears that also the measured values of the loss index of this sample are notably lower than the values measured for the HVOF sample. In the measurements of the HVOF sprayed sample, a linear relation between the loss index and the frequency was observed. A similar observation can be made of the flexicord sprayed sample, the main difference is that the measurements at a relative humidity of 60% only show that linear relation at frequencies below 1 Hz.

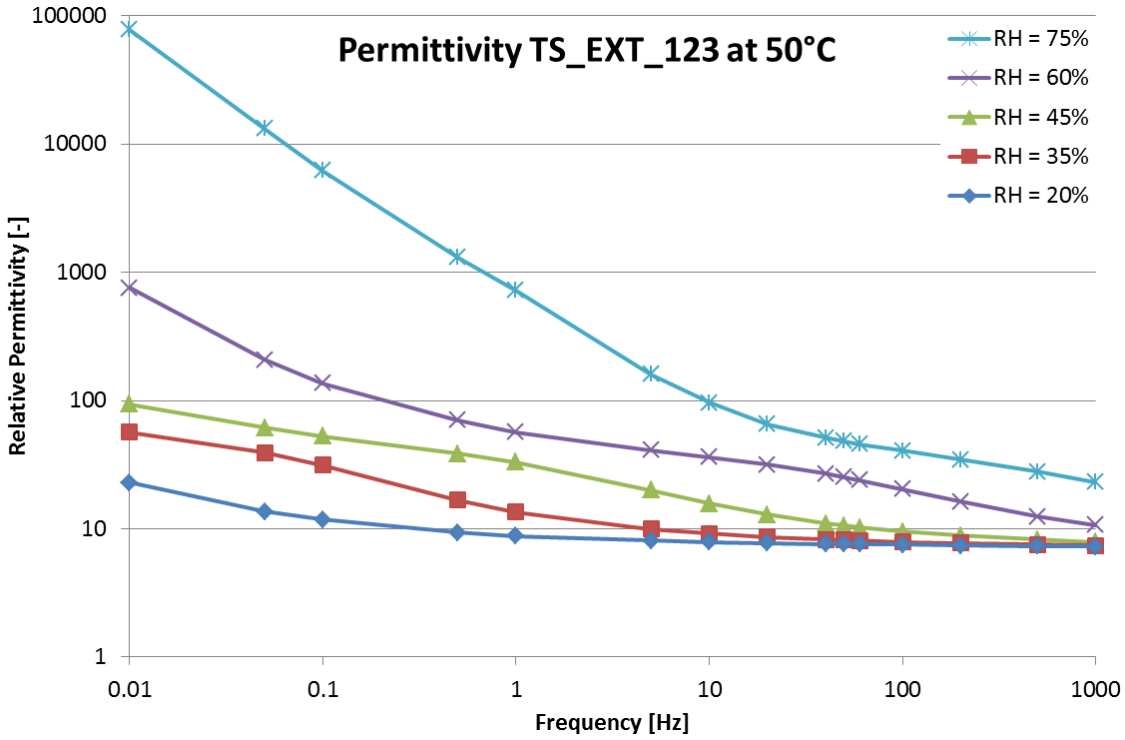

Figure 5.7. Relative permittivity of sample TS_EXT_123 at a temperature of 50°C.

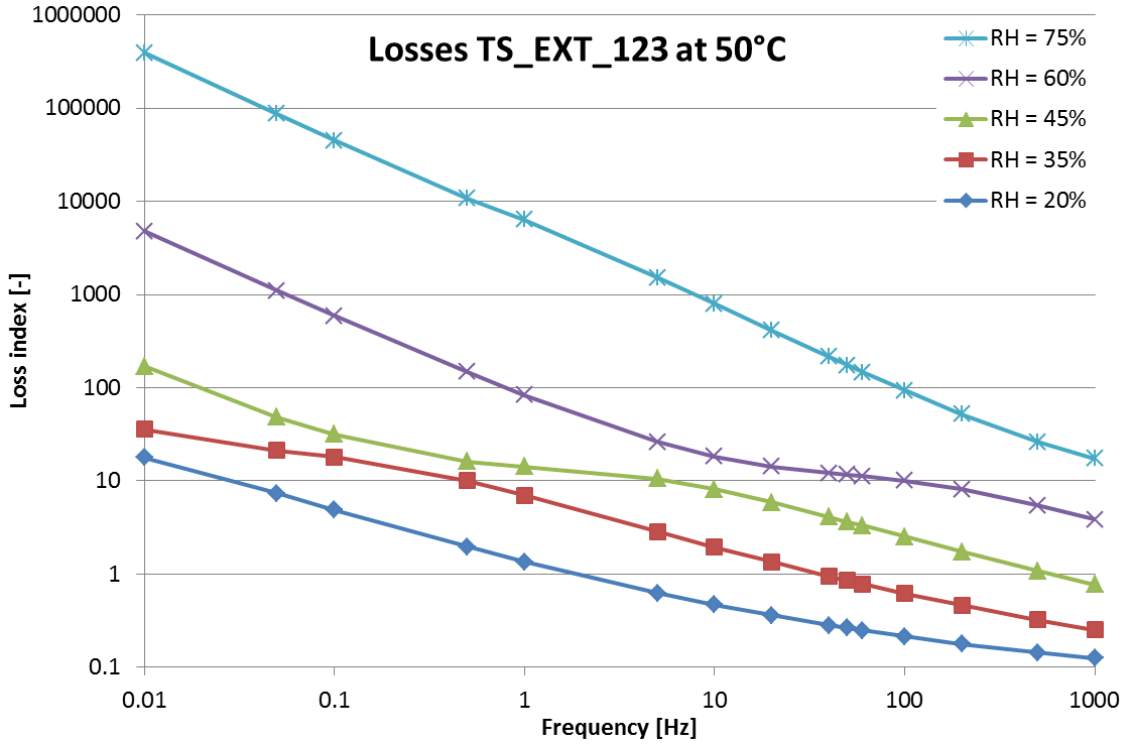

Figure 5.8. Loss index of sample TS_EXT_123 at a temperature of 50°C.

Plasma sprayed sample

In Figure 5.9, the relative permittivity of sample #184 alu, with the atmospheric plasma sprayed coating, is shown at a temperature of 50°C. In these measurement results, it can also be observed that the relative permittivity decreases with decreasing humidity and increasing frequency. The values of the relative permittivity are in general slightly higher than the values measured in the HVOF sprayed sample under the same circumstances.

Also in the measurement results of the plasma sprayed sample, a clear increase in permittivity with decreasing frequency can be seen at lower frequencies. This phenomenon can be observed in the measurements made at a relative humidity of 60% and 75%, but also, although a less severe increase, at a relative humidity of 45%. At lower frequencies, the relative permittivity tends to stabilize around the same value as observed in the HVOF sprayed sample.

The measured loss index of the plasma sprayed sample is shown in Figure 5.10. By comparing Figure 5.4 with Figure 5.10, it appears that the loss index measured in the plasma sprayed sample is slightly higher than the loss index measured in the HVOF sprayed sample. In the plasma sprayed sample, the relation between the loss index and the frequency is linear for the measurements performed at a relative humidity of 75% and 90%. At frequencies below 10 Hz, the measurements made at a relative humidity of 45% have also this linear relation.

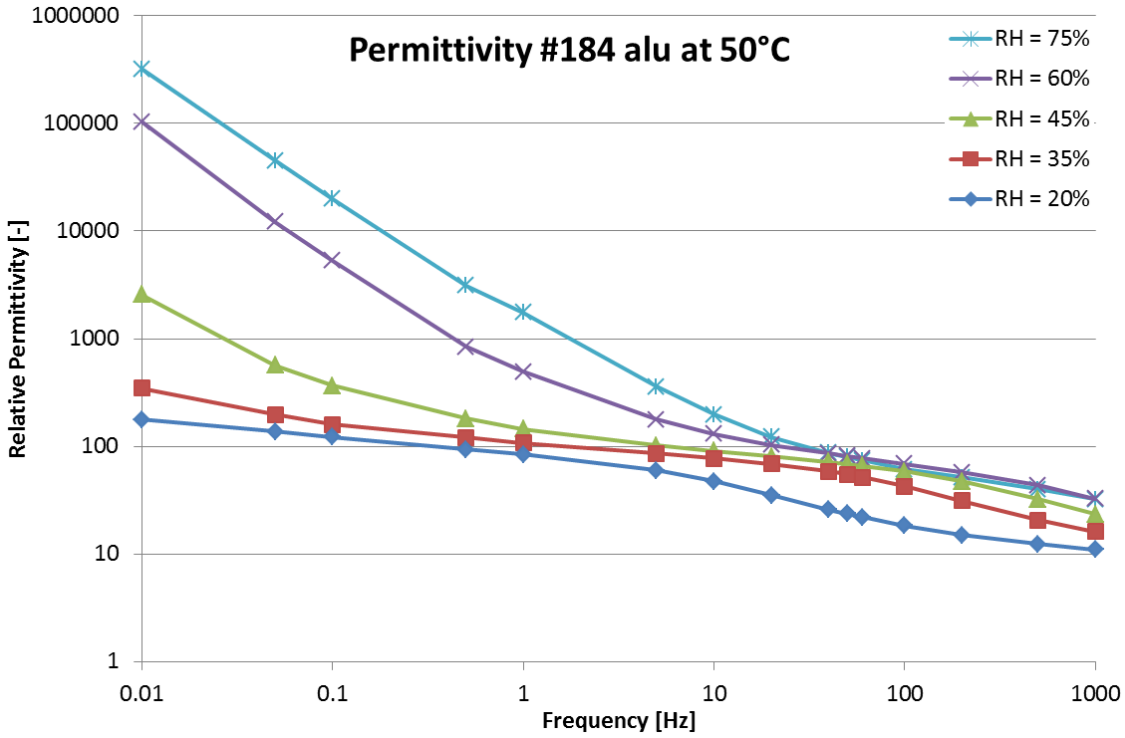

Figure 5.9. Relative permittivity of sample #184 alu at a temperature of 50°C.

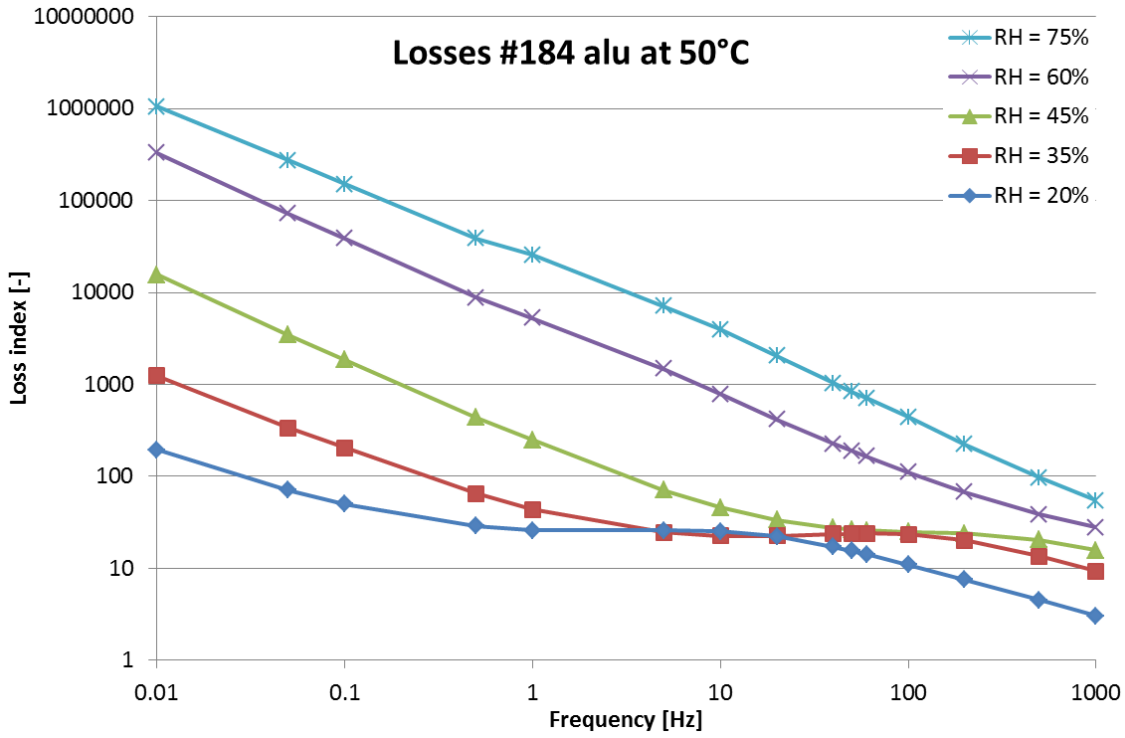

Figure 5.10. Loss index of sample #184 alu at a temperature of 50°C.

5.2.2 Constant relative humidity, variating temperature

HVOF sprayed sample

In Figure 5.11, the relative permittivity of sample 653_14, with the ethylene-HVOF sprayed coating, is shown at a relative humidity of 20% as a function of the frequency at all measured temperatures. It can be seen that the relative permittivity decreases with increasing frequency and decreasing temperature. In Appendix B, figures presenting the relation between the relative permittivity and the temperature are shown for all samples at 0.01 Hz, 50 Hz and 1000Hz.

By comparing this figure with Figure 5.13 and Figure 5.15, the results of the measurements at a relative humidity of 45% and 75% respectively, it is shown that the relative permittivity increases with increasing temperature. This was also concluded in Section 5.2.1.

In Figure 5.11, it can be seen that at a relative humidity of 20%, the relative permittivity steadily increases with decreasing frequency. The results of the measurements performed at a relative humidity of 45% show that the measurements at a temperature of 70°C tend to have a stronger increase in relative permittivity at the lowest frequencies. Figure 5.15 illustrates that at a relative humidity of 75%, the increase in relative permittivity with decreasing frequency is strong in all measured temperatures in the whole frequency range.

The loss index of the HVOF sprayed sample at a relative humidity of 20% is shown in Figure 5.12. It can be seen that also the loss index generally decreases with increasing frequency and with decreasing temperature. In Appendix B, figures presenting the relation between the loss index and the temperature are shown for all samples at 0.01 Hz, 50 Hz and 1000Hz.

By comparing these measurements with the measurements made at a relative humidity of 45% and 75%, respectively Figure 5.14 and Figure 5.16, it can be observed that the loss index strongly increases with increasing relative humidity. This was also noted in Section 5.2.1.

In Figure 5.12, it is shown that at a relative humidity of 20%, there is for each temperature a certain frequency range in which the losses are stable, even though the permittivity is not. It can be observed that that frequency-range shifts to higher frequencies with increasing temperature. By comparing Figure 5.12 with Figure 5.14, it can be seen that the frequency range whereat the loss index is stable shifts also to higher frequencies with increasing relative humidity. At a relative humidity of 75%, there is no such frequency range noticeable.

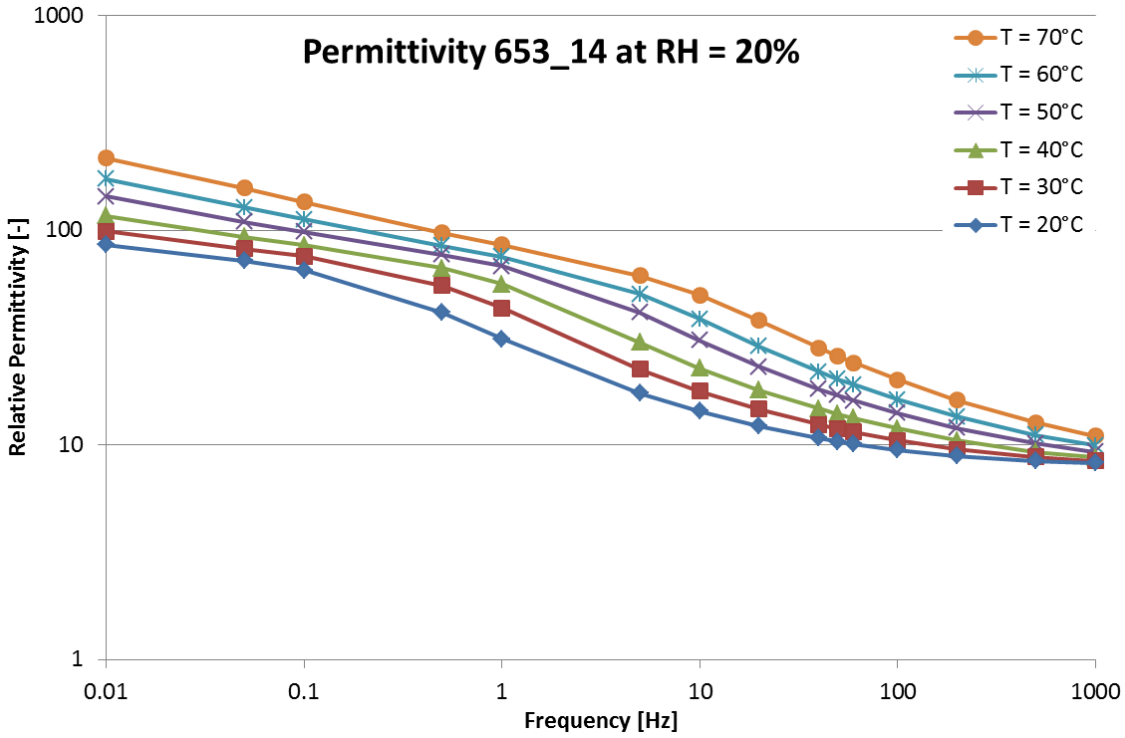

Figure 5.11. Relative permittivity of sample 653_14 at relative humidity of 20%.

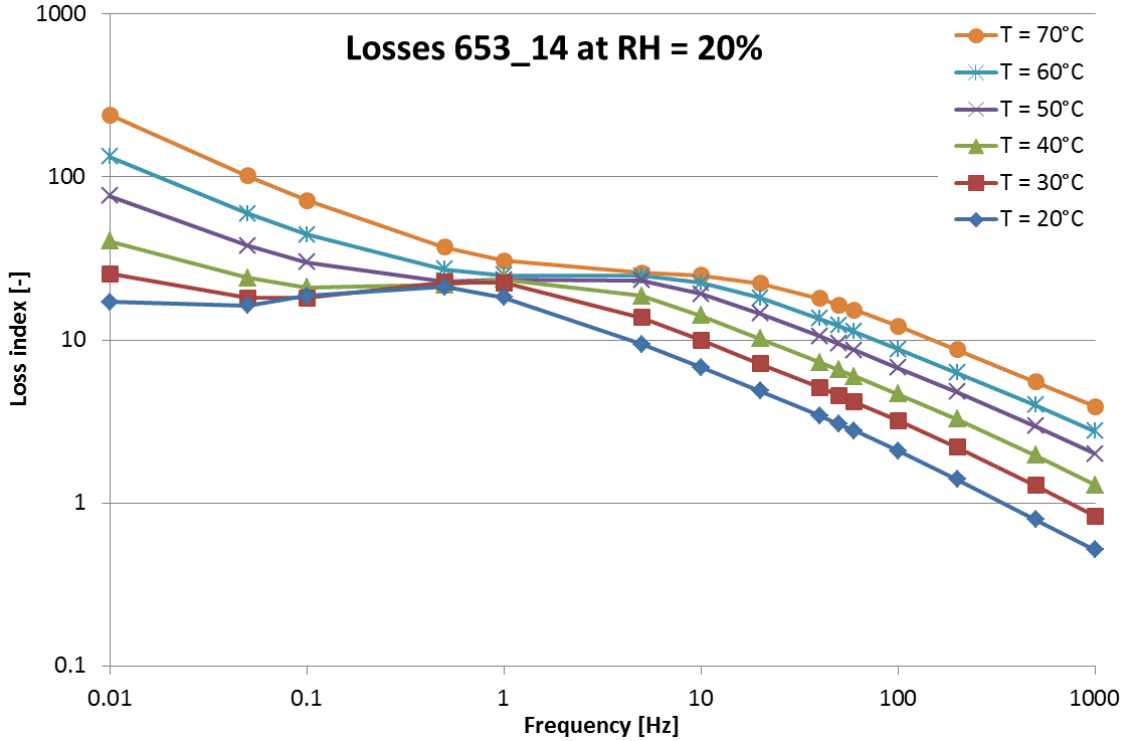

Figure 5.12. Loss index of sample 653_14 at a relative humidity of 20%.

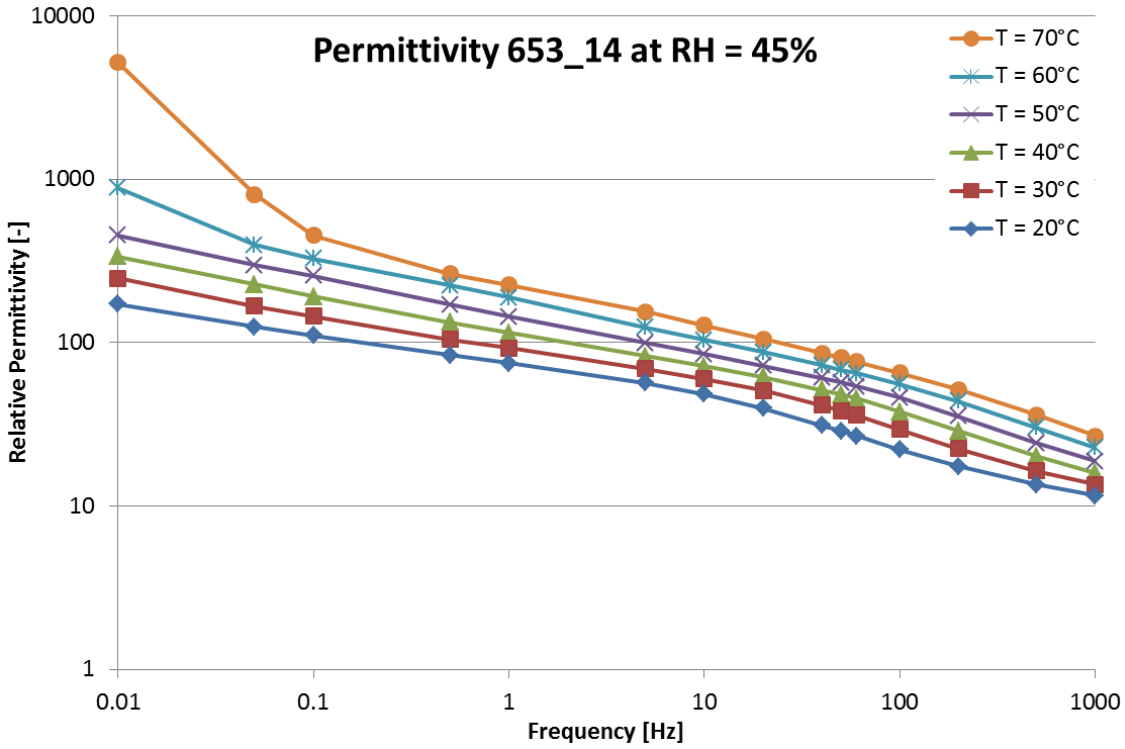

Figure 5.13. Relative permittivity of sample 653_14 at relative humidity of 45%.

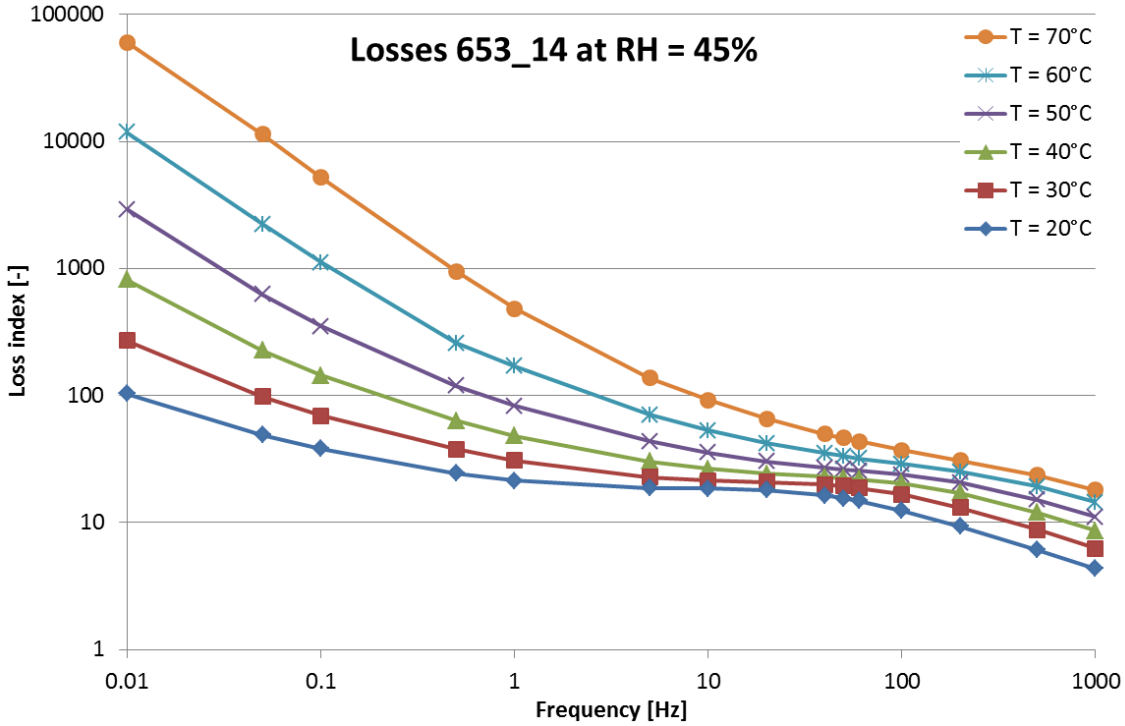

Figure 5.14. Loss index of sample 653_14 at a relative humidity of 45%.

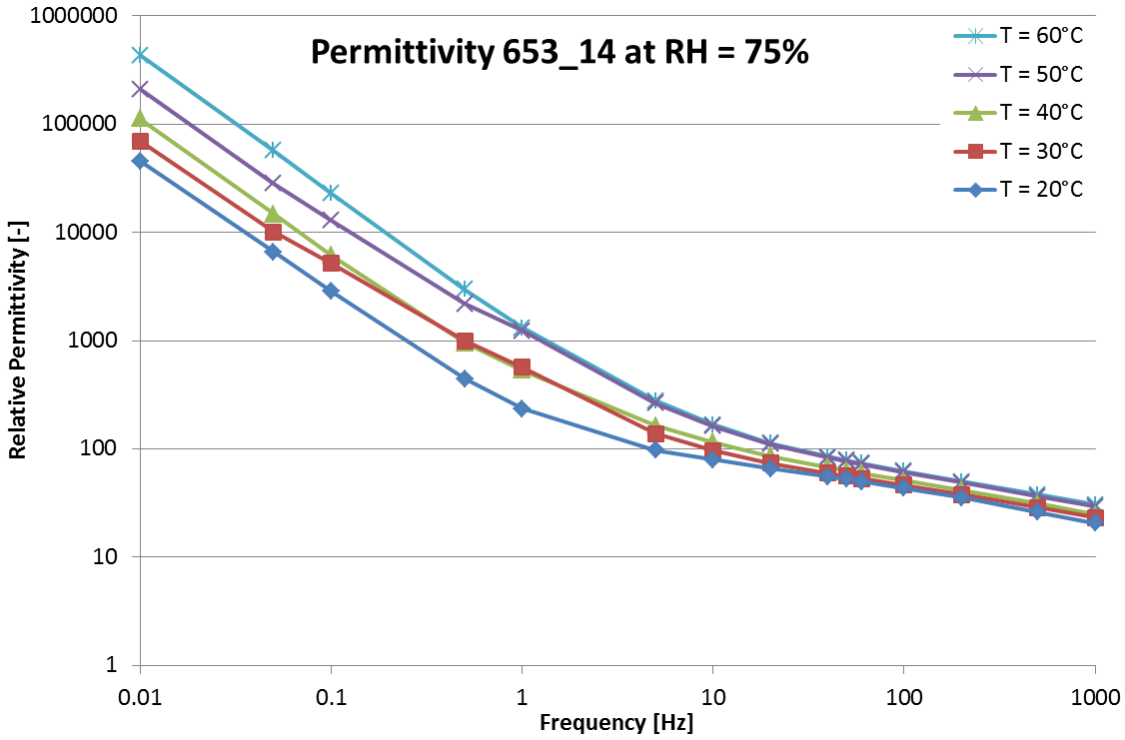

Figure 5.15. Relative permittivity of sample 653_14 at relative humidity of 75%.

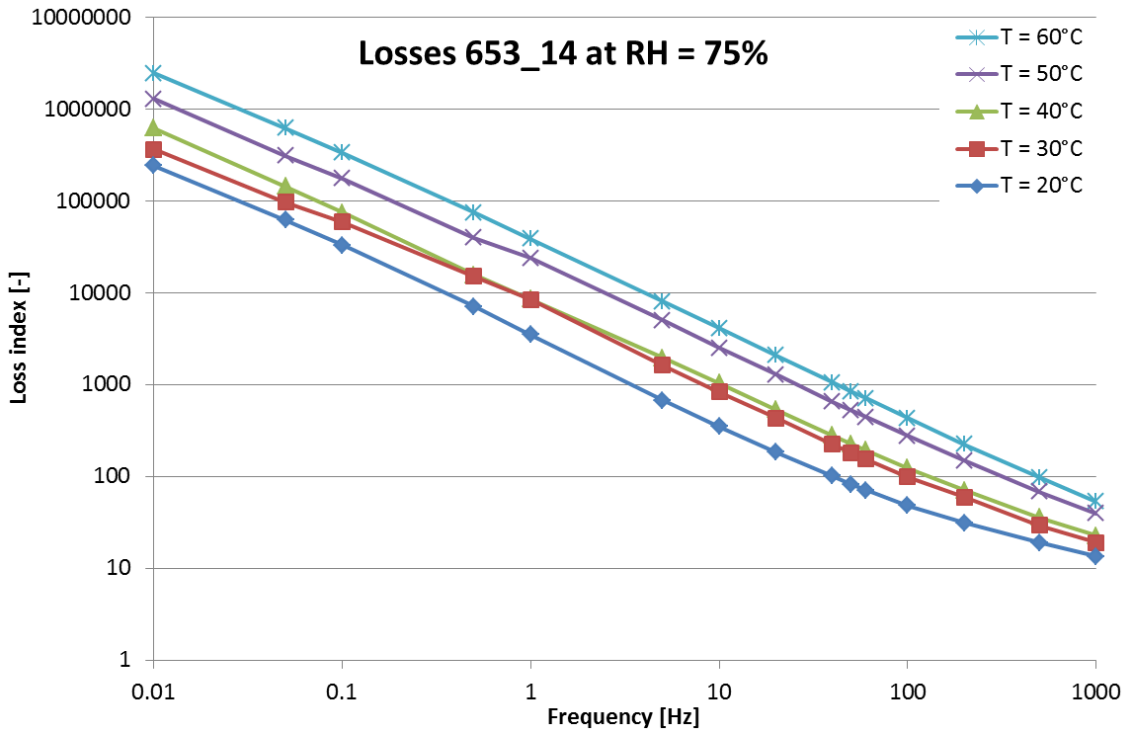

Figure 5.16. Loss index of sample 653_14 at a relative humidity of 75%.

Flexicord sprayed sample

The relative permittivity of the flexicord sprayed coating at a relative humidity of 45% is shown in Figure 5.17. These measurement results are very similar to the measurement results of the HVOF sprayed coating made at a relative humidity of 20%. Hence, the relative permittivity of the flexicord sprayed sample at a relative humidity of 45% is remarkably lower than the relative permittivity of the HVOF sprayed sample under the same circumstances.

Figure 5.18 depicts the loss index of the flexicord sprayed sample at a relative humidity of 45%. By comparing this figure with Figure 5.14, it can be observed that also the loss index of the flexicord sprayed sample is remarkably lower than the loss index of the HVOF sprayed sample at the same conditions.

In the measurements of the HVOF sprayed sample, a frequency range in which the loss index was more or less stable was observed at a relative humidity of 45%. The same observation can be made in the measurements of the flexicord sprayed sample. By comparing these two measurement results, a shift of the relevant frequency range to lower frequencies for the flexicord sprayed sample can be observed.

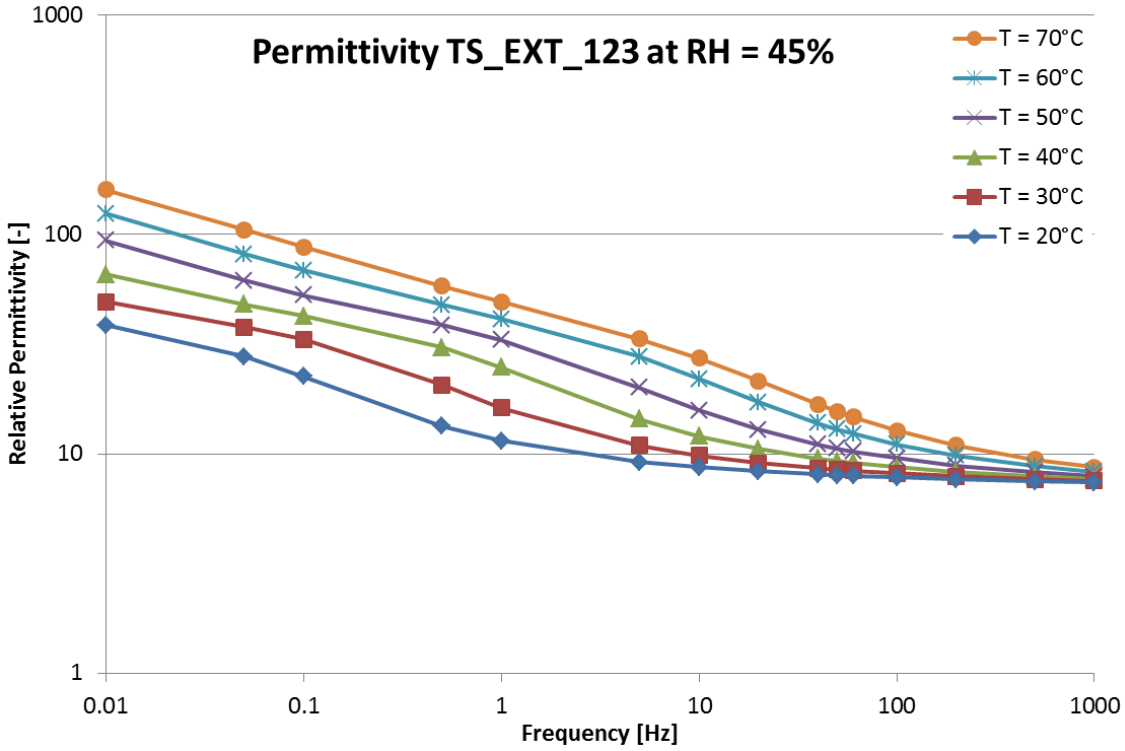

Figure 5.17. Relative permittivity of sample TS_EXT_123 at relative humidity of 45%.

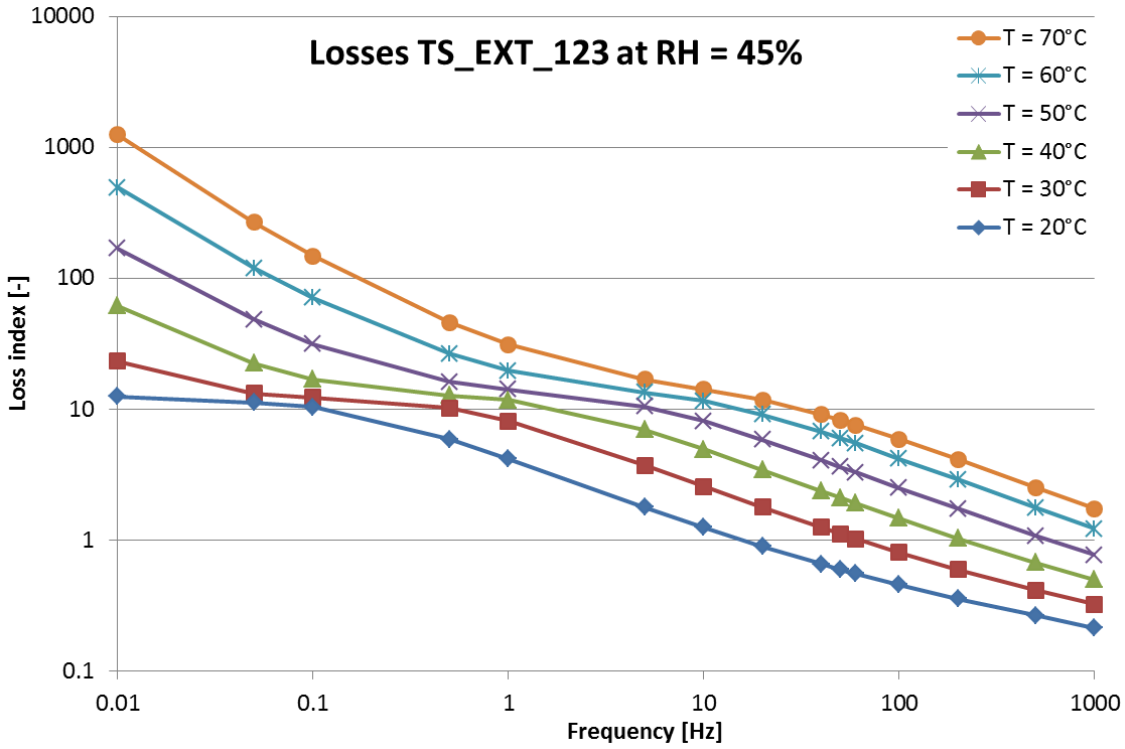

Figure 5.18. Loss index of sample TS_EXT_123 at a relative humidity of 45%.

Plasma sprayed sample

In Figure 5.19, the relative permittivity of the atmospheric plasma sprayed coating is shown at a relative humidity of 45%. By comparing Figure 5.13 with Figure 5.19, it can be observed that the increase in relative permittivity with increasing temperature at lower frequencies is stronger in the plasma sprayed sample than in the HVOF sprayed sample.

The loss index of the plasma sprayed coating is depicted in Figure 5.20. It is observed that the loss index is generally higher than the loss index observed in the other coatings. Also in this sample, there is a frequency range in which the loss index is more or less stable. That frequency range is about the same as observed in the HVOF sprayed sample.

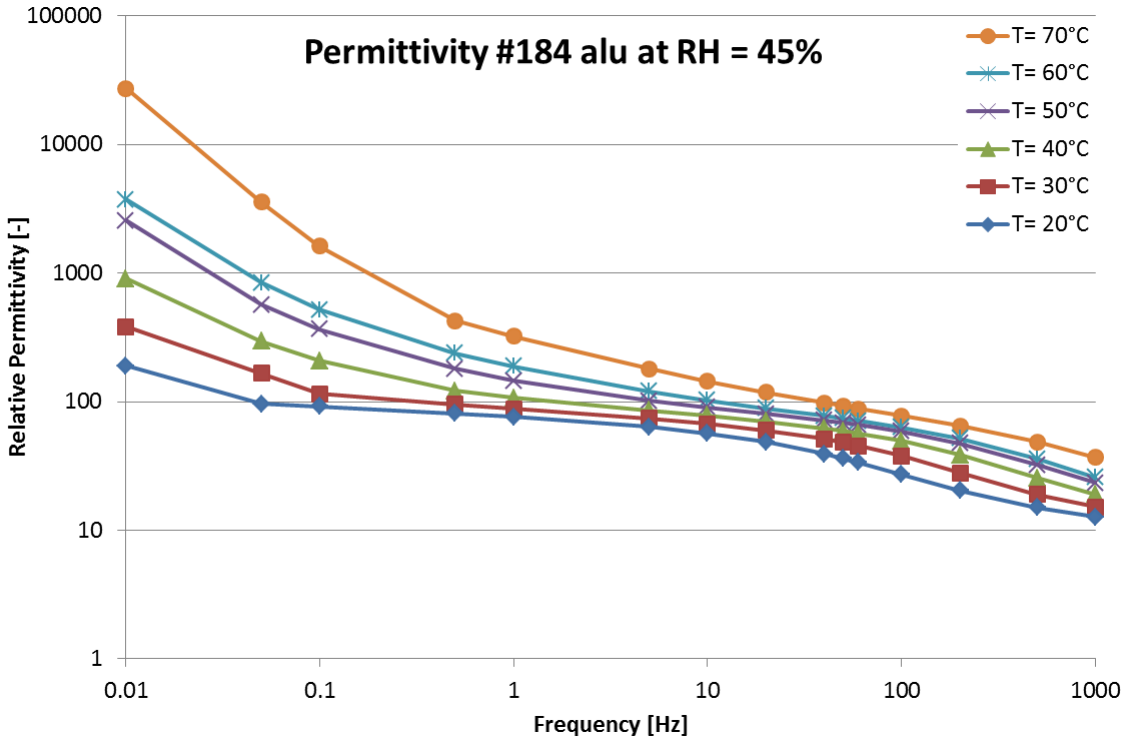

Figure 5.19. Relative permittivity of sample #184 alu at relative humidity of 45%.

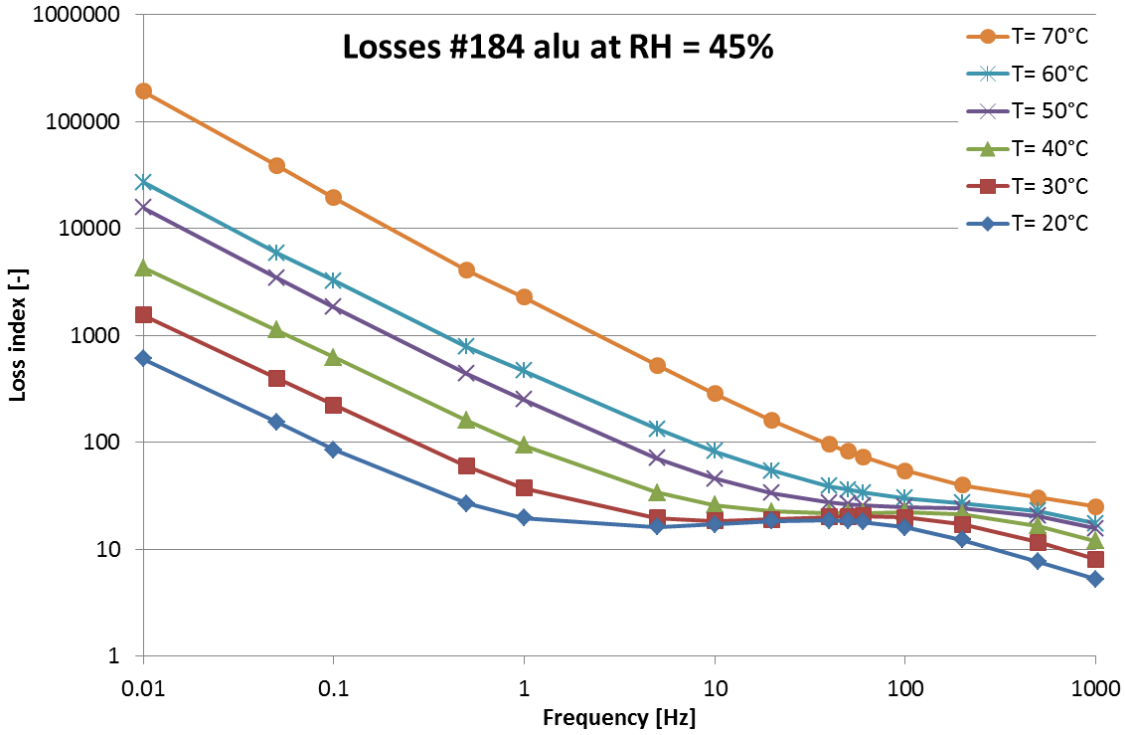

Figure 5.20. Loss index of sample #184 alu at a relative humidity of 45%.

5.2.3 Comparison of studied samples

In this section, the different samples are compared under four different circumstances. These circumstances are chosen because they show the evolution of the mutual relation between the different samples, starting at the lowest temperature and the lowest relative humidity, increasing to the most demanding conditions. By observing the results shown in Section 5.2.1 and Section 5.2.2, it can be observed that the measured values are particularly influenced by differences in relative humidity. Therefore, the relative humidity is mostly referred to when comparing the samples.

Figure 5.21 compares the relative permittivity of the different samples at a relative humidity of 20% and a temperature of 20°C. In these conditions, the relative permittivity of the plasma sprayed sample, #184 alu, is the highest at each frequency. The curve of the ethylene-HVOF sprayed sample, 653_14, has the same form as the curve of the plasma sprayed sample, but the relative permittivity is slightly lower at each frequency. The relative permittivity of the flexicord sprayed sample, TS_EXT_123, is the lowest at all frequencies. Because of the flatness of the latter curve, the difference in relative permittivity is larger at the lower frequencies.

The comparison of the loss index of the different samples in these conditions is depicted in Figure 5.22. The relation between the loss indexes of the different samples is similar to the relation observed between the relative permittivities. The only differences are the less flatness of the curve of the flexicord sprayed sample and the similar values for the HVOF and plasma sprayed samples at a frequency of 0.1 Hz and 0.5 Hz.

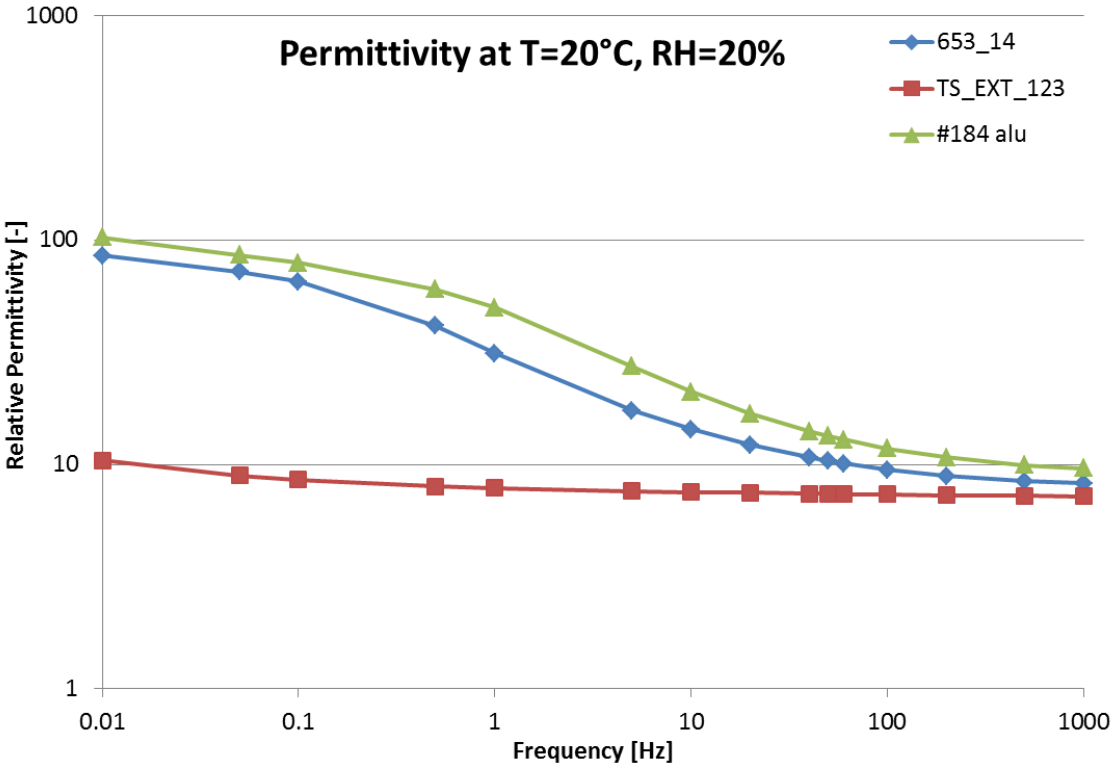

Figure 5.21. Comparison of the relative permittivity at T=20°C and RH=20%.

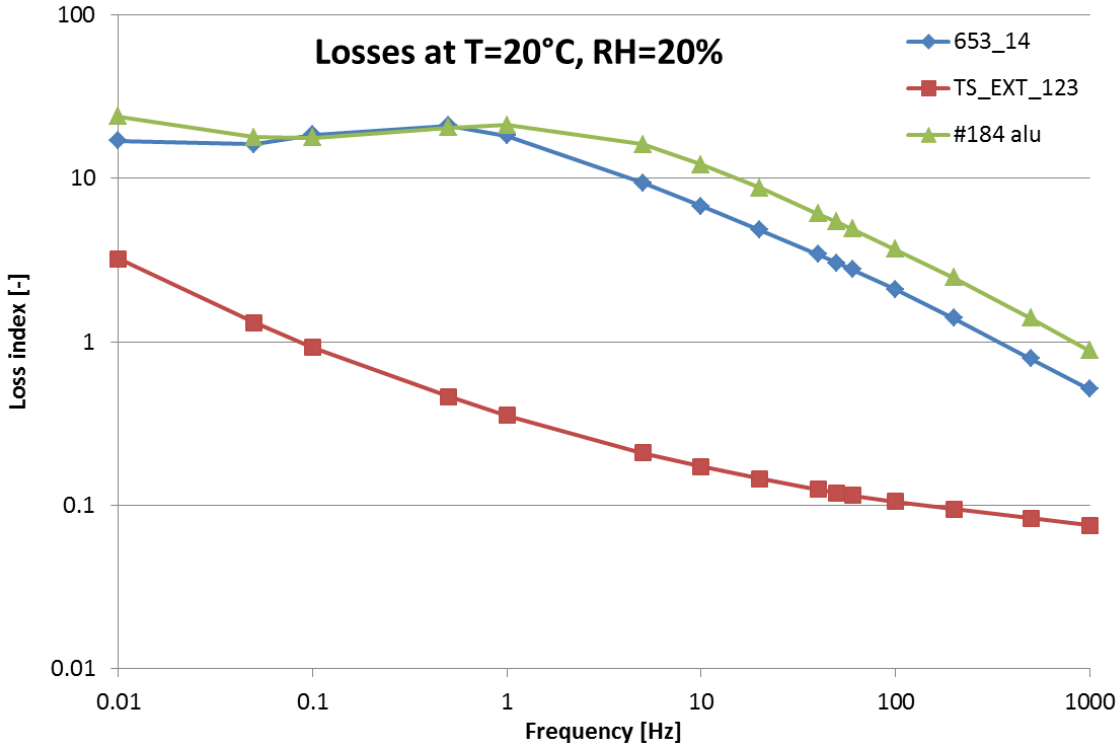

Figure 5.22. Comparison of the loss index at T=20°C and RH=20%.

In Figure 5.23, the relative permittivity of the different samples is shown at a relative humidity of 45% and a temperature of 40°C. Figure 5.24 depicts the relative permittivity of the samples at a relative humidity of 75% and a temperature of 30°C. The relative permittivity of the samples at a humidity of 90% and a temperature of 30°C is shown in Figure 5.25. By comparing these figures with Figure 5.21, the evolution of the three samples to more demanding conditions can be observed.

It appears that at a relative humidity of 45%, the difference in relative permittivity between the plasma sprayed and the HVOF sprayed sample is reduced at the higher frequencies. At the lower frequencies, the plasma sprayed sample shows a more strong increase in relative permittivity with increasing frequency, compared to the other samples. At a relative humidity of 75% or higher, the HVOF sprayed sample shows the same increase in relative permittivity at the lower frequencies. Therefore the HVOF sprayed and the plasma sprayed sample have a similar relative permittivity under these circumstances. It can be seen that the difference between these two samples and the flexicord sprayed sample is reduced with increasing relative humidity. At a relative humidity of 90%, the three samples have the same relative permittivity in the frequency range from 1 Hz to 10 Hz. At the other frequencies, the flexicord sprayed sample has a slightly lower relative permittivity compared to the other two samples.

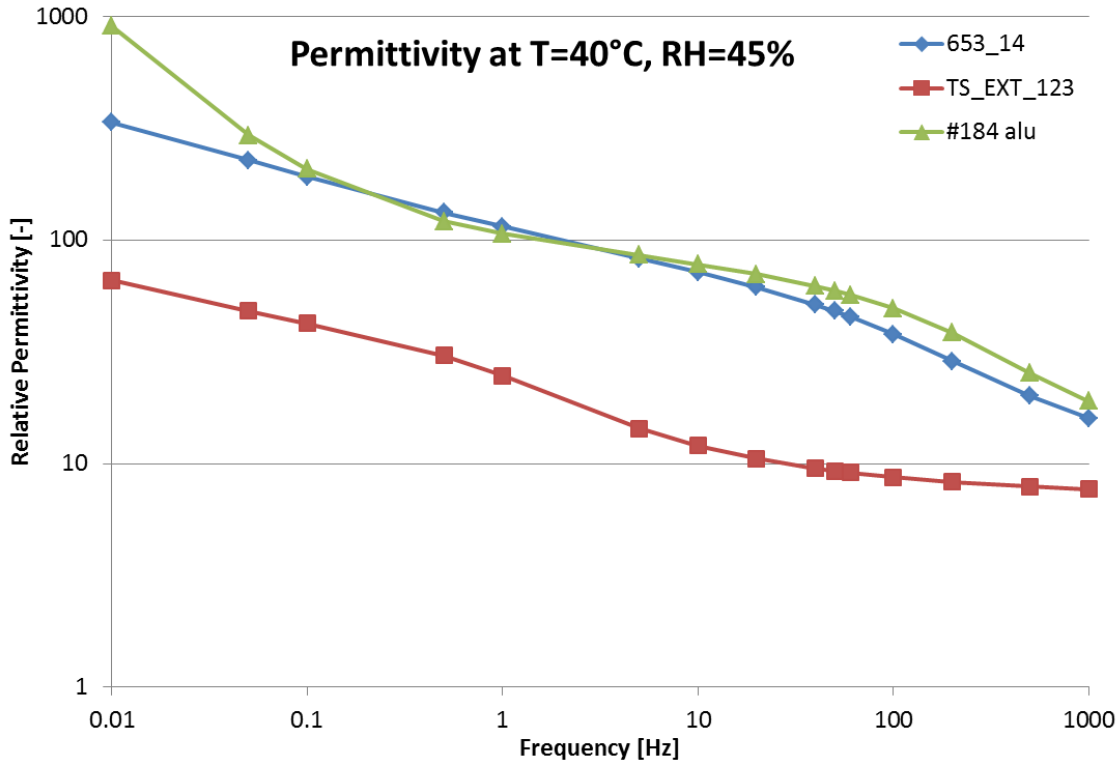

Figure 5.23. Comparison of the relative permittivity at T=40°C and RH=45%.

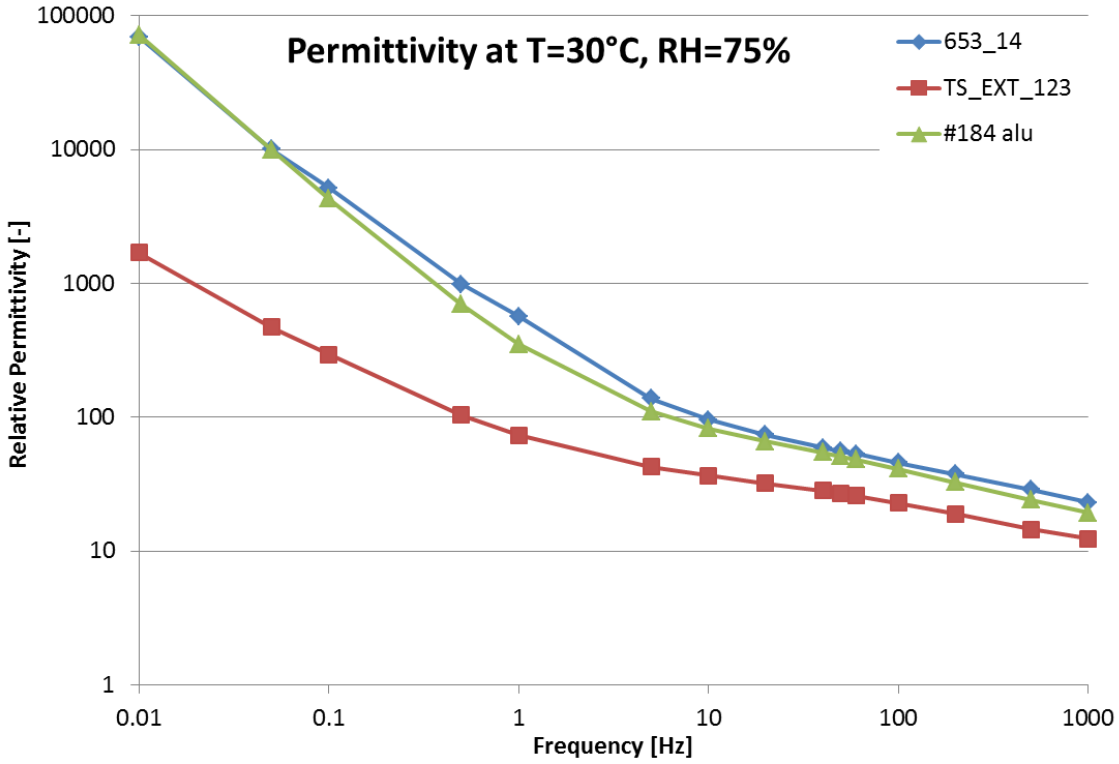

Figure 5.24. Comparison of the relative permittivity at T=30°C and RH=75%.

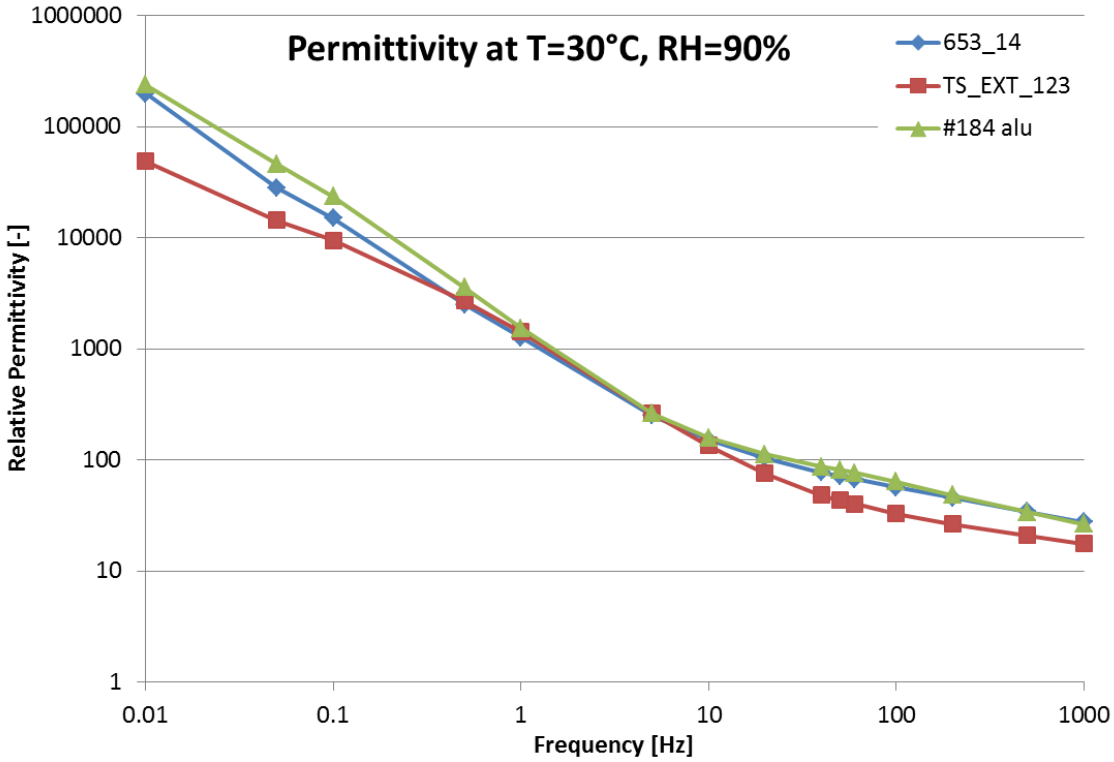

Figure 5.25. Comparison of the relative permittivity at T=30°C and RH=90%.

The loss index of the different samples at a relative humidity of 45% and a temperature of 40°C is depicted in Figure 5.26. In Figure 5.27 the comparison of the loss indexes at a relative humidity of 75% and a temperature of 30°C is shown. Figure 5.28 depicts the loss index of the samples at a relative humidity of 90% and a temperature of 30°C.

It appears that the evolution in the loss index is similar to the above observed evolution in relative permittivity. At a relative humidity of 45%, the plasma sprayed sample and the HVOF sprayed sample show similar values at the higher frequencies. The values at the lower frequencies are higher for the plasma sprayed sample than for the HVOF sprayed sample. At a relative humidity of 75% and 90%, both samples have a comparable loss index. It can be seen that the difference in loss index between these two samples and the flexicord sprayed sample is reducing with an increasing relative humidity.

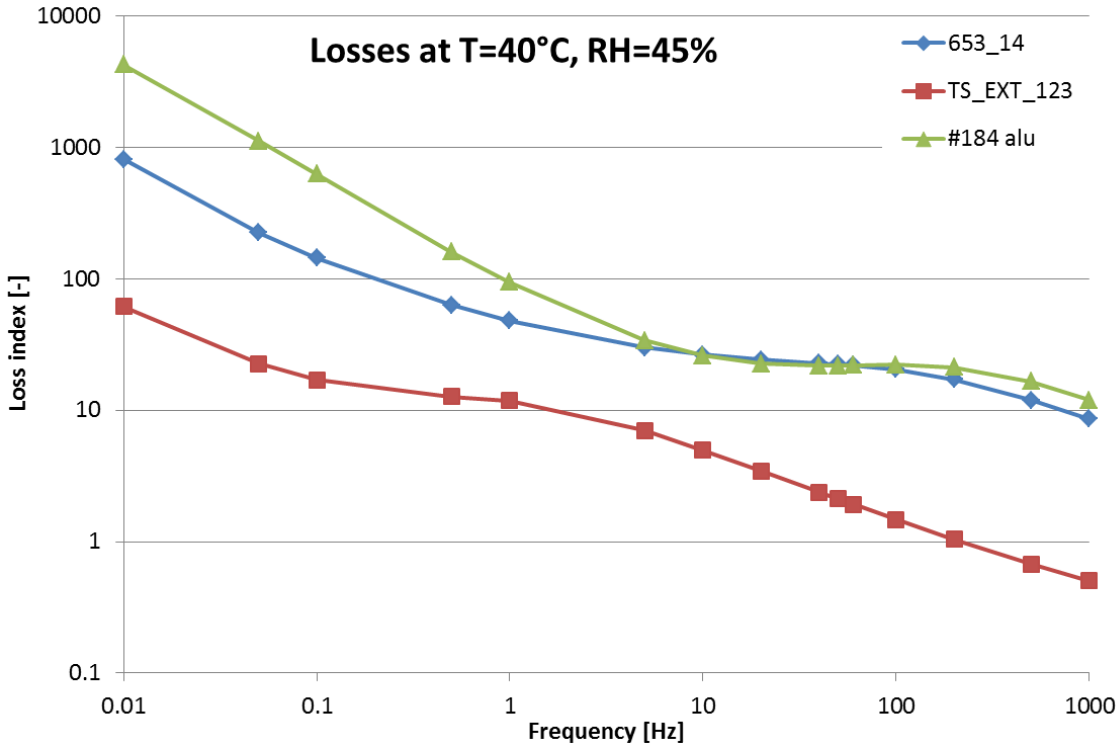

Figure 5.26.Comparison of the loss index at T=40°C and RH=45%.

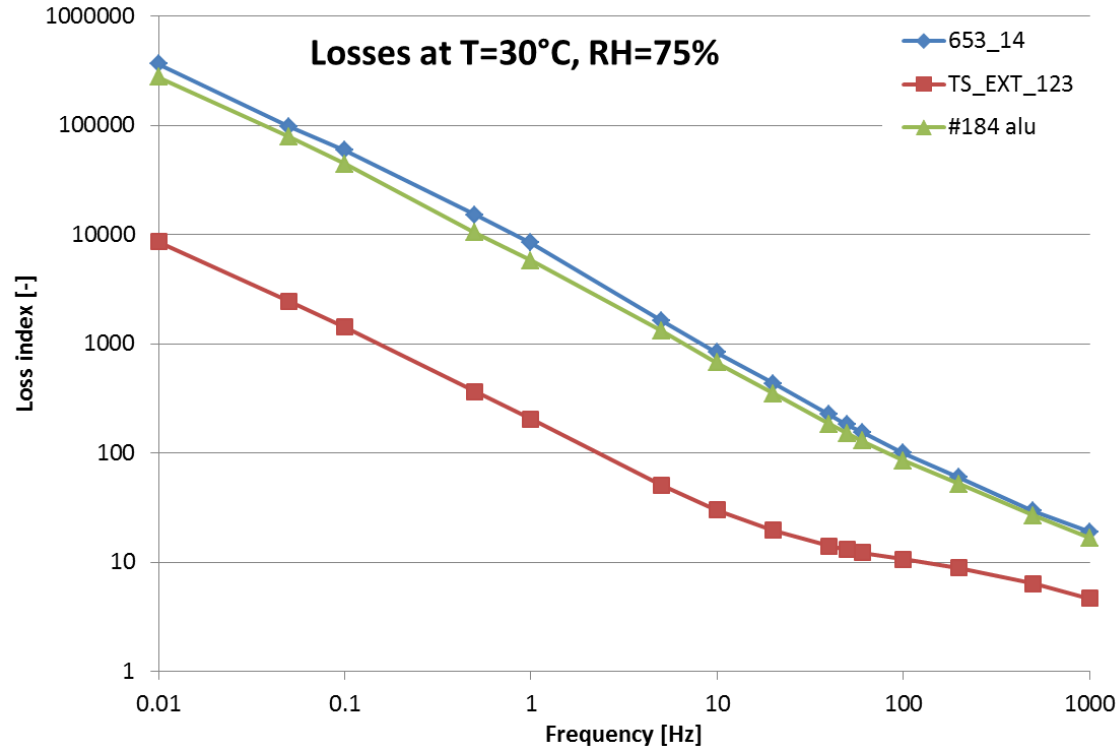

Figure 5.27. Comparison of the loss index at T=30°C and RH=75%.

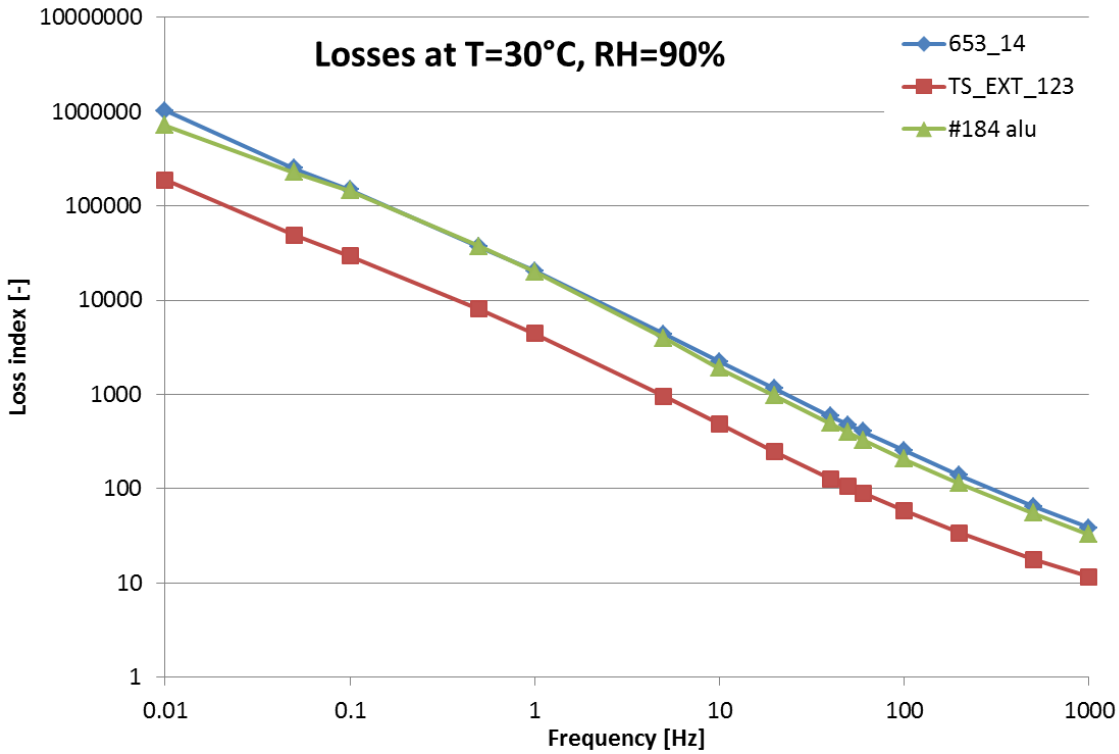

Figure 5.28. Comparison of the loss index at T=30°C and RH=90%.

5.2.4 Reliability of measurements below 100°C

As explained in Chapter 4, every sample was measured three times in every condition. Every result shown in Section 5.2 is the average of those three measurements. The electrodes were detached and re-attached before every measurement in order to eliminate coincidences due to the connection between the electrodes and the sample.

The repeatability was very high in the measurements performed below a relative humidity of 60%. This is shown in Figure 5.29, where the measurement of the relative permittivity of the HVOF sprayed sample at a temperature of 40°C and a relative humidity of 45% is depicted. At higher humidities, the repeatability of the measurements was less high, but still well acceptable. This is shown in Figure 5.30, the measurement of the HVOF sprayed sample at a temperature of 30°C and a relative humidity of 90%.

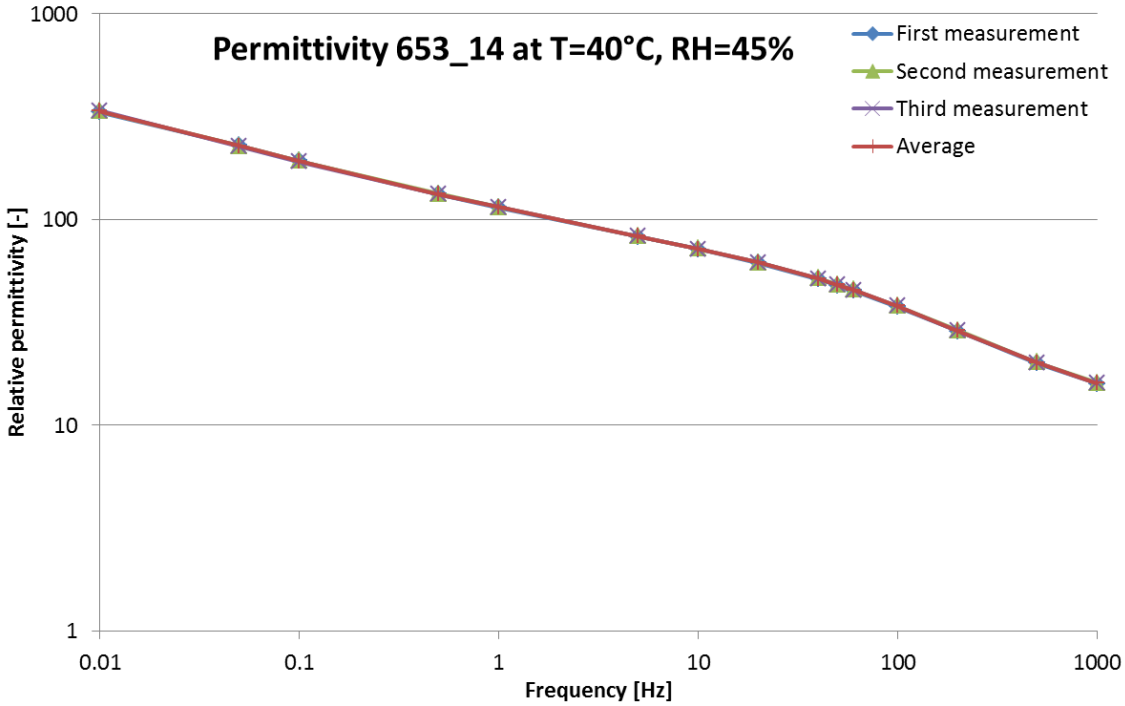

Figure 5.29. Repeatibility of measurements at a relative humidity below 60%.

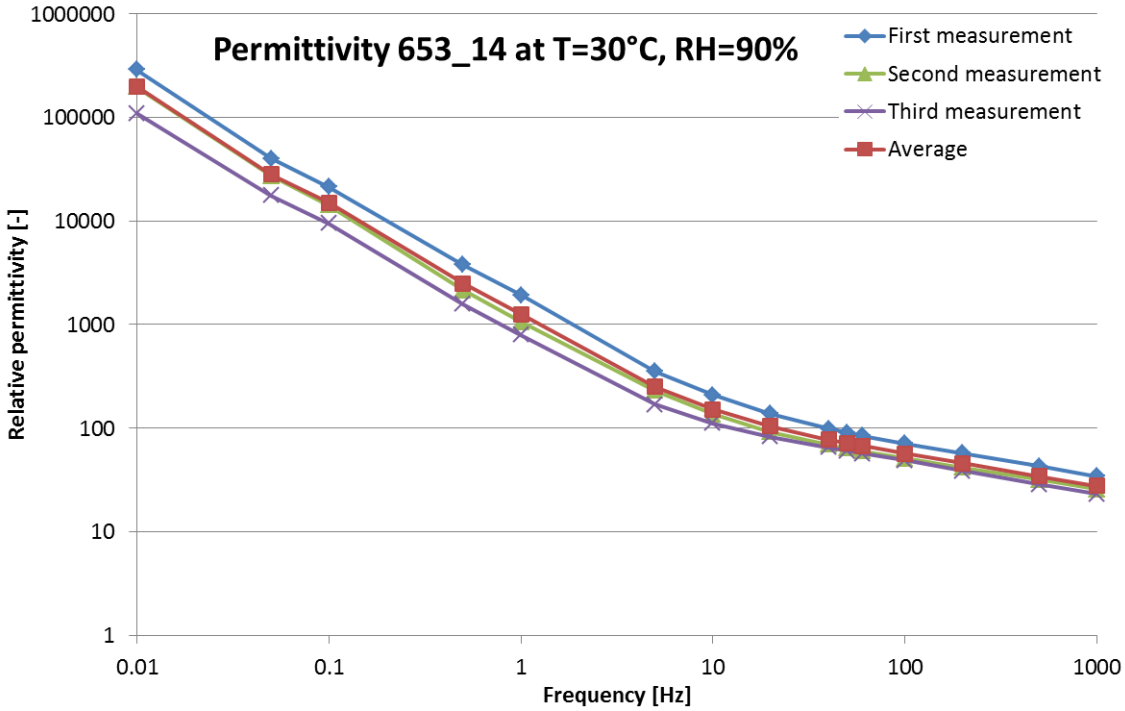

Figure 5.30. Repeatibility of measurements at higher relative humidities.

In order to determine the reliability of the acquired data, the measurements at a temperature of 30°C and a relative humidity of 20% were retaken after finishing all the measurements below 100°C. The comparison of the measured relative permittivity in those measurements is shown in Figure 5.31, Figure 5.32 and Figure 5.33 for the HVOF sprayed, the flexicord sprayed and the plasma sprayed sample, respectively.

It can be observed that the relative permittivity of both the HVOF and the plasma sprayed sample are decreased after performing all the measurements below 100°C. On the other hand, the relative permittivity of the flexicord sprayed sample is increased.

The loss indexes of the HVOF sprayed, the flexicord sprayed and the plasma sprayed sample are shown in respectively Figure 5.34, Figure 5.35 and Figure 5.36. Comparing these results, a similar observation as above can be made. The HVOF sprayed and the plasma sprayed sample behave in a similar way. After the measurements, both samples show a decrease in the loss index at the higher frequencies, but a severe increase in the loss index at the lower frequencies. On the other hand, the loss index in the flexicord sprayed sample shows in the whole frequency range a severe increase in the loss index after performing the measurements below 100°C.

It should be noted that the flexicord sprayed sample showed visible corrosion after performing all the measurements below 100°C, as shown in Figure 5.37. The visible corrosion was first detected after the measurements at a relative humidity of 90% and a temperature of 20°C. So if the measurement results are influenced by the corrosion, what can be expected regarding the different behaviour of the flexicord sprayed sample, mainly the last two measurements are affected.

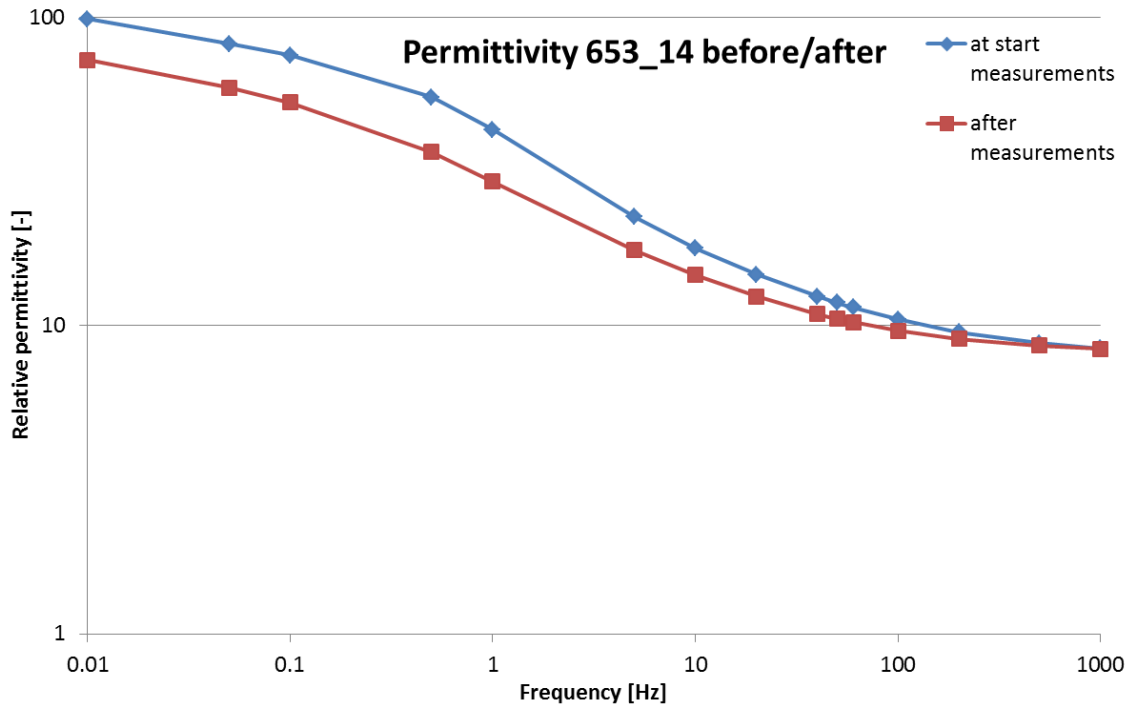

Figure 5.31. Relative permittivity of sample 653_14 before and after the measurements.

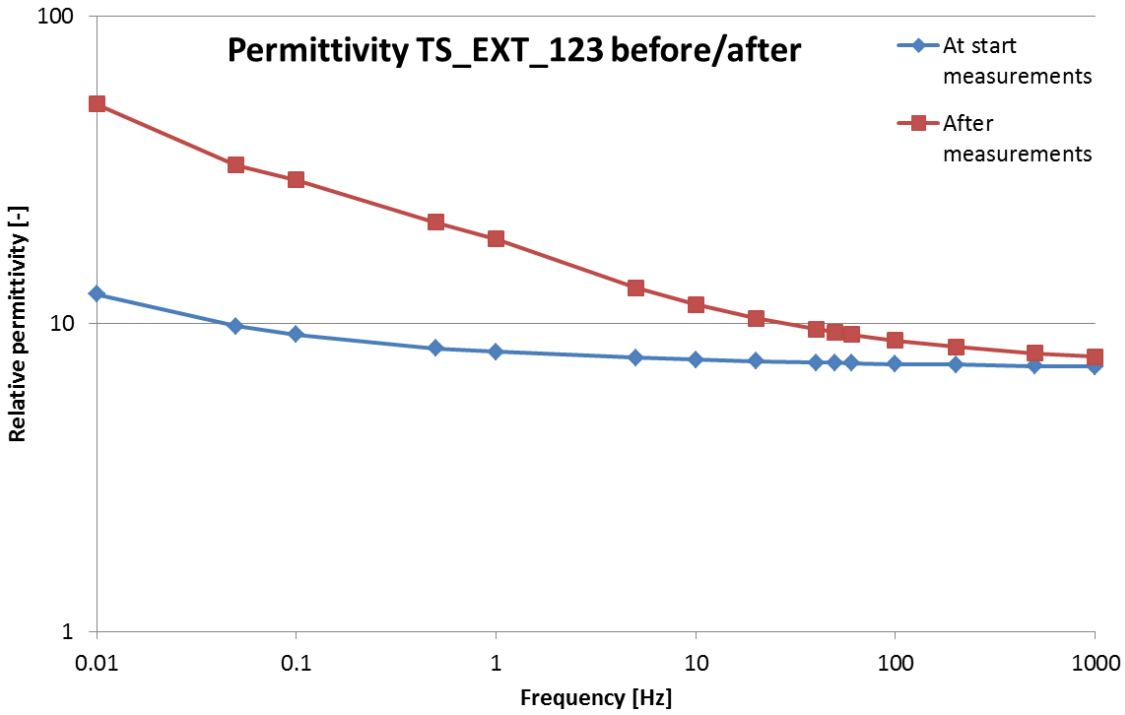

Figure 5.32. Relative permittivity of sample TS_EXT_123 before and after the measurements.

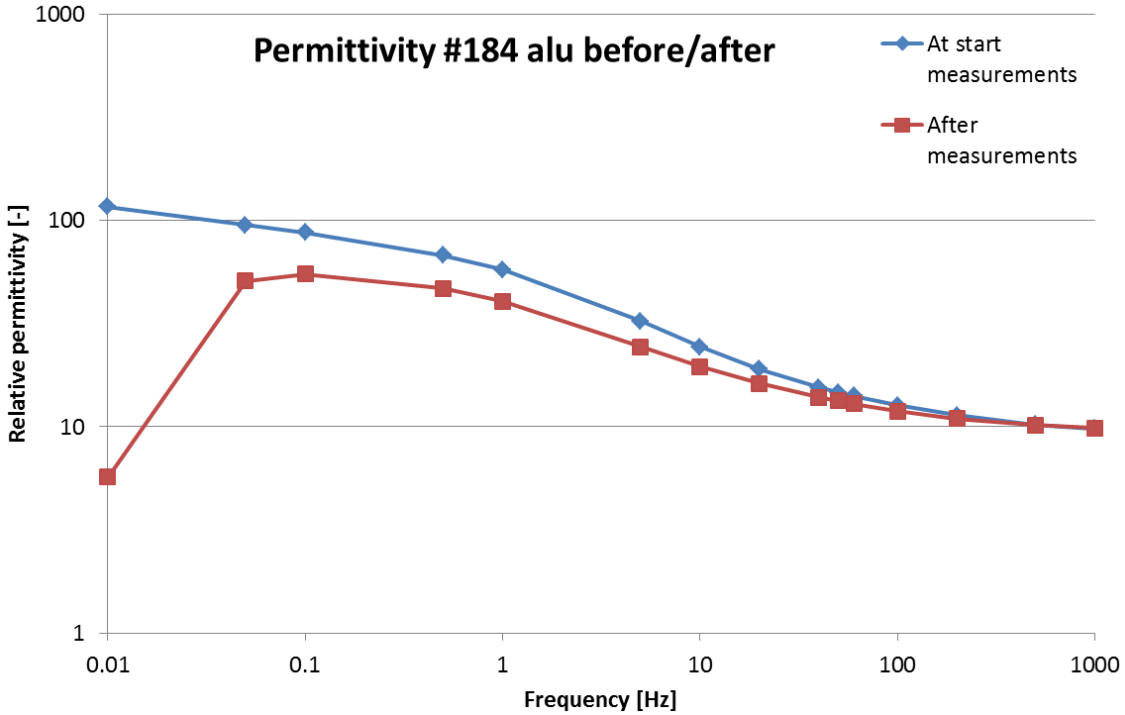

Figure 5.33. Relative permittivity of sample #184 alu before and after the measurements.

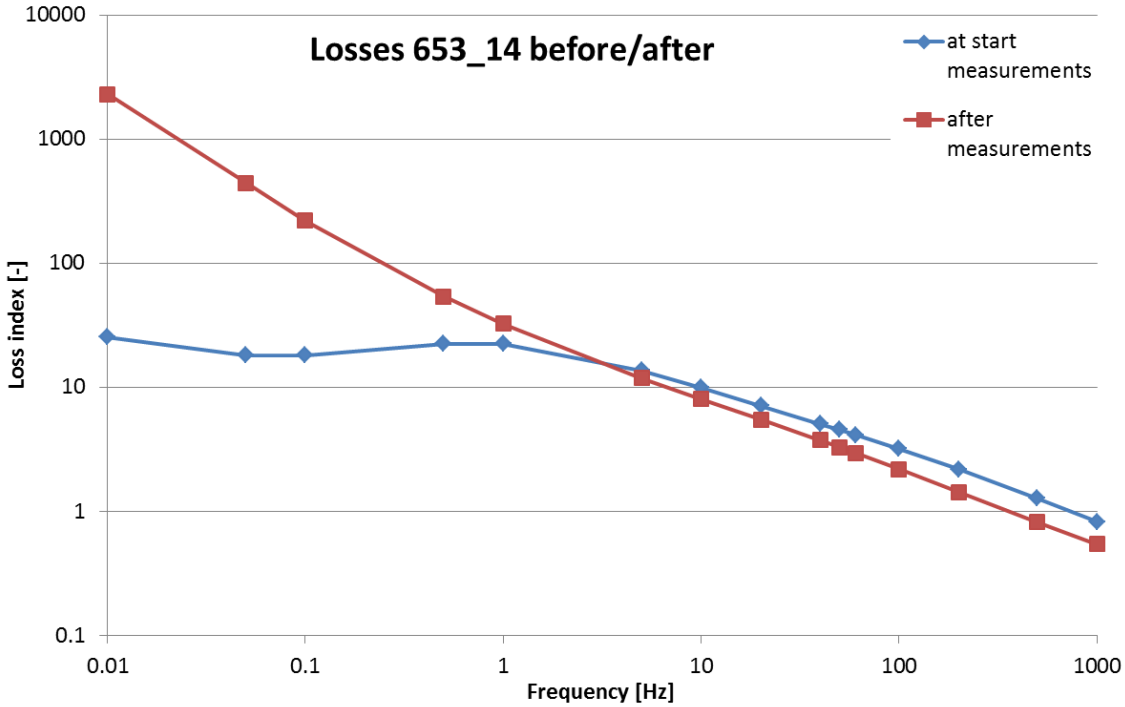

Figure 5.34. Loss index of sample 653_14 before and after the measurements.

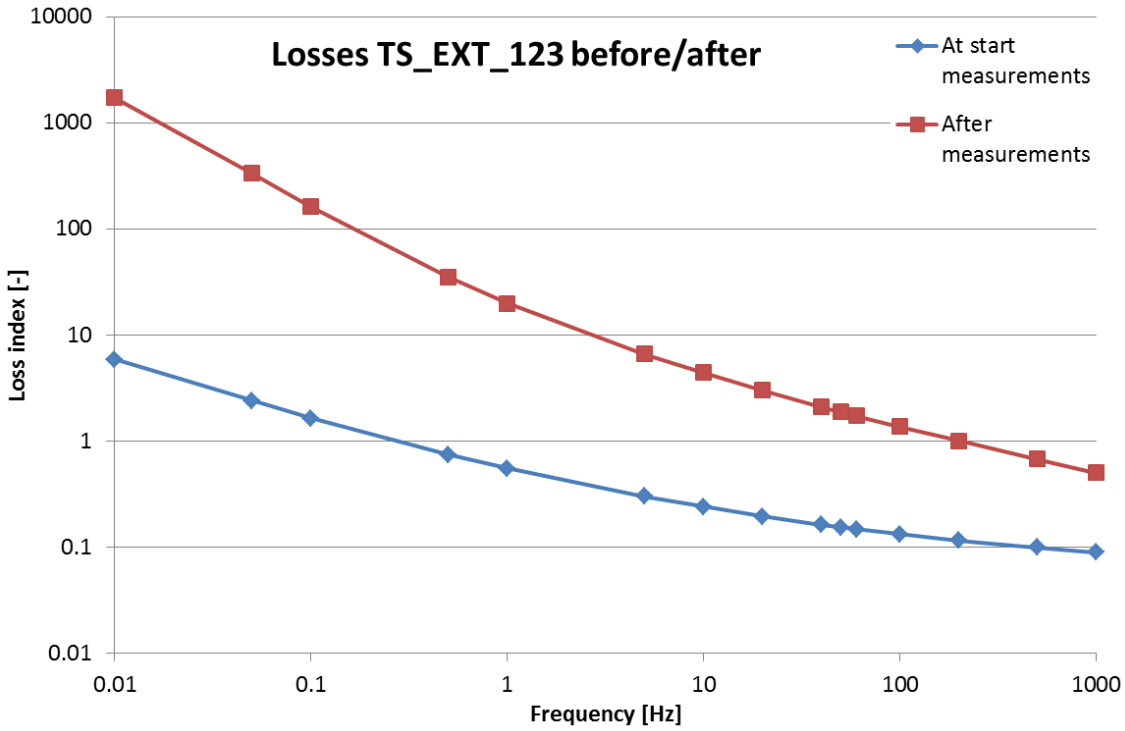

Figure 5.35. Loss index of sample TS_EXT_123 before and after the measurements.

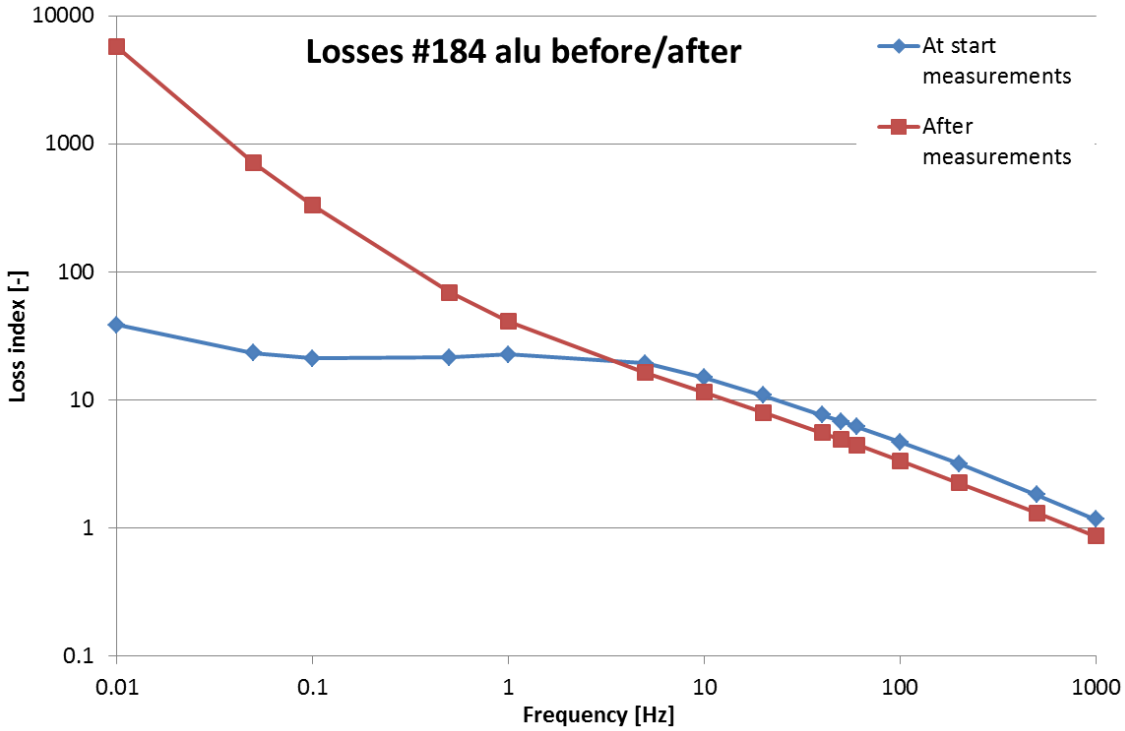

Figure 5.36. Loss index of sample #184 alu before and after the measurements.

Figure 5.37. The flexicord sprayed sample, TS_EXT_123, after the measurements. The orange spots are corroded.

5.3 Measurements above 100°C

The plan for this measurement series was to perform the same measurements as made in Section 5.2.2, but for temperatures higher than 100°C: at 105°C, 120°C, 150°C and 180°C. The measurements would be made in the oven, which would be placed in the climate room at a constant humidity. However, while trying to determine the stabilizing time of the samples at these temperatures, no clear stabilization was observed. Therefore it was decided to change the original plan to the examination of the stabilization behaviour at temperatures above 100°C. The flexicord sprayed sample was not used in these measurements, because of the severe corrosion and the lack of a new sample.

5.3.1 Stabilization of HVOF sprayed sample

As mentioned in Chapter 4, a new sample was used for these measurements to prevent any influences, as oxidation, from the earlier measurements. Figure 5.38 depicts the evolution of the relative permittivity of the HVOF sprayed sample after certain time periods at a temperature of 120°C. It can be seen that the relative permittivity decreases the longer the sample is in this condition. There is no noticeable stabilization after a time period of ten hours. The evolution of the relative permittivity at a temperature of 150°C is shown in Figure 5.39. At this temperature the measuring time has been extended to 25.5 hours. By comparing the measurements after 23.5 and 25.5 hours, it can be observed that the system appears stabilized. The evolution in relative permittivity at a temperature of 180°C is depicted in Figure 5.40. It can be observed that the decrease in relative permittivity is less quick, but also in these conditions there is no noticeable stabilization of the system after a measuring time of ten hours.

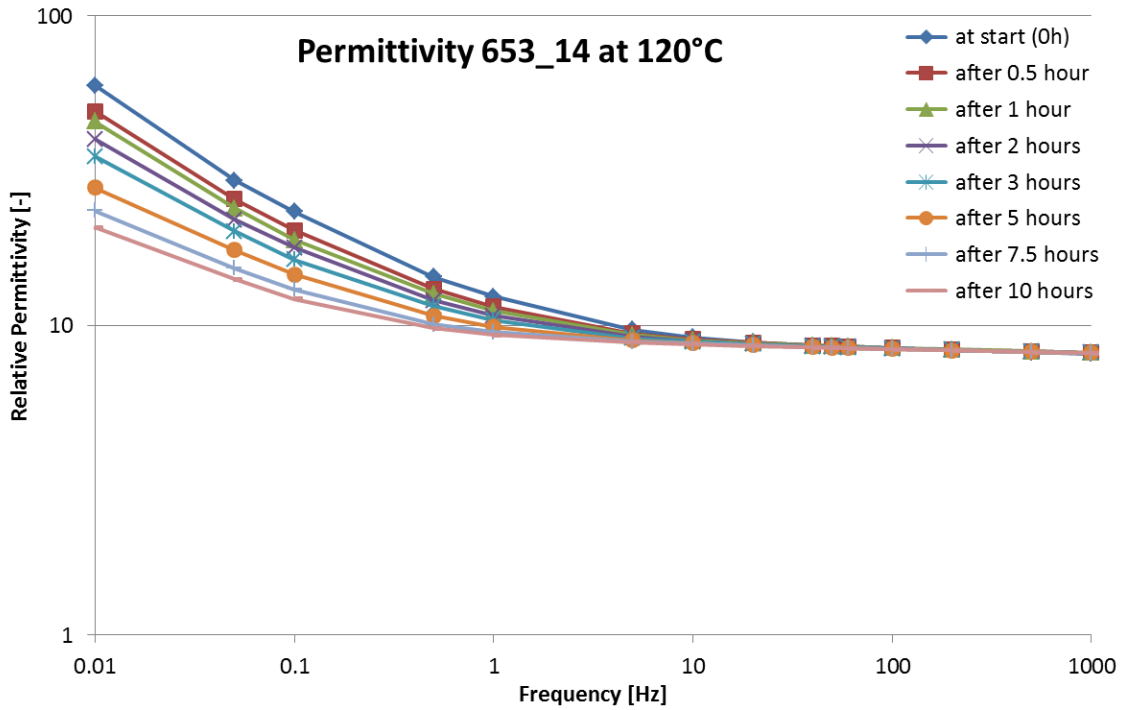

Figure 5.38. Permittivity of sample 653_14 with increasing heating time at 120°C.

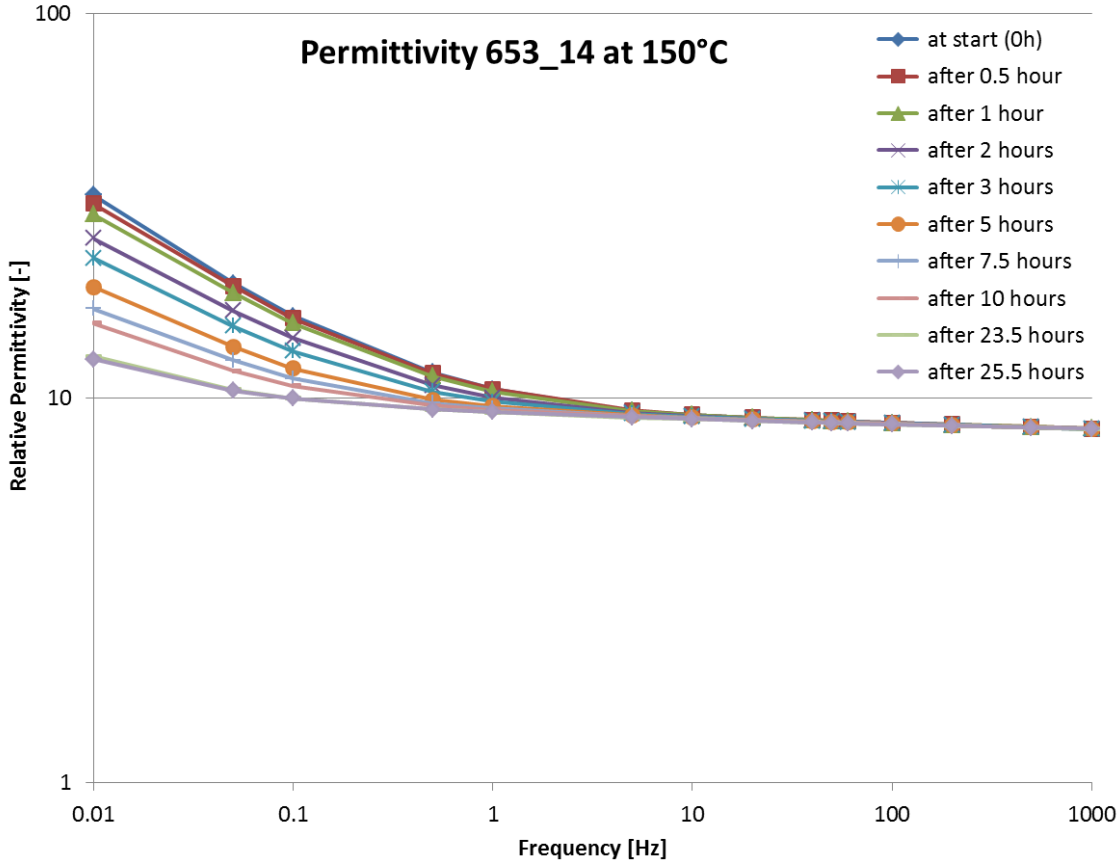

Figure 5.39. Permittivity of sample 653_14 with increasing heating time at 150°C.

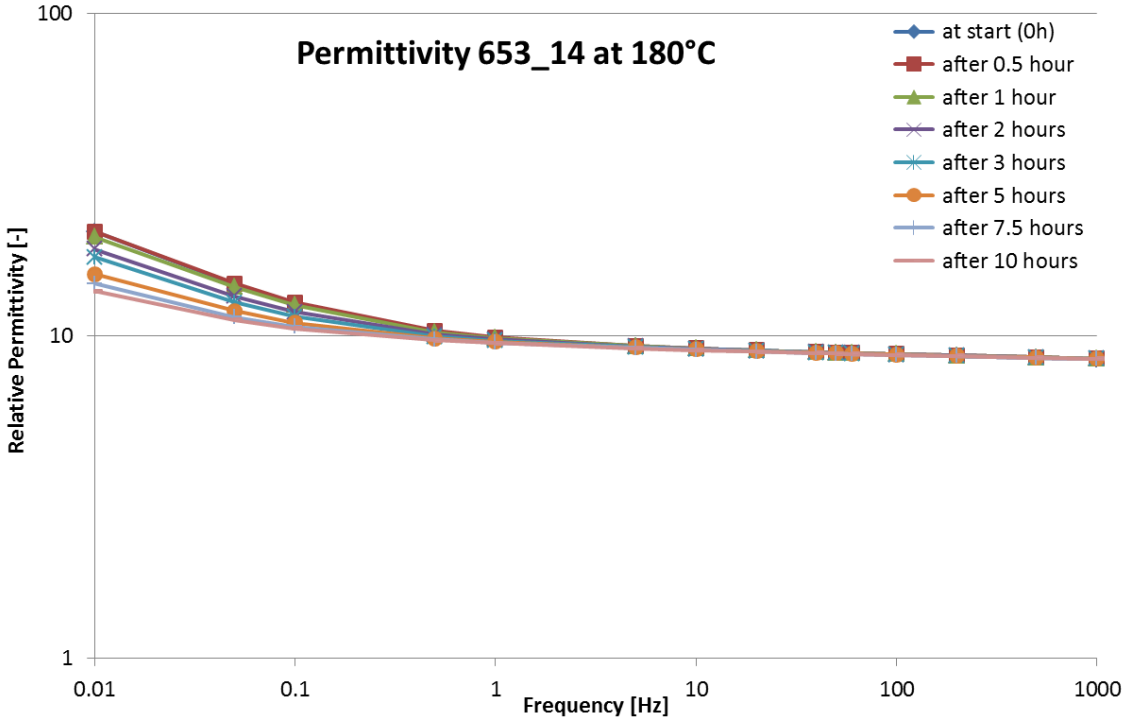

Figure 5.40. Permittivity of sample 653_14 with increasing heating time at 180°C.

The evolution of the loss index of the HVOF sprayed sample at a temperature of 120°C, 150° and 180°C is depicted in Figure 5.41, Figure 5.42 and Figure 5.43, respectively. The same tendency, as observed in the permittivity, can be seen in the loss index, it decreases the longer the system is heated. There is no noticeable stabilization after a time period of ten hours. After 23.5 hours, the difference in loss index between consequent measurements with a time difference of two hours is very small, what indicates an evolution to a stabilized state.

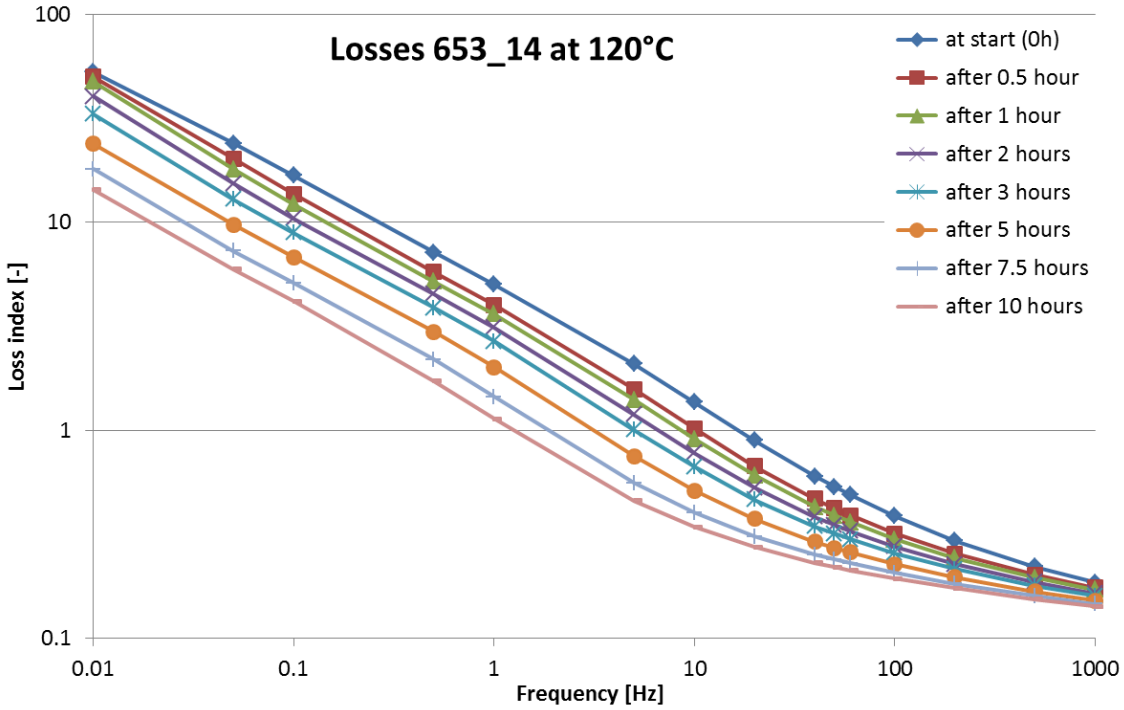

Figure 5.41. Loss index of sample 653_14 with increasing heating time at 120°C.

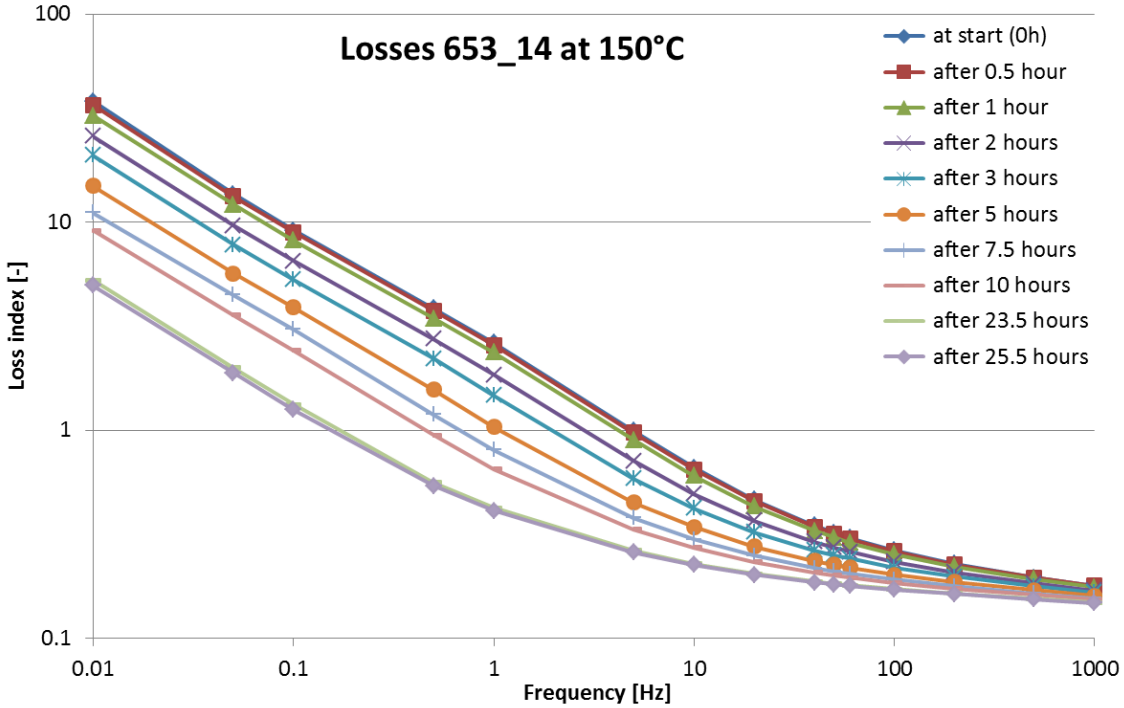

Figure 5.42. Loss index of sample 653_14 with increasing heating time at 150°C.

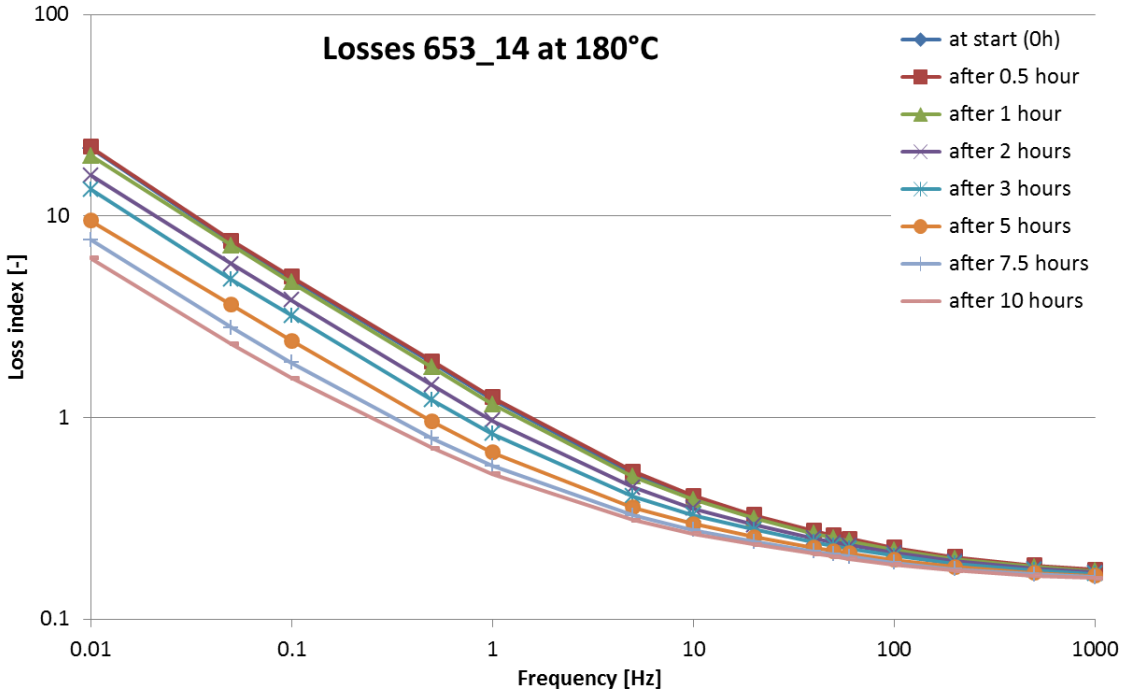

Figure 5.43. Loss index of sample 653_14 with increasing heating time at 180°C.

After each heating cycle, the relative permittivity and the loss index of the sample were measured in a reference environment. This was at a temperature of 30°C and a relative humidity of 20%. In Figure 5.44 and Figure 5.45, it appears that the relative permittivity and the loss index were decreased after each heating cycle. It can

be observed that the heating cycle at 150°C had the most influence on these quantities. The relative permittivity and the loss index were measured again a week after the last heating cycle. After this time period, the loss index showed a slight increase.

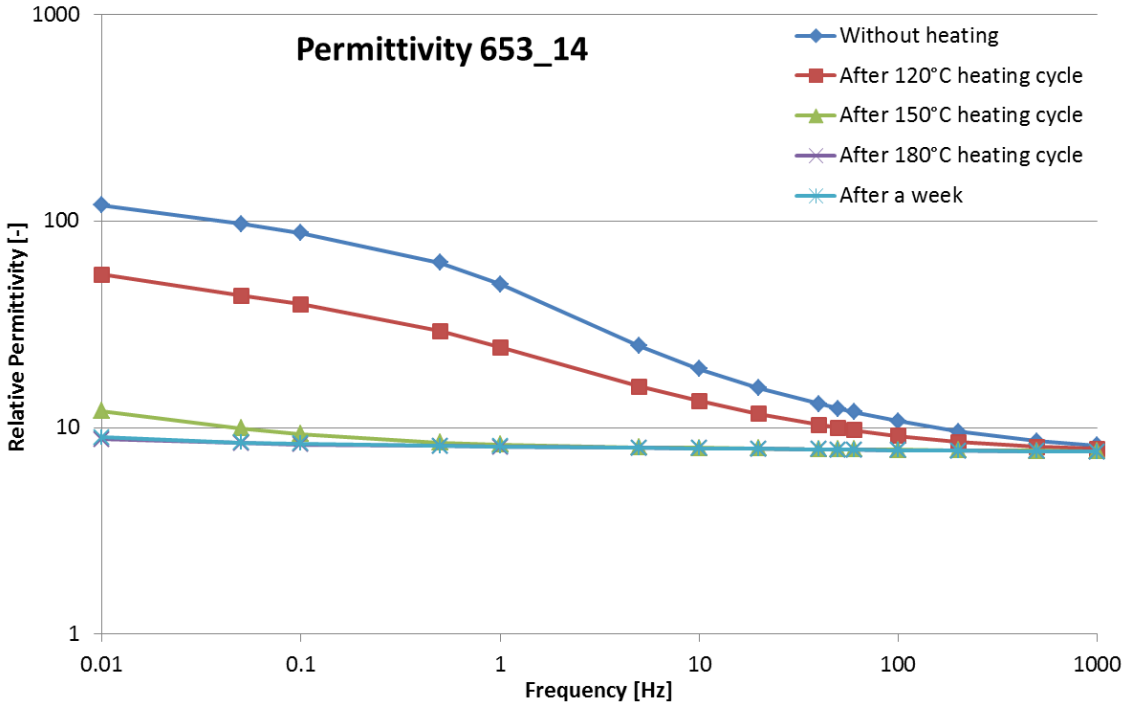

Figure 5.44. Permittivity of sample 653_14 after heating cycles.

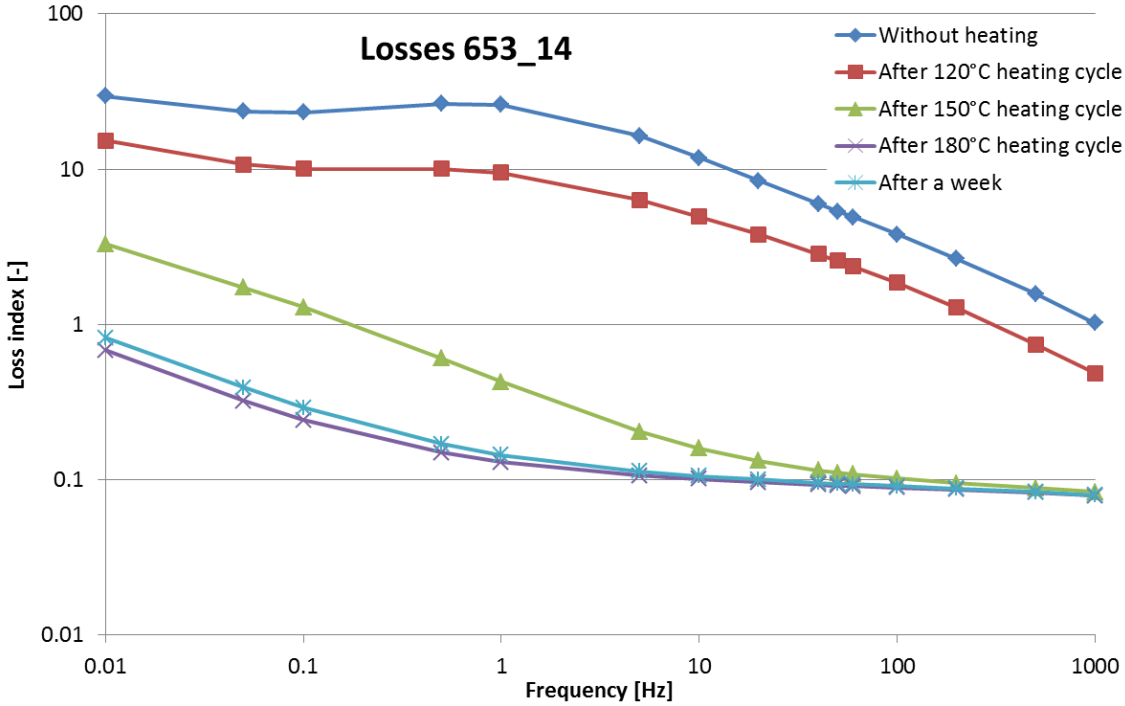

Figure 5.45. Loss index of sample 653_14 after heating cycles.

5.3.2 Stabilization of plasma sprayed sample

The substrate of the HVOF sprayed sample is carbon steel. In order to assess the influence of the substrate, also the stabilization behaviour of the plasma sprayed sample, coated on a stainless steel substrate, was determined. Because of the stainless steel substrate, less oxidation was expected. Thereby the sample used for the measurements below 100°C, was also used for these measurements. In the earlier measurements, the sample has been heated up eight times for two hours to a temperature of 120°C. Thereby the stabilization behaviour at a temperature of 150°C was examined in these measurements.

Figure 5.46 and Figure 5.47 show respectively the evolution of the relative permittivity and the loss index with an increasing heating time. It can be seen that these measurements show the same evolution as observed in the sample sprayed on carbon steel. Both the relative permittivity and the loss index decrease with an increasing heating time and there is no noticeable stabilization after a heating period of ten hours.

The measurements of the relative permittivity and the loss index in the reference environment are depicted in Figure 5.48 and Figure 5.49, respectively. Both the relative permittivity and the loss index appear to decrease after the heating cycle at 150°C, as observed in the measurements of the HVOF sprayed sample. The measurements before the heating cycle at 150°C are not the same measurements as depicted in Figure 5.33. For the measurements shown in these figures, the sample was measured again after another heat treatment at 120°C.

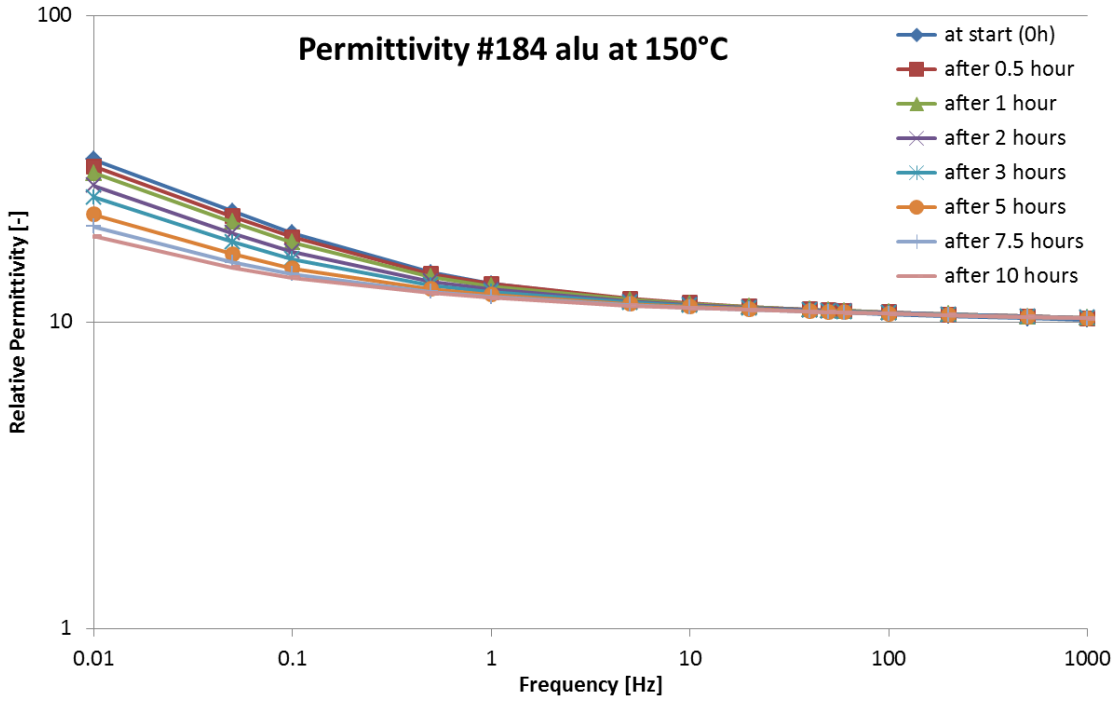

Figure 5.46. Permittivity of sample #184 alu with increasing heating time at 150°C.

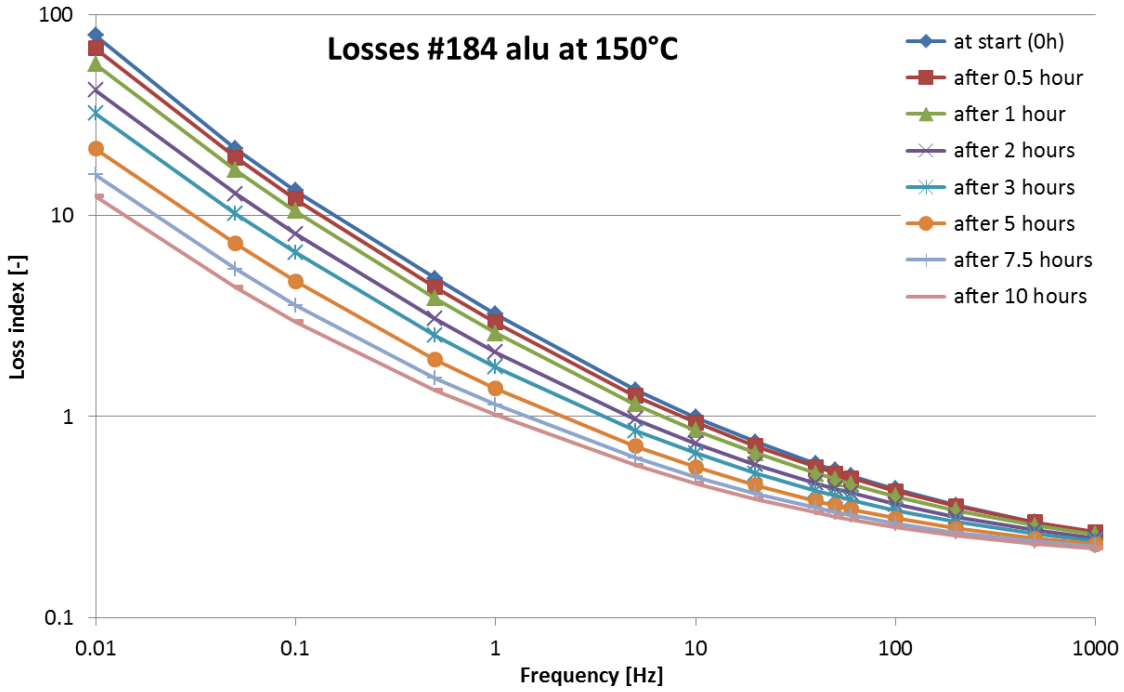

Figure 5.47. Loss index of sample #184 alu with increasing heating time at 150°C.

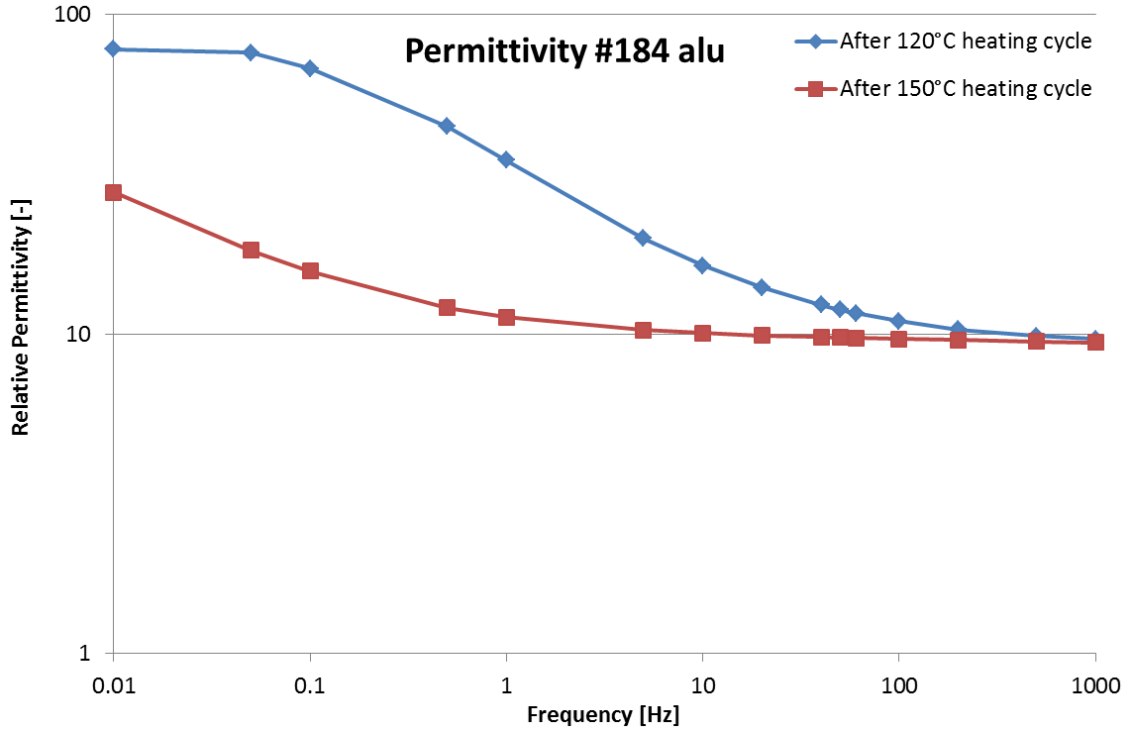

Figure 5.48. Permittivity of sample #184 alu before and after heating cycle at 150°C.

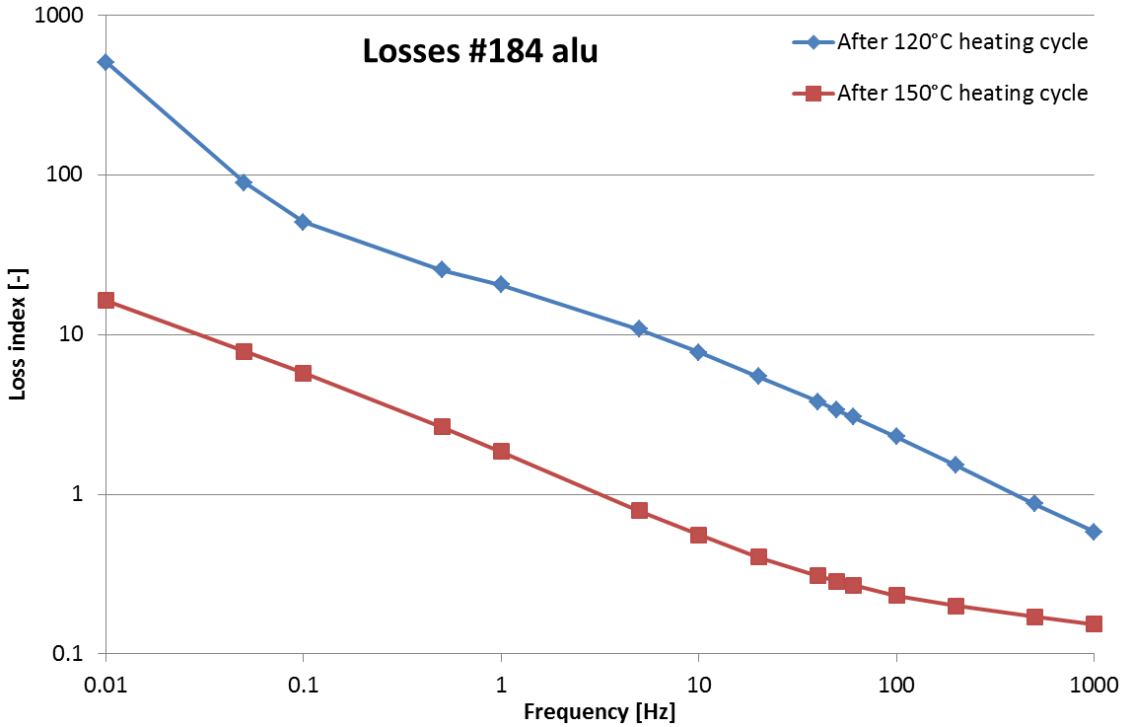

Figure 5.49. Loss index of sample #184 alu before and after heating cycle at 150°C.

6 DISCUSSION

6.1 Summary of measurement results

In Section 5.2, it was observed that in every sample both the relative permittivity and the loss index were increasing with increasing temperature, increasing relative humidity and decreasing frequency. The samples have shown to be more sensitive to an increase in relative humidity than to an increase in temperature.

At the lower relative humidities, the plasma sprayed sample showed the highest permittivity, the highest loss index and the highest sensitivity to an increase in temperature or humidity. The HVOF sprayed sample had slightly lower values for both relative permittivity and loss index and was less sensitive to an increase in temperature or humidity. The flexicord sprayed sample showed clearly lower values for both permittivity and loss index and the lowest sensitivity to changing conditions. At the highest humidity, all the samples had similar values for both the relative permittivity and the loss index.

After all the measurements below 100°C, the samples were measured again at a relative humidity of 20% and a temperature of 30°C. By comparing this measurement with the measurement performed earlier under the same circumstances, it was observed that the HVOF and the plasma sprayed samples showed a similar behaviour. The loss index was decreased at the higher frequencies, but it was severely increased at the lower frequencies. The relative permittivity was decreased in the whole frequency range. On the other hand, the flexicord sample showed a severe increase in both relative permittivity and loss index in the whole frequency range. It should be noted that this sample showed visible corrosion, first observed while performing the measurements at a relative humidity of 90%.

In Section 5.3, it was observed that the HVOF and the plasma sprayed sample showed unexpected behaviour at temperatures higher than 100°C. The flexicord sprayed sample was not used in this measurement sequence, because of the corrosion and the lack of a new sample. It was observed that both the relative permittivity and the loss index were decreasing with an increase in heating time. There was no noticeable stabilization after a heating time of 10 hours. The HVOF sprayed sample was heated up to a temperature of 150°C for 25.5 hours, at that point there were clear signs of stabilization of the system.

The samples were measured in a reference condition after each heating cycle. It could be seen that both the relative permittivity and the loss index were decreased after each heating cycle.

6.2 Discussion of measurement results

In Chapter 5, it was observed that the relative permittivity, the dissipation factor and hence the loss index are dependent on the frequency. This is a consequence of the frequency dependence of the different polarization mechanisms and can be described by the Debye equations. This relation is thoroughly discussed in Sections 2.3 and 2.4. The shift of the polarization mechanisms to higher frequencies with an increase in temperature can be modelled by the *Arrhenius equation* and is described in Section 2.4.3. The sensitivity of thermally sprayed Al_2O_3-coatings to humidity was also observed in the literature. The explanation of this behaviour is discussed in Section 3.3.7 and summarized in Figure 3.7.

It should be noted that the results shown in Section 5.2.2, the measurements at a constant relative humidity and variable temperature, do not show the pure effect of temperature on the dielectric properties of the samples. The reason for this is the increase in absolute humidity with an increase in temperature at a constant relative humidity. In the *Mollier diagram*, it can be seen that the absolute humidity is 9 g water/kg air at a temperature of 20°C and a relative humidity of 60% and at a temperature of 40°C and a relative humidity of 20%. The relative permittivity and the loss index of the HVOF sprayed sample at these conditions are compared in Figure 6.1 and Figure 6.2, respectively. It can be observed that both the relative permittivity and the loss index actually decrease with an increase in temperature at a constant absolute humidity. The same observations can be made in the other examined coatings, as depicted in Appendix C.

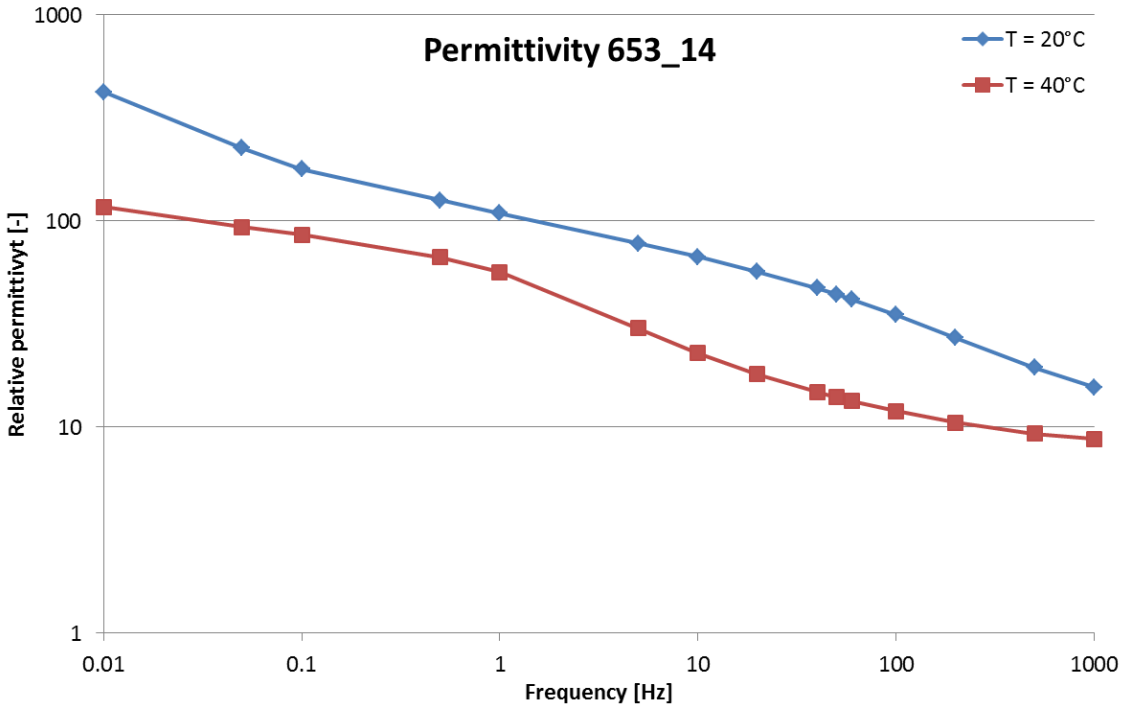

Figure 6.1. Permittivity of sample 653_14 at a constant absolute humidity of 9 g/kg.

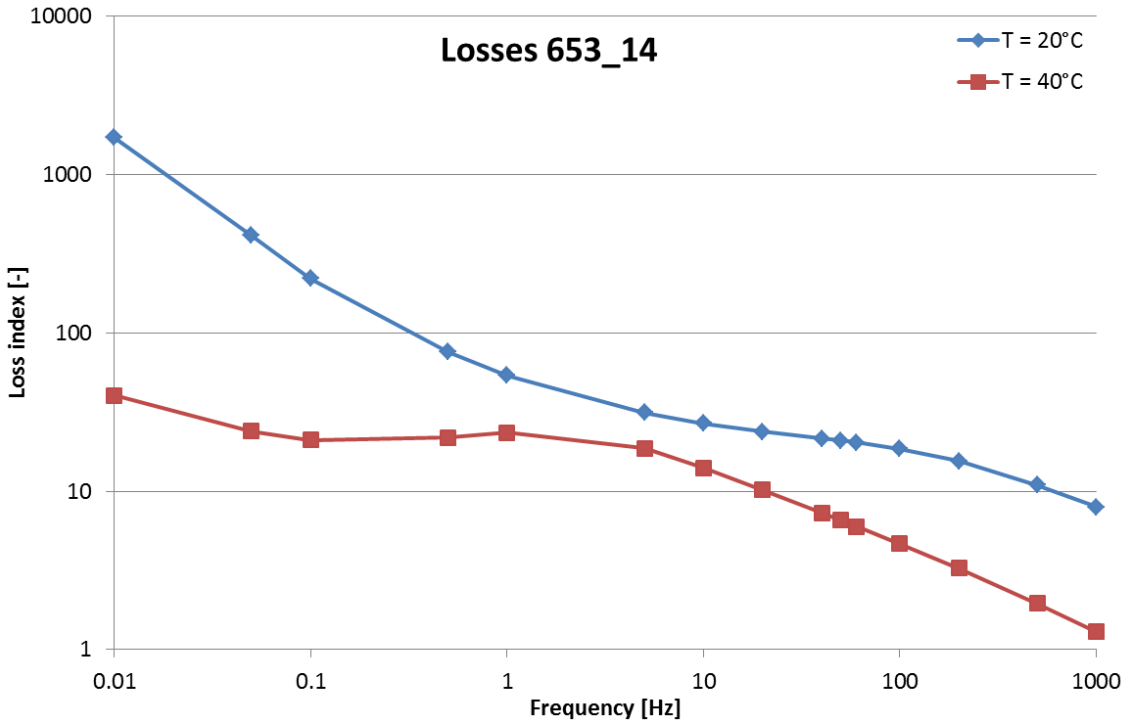

Figure 6.2. Loss index of sample 653_14 at at a constant absolute humidity of 9 g/kg.

In Section 5.2.1, a stabilization in relative permittivity at the higher frequencies was observed for the HVOF and the plasma sprayed sample, even though the relative humidity increased. At a frequency of 50 Hz, the relative permittivity appeared to stabilize around the value 80. This is the typical value for the relative permittivity of water at 50 Hz [38]. The observed linear relation between the frequency and the loss index in these measurements is a typical sign of dominating conductive current over the other parts of the resistive current and thus an indication of lossy insulation.

In Table 6.1, the relative permittivities and the loss indexes of different materials are compared. The values for the measured coatings are the results at 1 kHz, a temperature of 20°C and a relative humidity of 20%. It should be noted that the values for the other ceramic materials are literature values at a frequency of 1 MHz. However, with reference to Figure 2.8, there is no big variation in relative permittivity or loss index expected in the frequency range between 1 kHz and 1 MHz for materials where orientational polarization does not extensively occurs.

Table 6.1 shows that the values for the relative permittivity of the measured coatings are similar to the values of other ceramic materials, such as alumina, porcelain and glass. On the other hand, the loss index of the measured coatings is clearly higher than the loss index of the other materials. Particularly the values for the HVOF and the plasma sprayed coating are striking. It can also be observed that the relative permittivity and loss index is typically higher in ceramic materials than in polymers, such as polyethylene.

Table 6.1. Relative permittivity and loss index of different materials. [3,39]

		ε_r	Loss index ε'' *(x 10^3)*
HVOF sprayed alumina	- *1 kHz*	8.2	515
Flexicord sprayed alumina	- *1 kHz*	7.2	75.3
Plasma sprayed alumina	- *1 kHz*	9.6	888
Alumina (99.9% Al_2O_3)	- *1 MHz*	10.1	2.02
Porcelain	- *1 MHz*	8.5	42.5
Silica (fused)	- *1 MHz*	3.2	14.4
Toughened glass: alkali lime silica	- *1 MHz*	7.1 – 7.5	35.5 – 90
Polyethylene (PE)	- *1 kHz*	2.3	0.46 – 2.3

The differences in relative permittivity and loss index between the studied samples are mainly caused by differences in phase composition and porosity. The phase composition of the samples was measured by X-ray diffraction (XRD). The results of those measurements, performed by VTT, are shown in Appendix D. It can be seen that the HVOF and the plasma sprayed samples have a very similar phase composition. The HVOF sprayed sample contains only γ-Al_2O_3 and amorphous alumina. The plasma sprayed sample is composed of the same phases and contains also a really small amount of α-Al_2O_3. The phase composition of the flexicord sample is different from these two. It contains a lot of the less hygroscopic α-Al_2O_3, due to a large number of unmolten particles in the coating.

Figure 6.3, Figure 6.4 and Figure 6.5 show the cross sections of the different samples. In these figures, the difference in porosity between the samples can be observed. It appears that the HVOF sprayed sample, shown in Figure 6.3, is the least porous coating and that the flexicord sprayed sample, shown in Figure 6.4 is the most porous coating. The lighter regions in the cross section of the flexicord sprayed sample are the unmolten α-Al_2O_3 particles.

The lower values of the permittivity and the loss index of the flexicord sprayed sample are due to the higher amount of the stable α-Al_2O_3. The difference in dielectric properties between the HVOF sprayed and the plasma sprayed sample is mainly caused by the difference in porosity. Table 6.2 summarizes the phase composition of the different samples and the measured values for the porosity, determined by VTT.

Table 6.2. Phase composition and porosity of the different samples.

	Phase composition	**Porosity** *[% of volume]*
Ethylene-HVOF sprayed	Amorphous, γ-Al_2O_3,	1.40
Flexicord sprayed	Amorphous, γ-Al_2O_3, α-Al_2O_3	2.62
Atmospheric plasma sprayed	Amorphous, γ-Al_2O_3, little α-Al_2O_3	2.26

Figure 6.3. Cross-section of the HVOF sprayed sample.

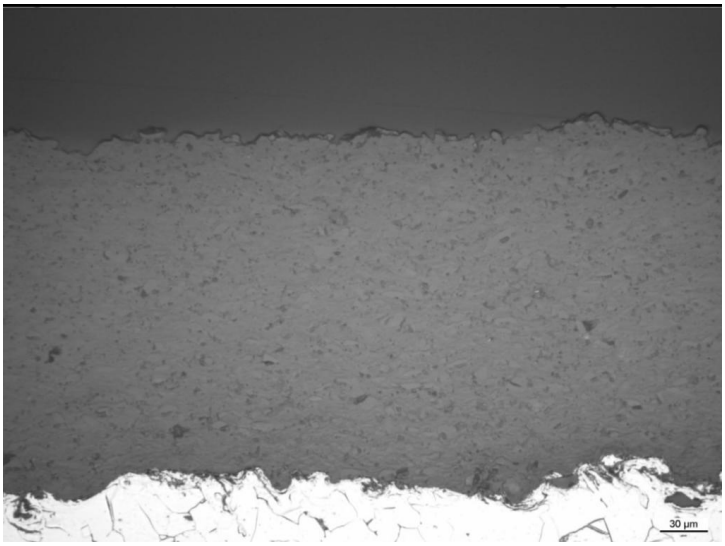

Figure 6.4. Cross-section of the flexicord sprayed sample.

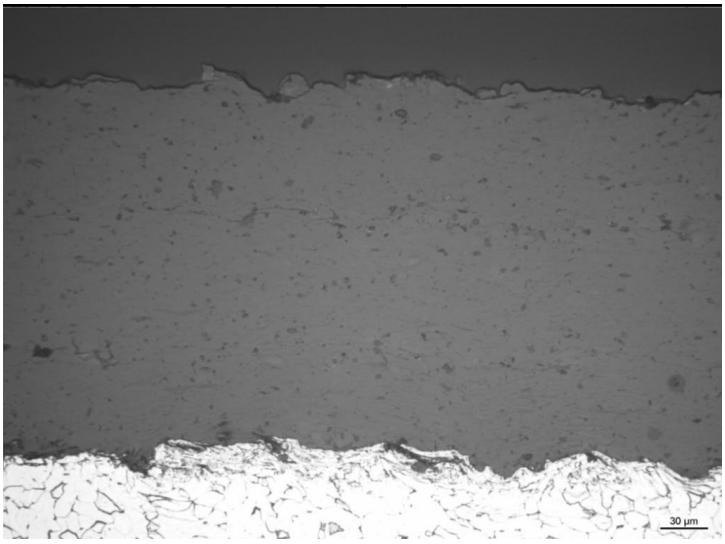

Figure 6.5. Cross-section of the plasma sprayed sample.

There are two mechanisms that are probably partly responsible for the observed permanent changes in permittivity and loss index during the measurements below 100°C. The first is oxidation, a thin layer of oxidation in the interface between substrate and coating can change the studied electric properties. The second mechanism is the formation of aluminium hydroxide (AlOH), as explained in Figure 3.7. This process is not totally reversible, as it causes changes in the electrical properties of the studied samples. Also the change in electrical properties at temperatures above 100°C can be explained by these mechanisms. Because of the high temperature, the changes in the material will occur faster and at lower humidities.

A phase transformation from the metastable γ-Al_2O_3 to the less hygroscopic α-Al_2O_3 was a third possible explanation for the observed change in dielectric properties. However, in the X-ray diffraction measurements, shown in Appendix D, there are no major phase changes noticeable after performing the measurements.

6.3 Recommendations for future work

The results obtained by using the developed measurement setup and measurement procedure, were highly repeatable and triggered the decision to use this setup and procedure in the further measurements for the HICC project. The only recommended modification in the measurement setup concerns the substrate on which the coating is sprayed. All the samples should be coated on a stainless steel substrate, in order to avoid severe oxidation.

The electrical properties of the samples changed during the measurement sequences performed for this thesis. The acquired results give a good insight into the behaviour of the different materials, but the results are not totally reliable regarding the use for future applications. In order to obtain more reliable results, the measurements should be performed on stabilized samples, of which the electrical properties do not change by heating the samples up to moderate temperatures, at approximately 200°C.

For this thesis, only measurements at temperatures of 20°C and higher were made. It can also be useful to study the dielectric properties of these materials at temperatures below 0°C. It can be expected that the freezing of the water inside the samples influences the properties.

In a later phase of the HICC-project, when the dielectric properties of more coatings are determined, maximum values for the loss index should be specified. Those values may serve as boundaries under which the losses and the permittivity of different materials are acceptable.

7 SUMMARY

The first objective of this thesis was to develop a test program to study the dielectric losses and the permittivity of thermally sprayed ceramic coatings. The second objective was to measure these properties for three different samples at different ambient conditions.

The first two chapters of the thesis are dedicated to a thorough literature study regarding general behaviour of insulating materials and thermally sprayed ceramic coatings. Next, the measurement setup and measurement procedure are discussed. The electrical properties were measured with the IDA 200 measurement device, using dielectric spectroscopy. The measurements were performed inside a Faraday cage, in order to prevent influences of external fields. Two measurement sequences were performed. The first measurement sequence was at temperatures below 100°C and examined the effect of temperature and humidity on the dielectric properties of the studied coatings. Between consecutive measurements at different conditions, the samples were acclimatized for at least four hours. The second measurement sequence was at temperatures above 100°C, where the effect of heating on the dielectric properties of the samples was examined.

The examined samples were all coated with aluminium oxide (Al_2O_3). Two samples were coated on a carbon steel substrate, one with ethylene-HVOF spraying, the other one with flexicord spraying. The third sample had an atmospheric plasma sprayed coating on a stainless steel substrate.

Generally, it was observed that both relative permittivity and loss index increased with decreasing frequency, increasing humidity and increasing temperature at a constant relative humidity. However, at a constant absolute humidity, the dielectric quantities decreased with an increase in temperature.

It was observed that the plasma sprayed sample showed the highest permittivity, loss index and sensitivity to an increase in temperature or humidity. The HVOF sprayed sample had slightly lower values for both permittivity and loss index and showed a lower sensitivity to changing conditions. The higher values of the plasma sprayed sample are due to a higher amount of porosities in the microstructure of the coating.

The flexicord sprayed sample had the lowest values for both permittivity and loss index and showed to be the least sensitive to changing conditions, despite the high porosity. The difference between the flexicord sprayed sample and the other samples is due to a different phase composition. The HVOF and the plasma sprayed samples are composed of the metastable γ-Al_2O_3 and amorphous alumina. The flexicord sample

contains also the stable, less hygroscopic α-Al_2O_3, due to unmolten particles in the coating.

The relative permittivity of the studied samples was similar to the relative permittivity of other ceramic materials. On the other hand, the loss index of the examined coatings was clearly higher than the loss index of other ceramics.

The first measurement was repeated after the whole measurement sequence below 100°C. The dielectric properties of the tested samples were compared before and after all the electrical and ambient stresses. It was observed that the permittivity and the loss index of the samples were changed during the measurement sequence. In the second measurement sequence, at temperatures above 100°C, it was observed that both permittivity and loss index changed with an increase in heating time, indicating permanent changes in the tested samples. These observations can be explained by two mechanisms. The first one is the formation of aluminium hydroxide (AlOH), the second mechanism is the formation of a thin layer of oxidation in the interface between the substrate and the coating.

In the last part of the thesis, recommendations for future research were given. After the first measurement sequence, at temperatures below 100°C, the flexicord sprayed sample was severely corroded. In order to prevent this heavy oxidation in the future, the next samples should be coated on a stainless steel substrate.

The electrical properties changed permanently during the measurements. The acquired results give a good insight into the dielectric properties of the different materials, but the results are not totally reliable. In order to obtain more reliable data, the measurements should be performed on stabilized samples. Nevertheless, comparing the observed permanent changes in the dielectric properties to the generally high variation of those properties due to ambient changes, the results of this thesis can be regarded as highly useful.

In future measurements, it would be interesting to extend the temperature range to temperatures below 0°C, because of the different dielectric properties of ice. In a later phase of the HICC-project, maximum acceptable values for the loss index should be specified.

REFERENCES

[1] J. Gerhold, "Dielectric properties," in *Handbook of Applied Superconductivity, Volume 2*, Bernd Seeber, Ed.: Taylor & Francis, 1998, pp. 1121 - 1137.

[2] Ruben D. Garzon, *High Voltage Circuit Breakers: Design and Applications*.: CRC Press, 2002.

[3] G. G. Raju, *Dielectrics in Electric Fields*. New York: Marcel Dekker Ltd, 2003.

[4] Joseph Callaway, *Band theory of solids*.: AccessScience, ©McGraw-Hill Companies, http://www.accesscience.com, 2008.

[5] D. J. David and Ashok Misra, *Relating Materials Properties to Structure with MATPROP Software Handbook and Software for Polymer Calculations and Materials properties*.: CRC Press, 2001, pp. 379 - 408.

[6] K. F. Etzold, "Dielectrics," in *RF and Microwave Passive and Active Technologies*, Mike Golio and Janet Golio, Eds.: CRC Press, 2008, ch. 27, pp. 1 - 8.

[7] Mario Rabinowitz and Steven A. Boggs, *Electrical insulation*.: AccessScience, ©McGraw-Hill Companies, http://www.accesscience.com, 2008.

[8] Michael B. Heaney, "Electrical Conductivity and Resistivity," in *Electrical Measurement, Signal Processing and Displays*, John G. Webster, Ed., 2003, ch. 7, pp. 1 - 14.

[9] John B. Goodenough, *Electric insulator*.: AccessScience, ©McGraw-Hill Companies, http://www.accesscience.com, 2008.

[10] Fred D. Barlow and Aicha Elshabini, Eds., *Ceramic Interconnect Technology Handbook*.: CRC Press, 2007.

[11] Ilkka Rytöluoto, "Application of polypropylene nanocomposites in metallized film capacitors under DC voltage," Department of Electrical Engineering, Tampere University of Technology, Tampere, Master of Science Thesis, 2011.

[12] James H. Calderwood, *Permittivity*.: AccessScience, ©McGraw-Hill Companies, http://www.accesscience.com, 2008.

[13] R. Bartnikas, "Dielectrics and Insulators," in *Electronics, Power Electronics, Optoelectronics, Microwaves, Electromagnetics and Radar*, Richard C Dorf, Ed.: CRC Press, 2006, ch. 29, pp. 1 - 20.

[14] William B. White, "Basic Science of Advanced Ceramics," in *Handbook of Advanced Ceramics*, Shigeyuki Sömiya, Ed.: Elsevier, 2003, pp. 3 - 80.

[15] Robert D. Waldron, *Polarization of dielectrics*.: AccessScience, ©McGraw-Hill Companies, http://www.accesscience.com, 2008.

[16] Hannes Ranta, "Long-term electrical properties of polypropylene nanocomposites for high voltage capacitor applications," Department of Electrical Engineering, Tampere University of Technology, Tampere, Master of Science Thesis, 2008.

[17] Tony Blythe and David Bloor, *Electrical Properties of Polymers*, 2nd ed. United Kingdom: Cambridge University Press, 2005, ch. 6.

[18] Dale E. Niesz, *Ceramics*.: AccessScience, ©McGraw-Hill Companies, http://www.accesscience.com, 2008.

[19] Kevin G. Ewsuk, "Ceramic processing," in *Encyclopedia of Chemical Physics and Physical Chemistry - 3 Volume Set*, John H. Moore and Nicholas D. Spencer, Eds.: Taylor & Francis, 2001.

[20] Arvind Agarwal, Srinivasa Rao Bakshi, and Debrupa Lahiri, *Carbon Nanotubes, Reinforced Metal Matrix Composites*.: CRC Press, 2010, pp. 17 - 70.

[21] J. Liebault, J. Vallayer, D. Goeuriot, D. Treheux, and F. Thevenot, "How the trapping of charges can explain the dielectric breakdown performance of alumina ceramics," *Journal of the European Ceramic Society*, vol. 21, pp. 389 - 397, 2001.

[22] M. Touzin, D. Goeuriot, C. Guerret-Piécourt, D. Juvé, and H.-J. Fitting, "Alumina based ceramics for high voltage insulation," *Journal of the European Ceramic Society*, vol. 30, pp. 805 - 817, 2010.

[23] Tadeusz Wierzchon and Tadeusz Burakowski, *Surface Engineering of Metals: Principles, Equipment, Technologies*.: CRC Press, 1998.

[24] A. A. Seireg, *Friction and Lubrication in Mechanical Design*.: CRC Press, 1998.

[25] Michael T. Powers et al., Eds., *Materials Processing Handbook*.: CRC Press, 2007.

[26] I. Zhitomirsky, "Electrophoretic and Electrolytic Deposition of Ceramic Coatings on Carbon Fibers," *Journal of the European Ceramic Society*, vol. 18, pp. 849 - 856, 1998.

[27] Lin Xie, Kiyoshi Funatani, and George E. Totten, Eds., *Handbook of Metallurgical Process Design*.: CRC Press, 2004, pp. 833 - 856.

[28] Mel Scwhartz, *Innovations in Materials Manufacturing, Fabrication and Environmental Safety*.: CRC Press, 2010, pp. 385 - 444.

[29] Maria Oksa, Erja Turunen, Tomi Suhonen, Tommi Varis, and Simo-Pekka Hannula, "Optimization and Characterization of High Velocity Oxy-fuel Sprayed Coatings: Techniques, Materials and Applications," *www.mdpi.com/journal/coatings*, 2011.

[30] R. Ahmed, N. H. Faisal, A. M. Paradowska, and M. E. Fitzpatrick, "Residual Strain and Fracture Response of Al2O3 Coatings Deposited via APS and HVOF Techniques," *Journal of Thermal Spray Technology*, vol. 21, pp. 23 - 40, January 2012.

[31] Filofteia-Laura Toma et al., "Comparative Study of the Electrical Properties and Characteristics of Thermally Sprayed Alumina and Spinel Coatings," *Journal of Thermal Spray Technology*, vol. 20(1-2), pp. 195 - 204, January 2011.

[32] E. Turunen et al., "On the role of particle state and deposition procedure on mechanical, tribological and dielectric response of high velocity oxy-fuel sprayed alumina coatings," *Materials Science and Engineering, Elsevier*, pp. 1 - 11, 2005.

[33] Bertil Helgee and Peter Bjellheim, "Electric Breakdown Strenght of Aromatic Polymers - Dependence on Film Thickness and Chemical Structure," *IEEE Transactions on Electrical Insulation*, vol. 26, no. 6, pp. 1147 - 1152, December 1991.

[34] W. Hauschild and W. Mosch, *Statistical techniques for high-voltage engineering*. London, United Kingdom: Peter Peregrinus Ltd, 1992, pp. 257 - 294.

[35] "IEC Standard 60672-2, Ceramic and glass insulating materials - Part 2: Methods of test," 1999.

[36] G.E. Services, "IDA 200 - Insulation Diagnostic System, User's Manual".

[37] "IEC Standard 60250, Recommended methods for the determination of the permittivity and dielectric dissipation factor of electrical insulating materials at power, audio and radio frequencies including metre wavelengths," 1969.

[38] Davide Tommasini. (2009, June) [Online]. *http://cas.web.cern.ch/cas/Belgium-2009/Lectures/PDFs/Tommasini.pdf* (last acces: May 17, 2012)

[39] J. S. T. Looms, *Insulators for high voltages*. London, United Kingdom: Peter Peregrinus Ltd., 1988, p. 26.

APPENDIX A – PROPERTIES AT CONSTANT TEMPERATURE

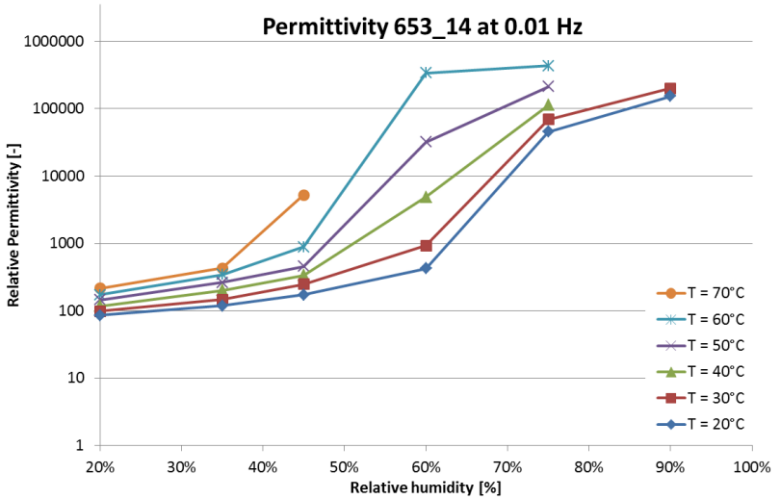

Figure A.1. Relative permittivity of 653_14 at 0.01 Hz as a function of relative humidity.

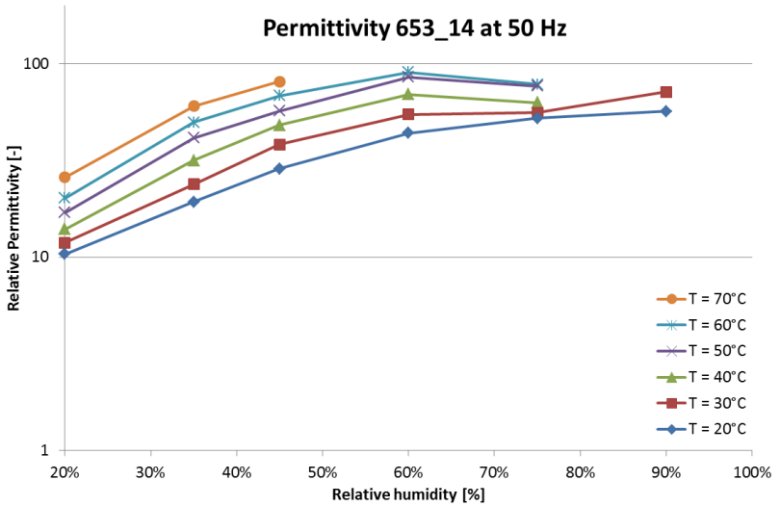

Figure A.2. Relative permittivity of 653_14 at 50 Hz as a function of relative humidity.

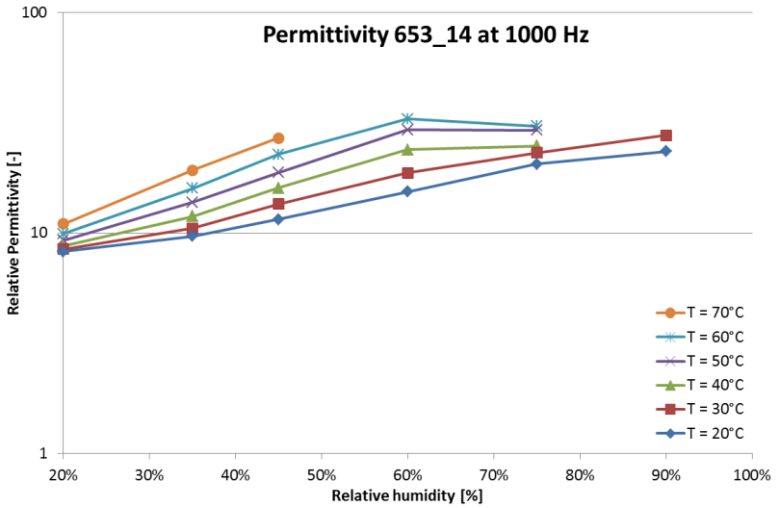

Figure A.3. Relative permittivity of 653_14 at 1000 Hz as a function of relative humidity.

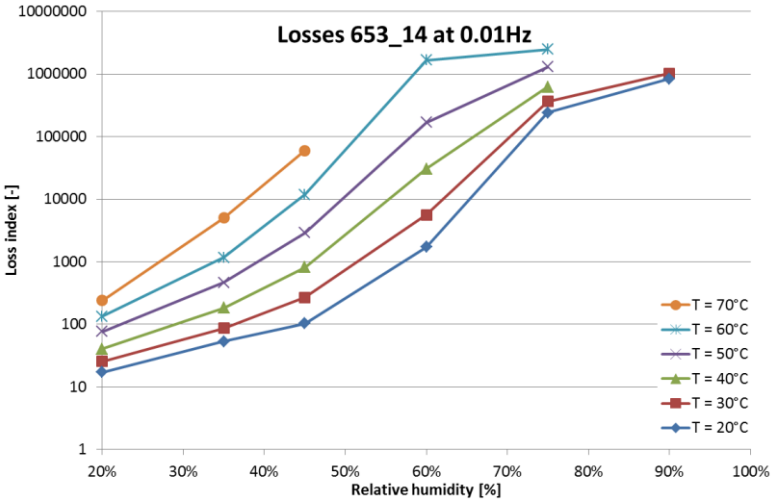

Figure A.4. Loss index of 653_14 at 0.01 Hz as a function of relative humidity.

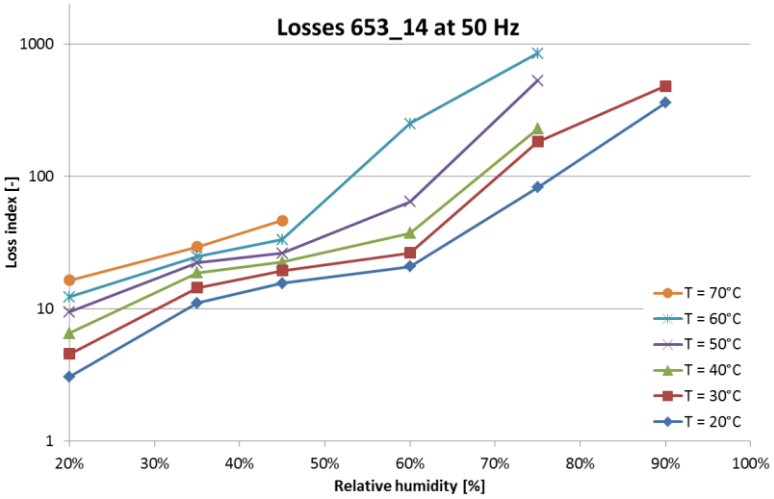

Figure A.5. Loss index of 653_14 at 50 Hz as a function of relative humidity.

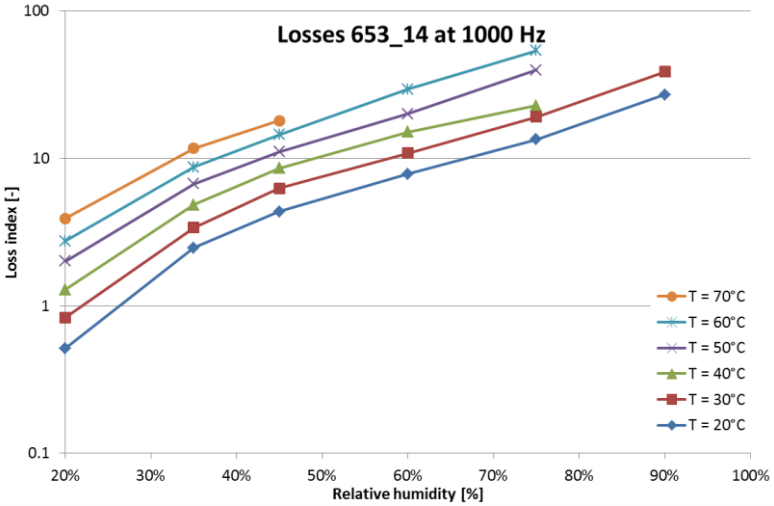

Figure A.6. Loss index of 653_14 at 1000 Hz as a function of relative humidity.

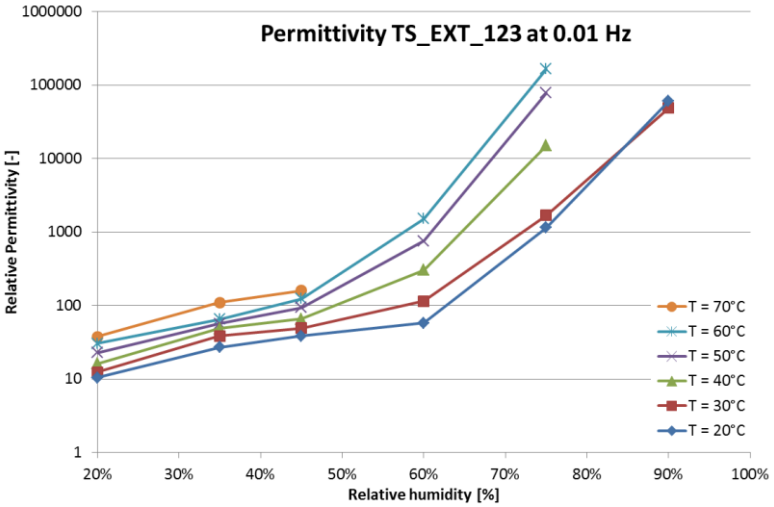

Figure A.7. Relative permittivity of TS_EXT_123 at 0.01 Hz as a function of relative humidity.

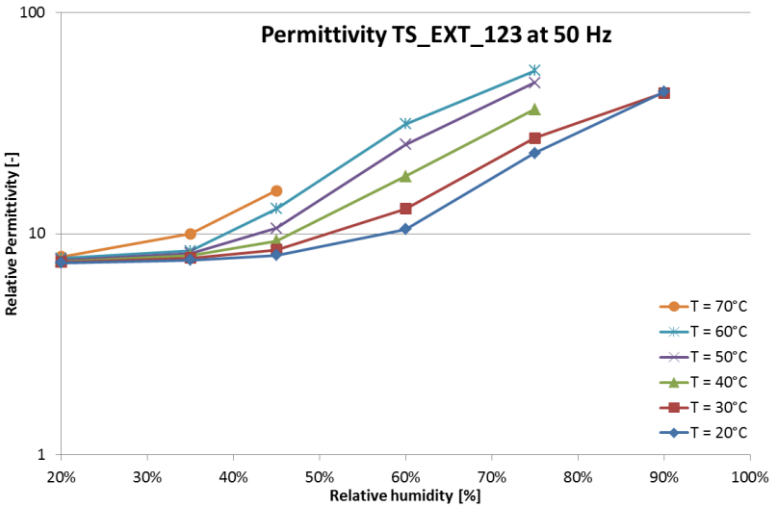

Figure A.8. Relative permittivity of TS_EXT_123 at 50 Hz as a function of relative humidity.

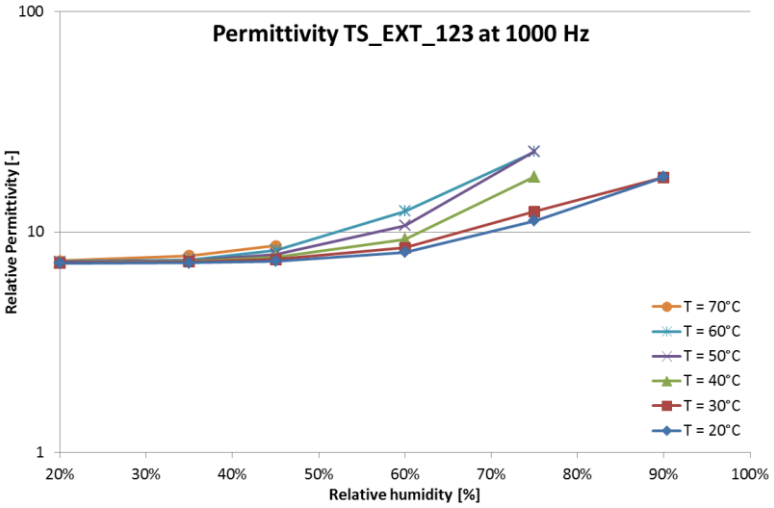

Figure A.9. Relative permittivity of TS_EXT_123 at 1000 Hz as a function of relative humidity.

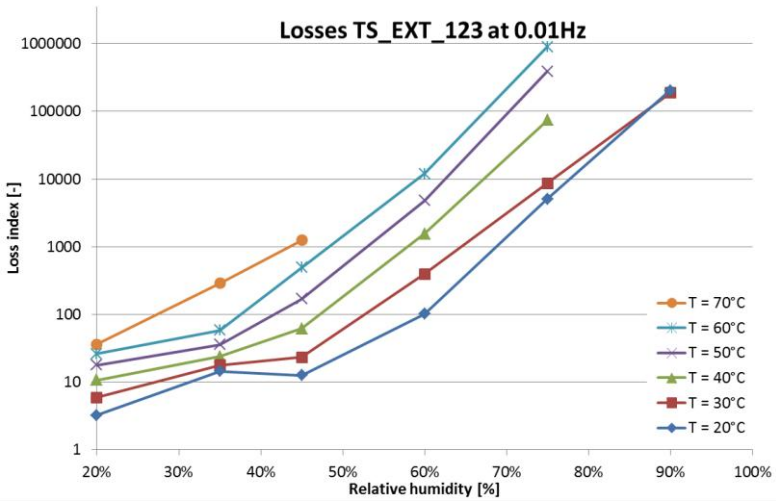

Figure A.10. Loss index of TS_EXT_123 at 0.01 Hz as a function of relative humidity.

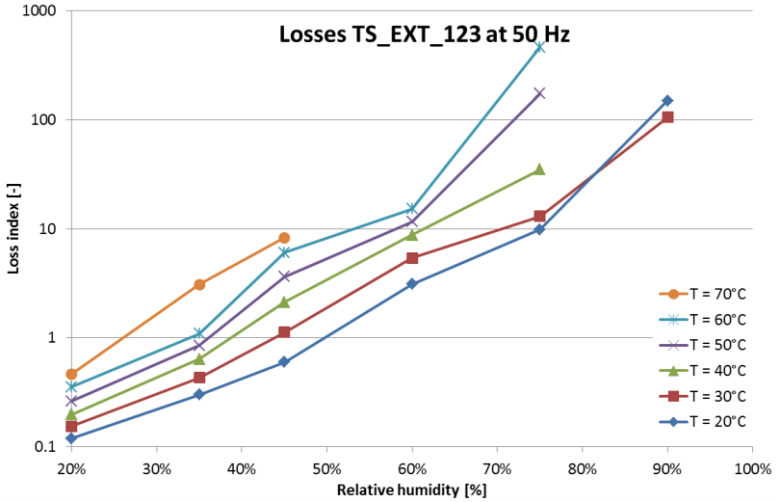

Figure A.11. Loss index of TS_EXT_123 at 50 Hz as a function of relative humidity.

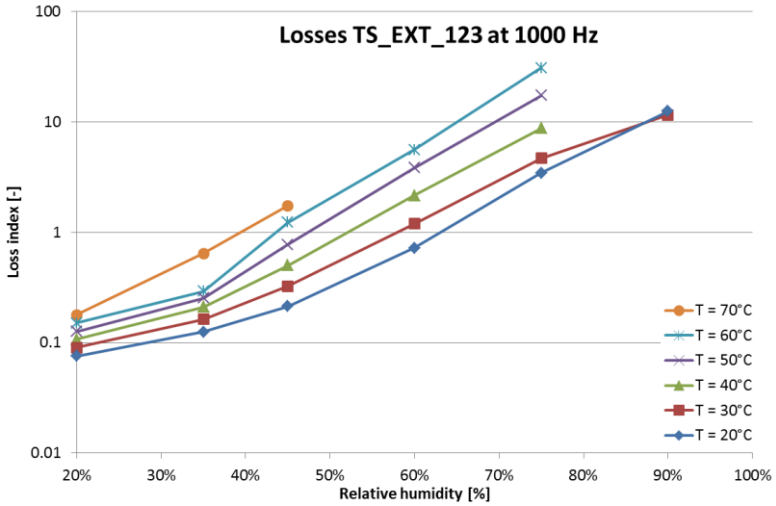

Figure A.12. Loss index of TS_EXT_123 at 1000 Hz as a function of relative humidity.

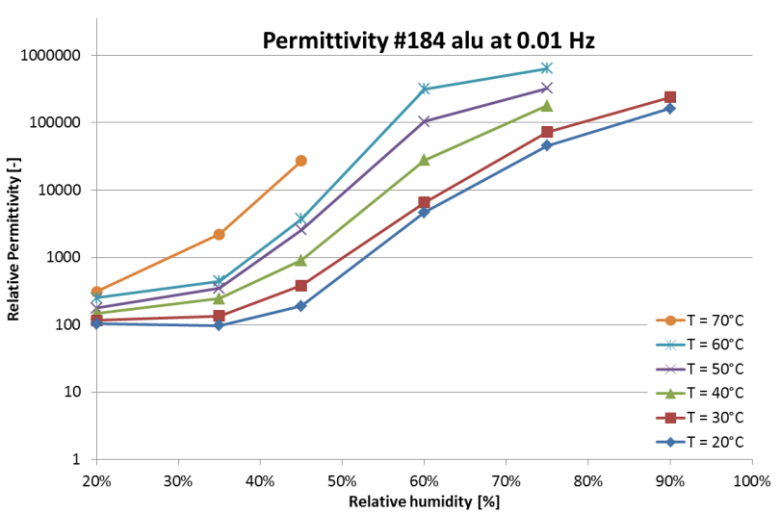

Figure A.13. Relative permittivity of #184 alu at 0.01 Hz as a function of relative humidity.

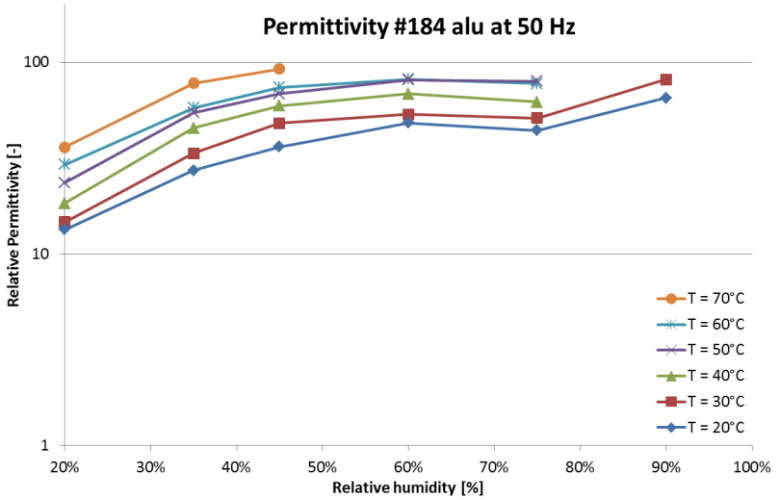

Figure A.14. Relative permittivity of #184 alu at 50 Hz as a function of relative humidity.

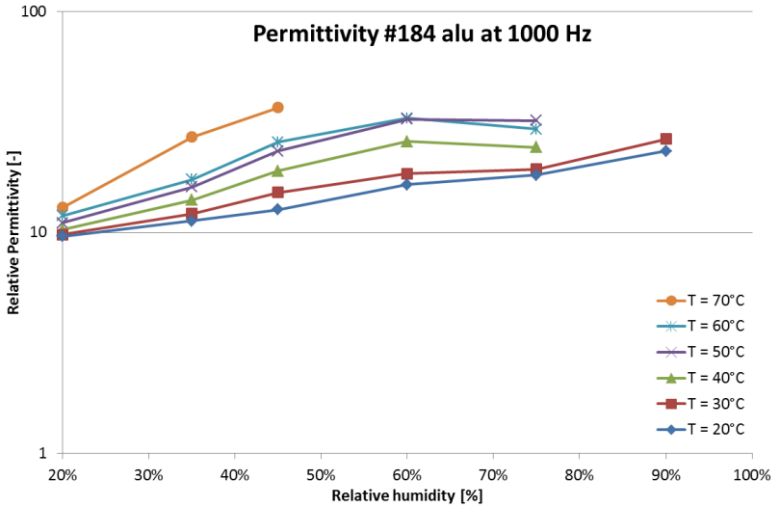

Figure A.15. Relative permittivity of #184 alu at 1000 Hz as a function of relative humidity.

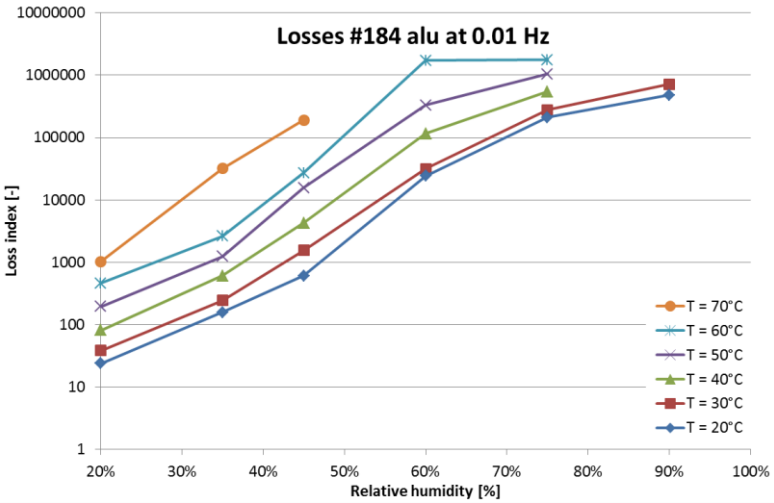

Figure A.16. Loss index of #184 alu at 0.01 Hz as a function of relative humidity.

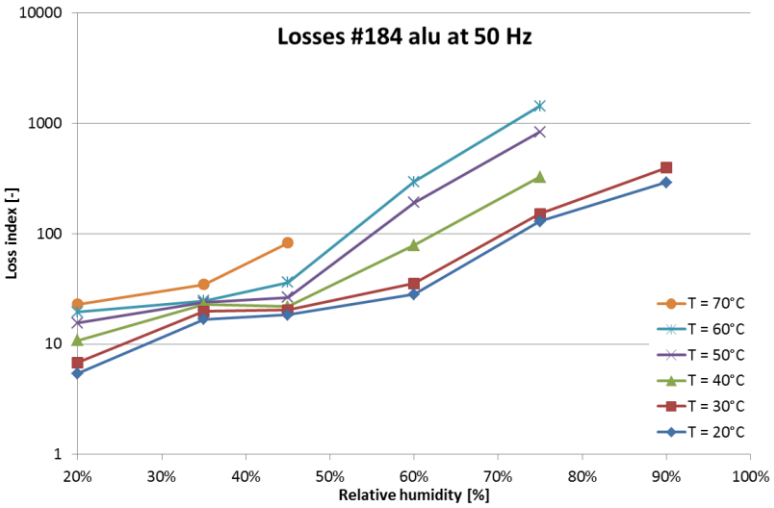

Figure A.17. Loss index of #184 alu at 50 Hz as a function of relative humidity.

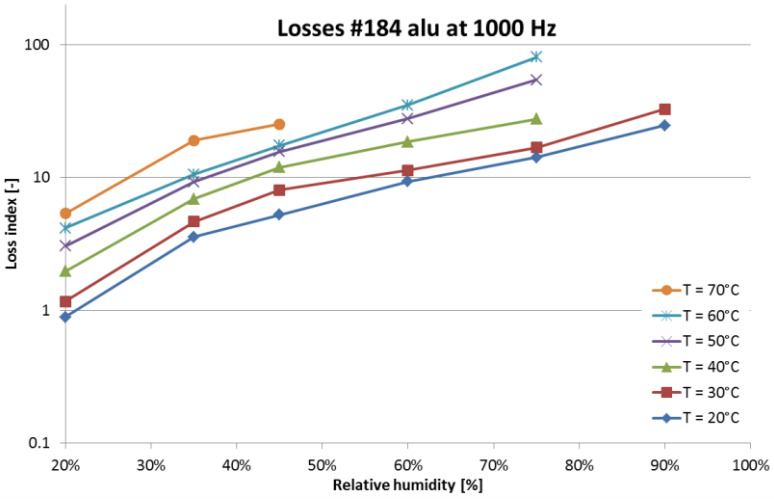

Figure A.18. Loss index of #184 alu at 1000 Hz as a function of relative humidity.

APPENDIX B – PROPERTIES AT CONSTANT RELATIVE HUMIDITY

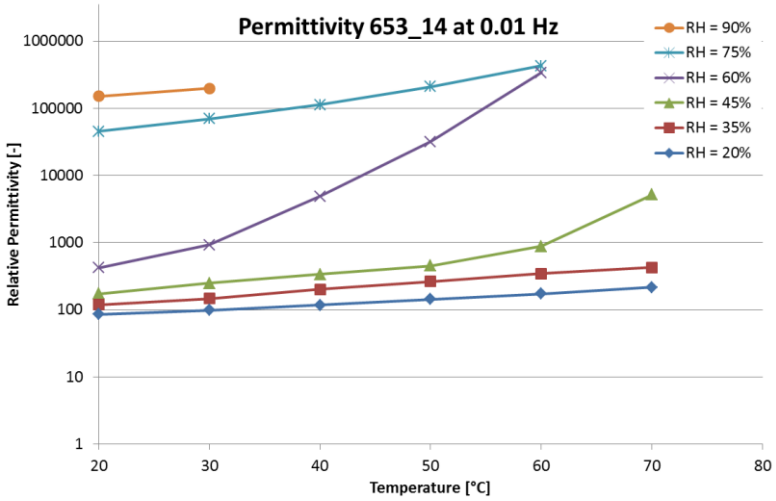

Figure B.1. Relative permittivity of 653_14 at 0.01 Hz as a function of temperature.

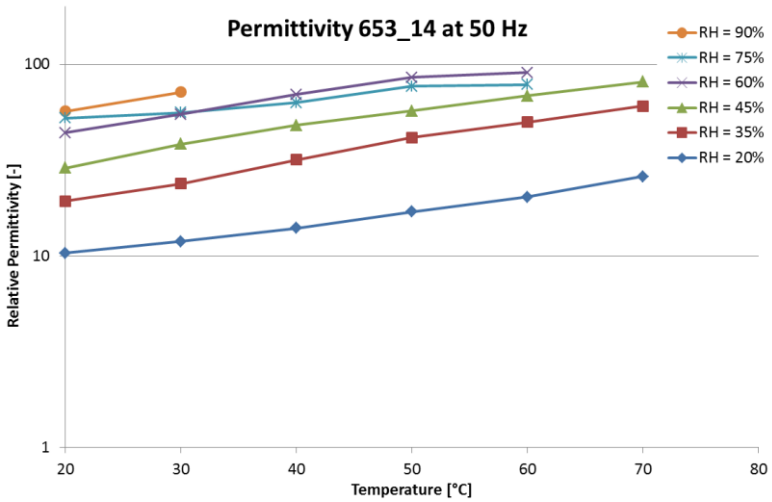

Figure B.2. Relative permittivity of 653_14 at 50 Hz as a function of temperature.

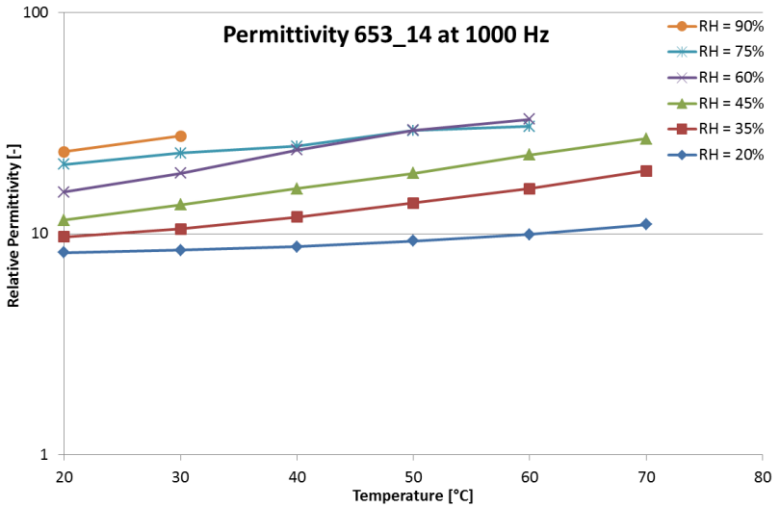

Figure B.3. Relative permittivity of 653_14 at 1000 Hz as a function of temperature.

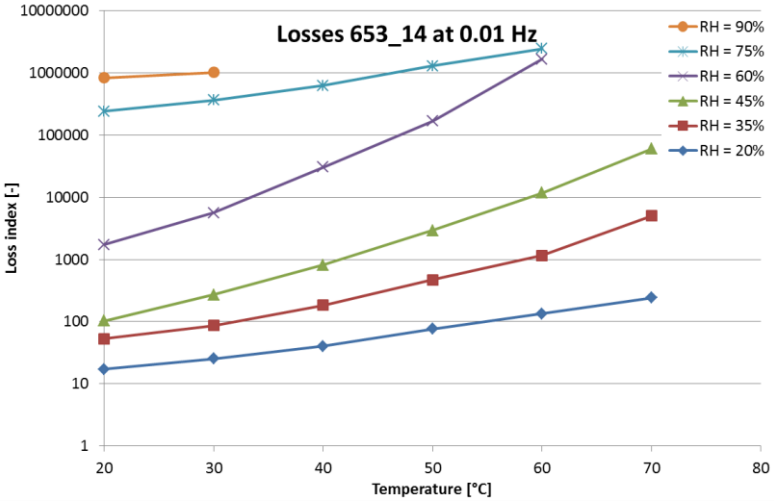

Figure B.4. Loss index of 653_14 at 0.01 Hz as a function of temperature.

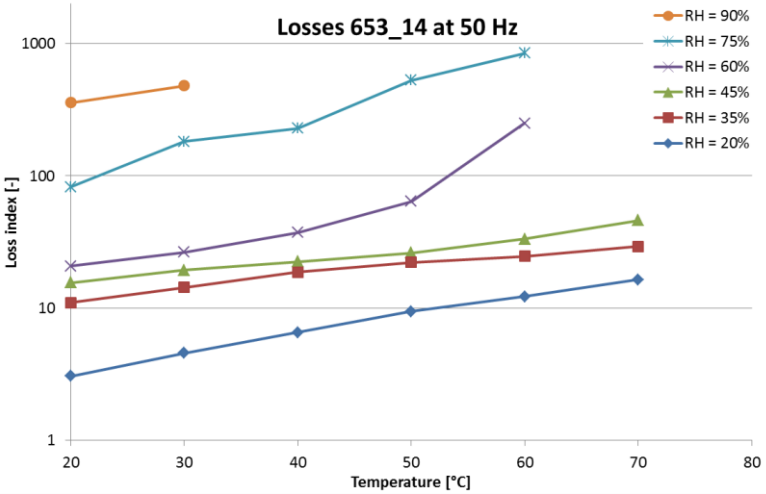

Figure B.5. Loss index of 653_14 at 50 Hz as a function of temperature.

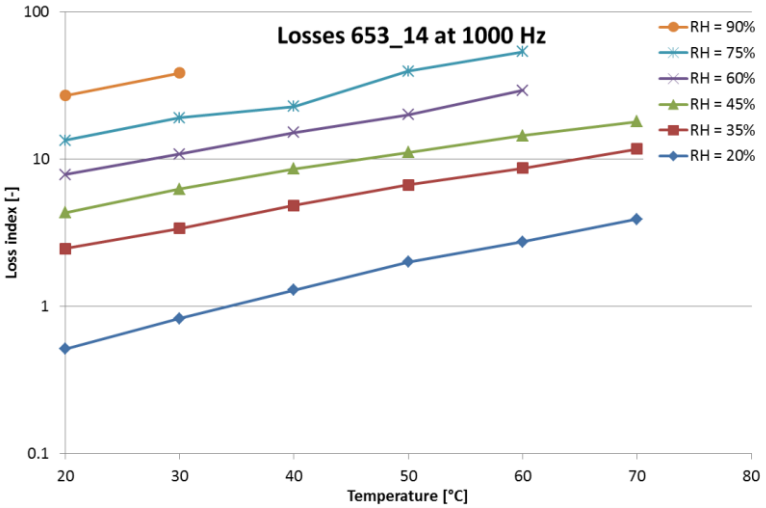

Figure B.6. Loss index of 653_14 at 1000 Hz as a function of temperature.

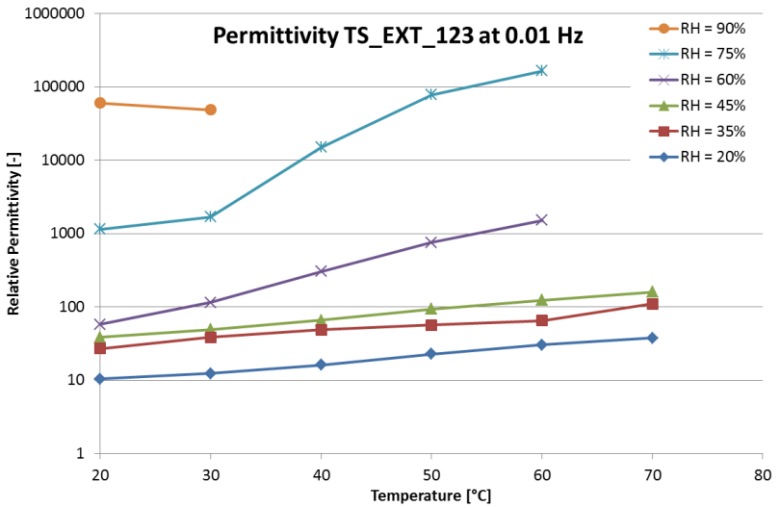

Figure B.7. Relative permittivity of TS_EXT_123 at 0.01 Hz as a function of temperature.

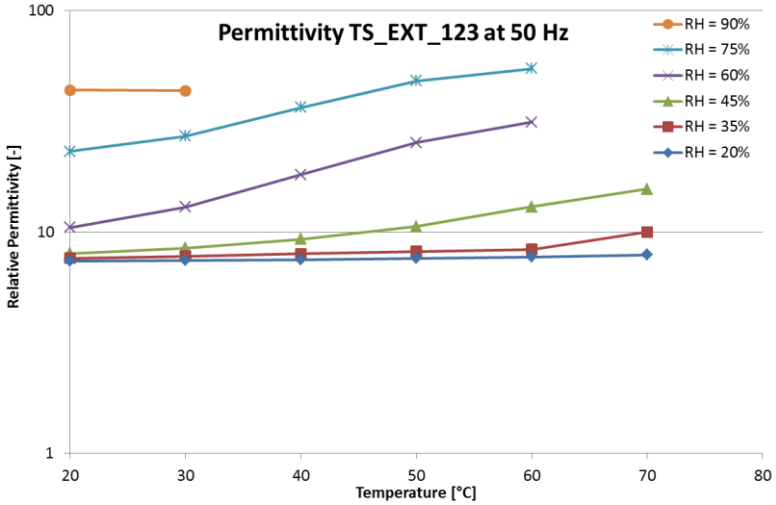

Figure B.8. Relative permittivity of TS_EXT_123 at 50 Hz as a function of temperature.

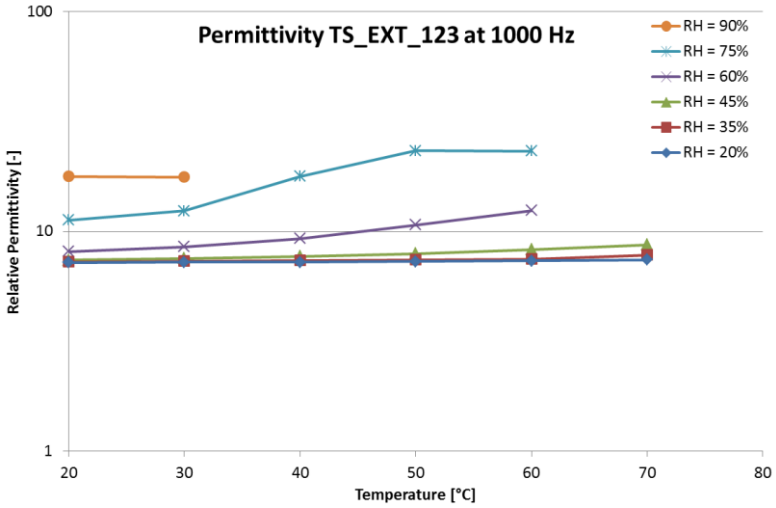

Figure B.9. Relative permittivity of TS_EXT_123 at 1000 Hz as a function of temperature.

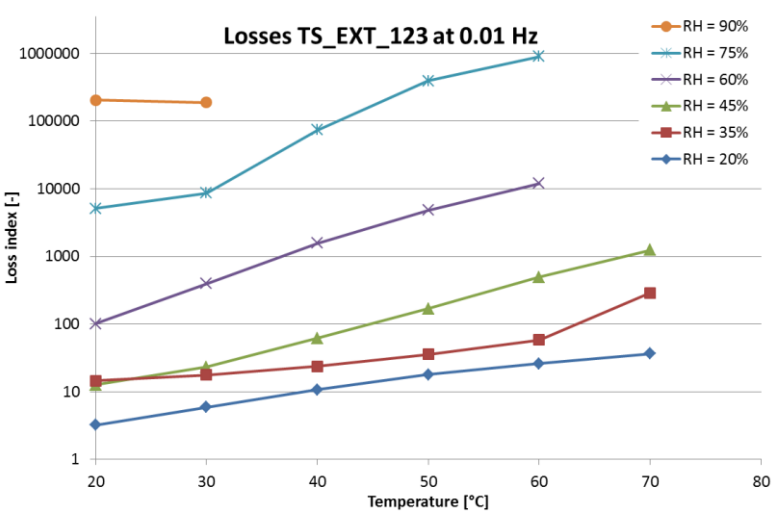

Figure B.10. Loss index of TS_EXT_123 at 0.01 Hz as a function of temperature.

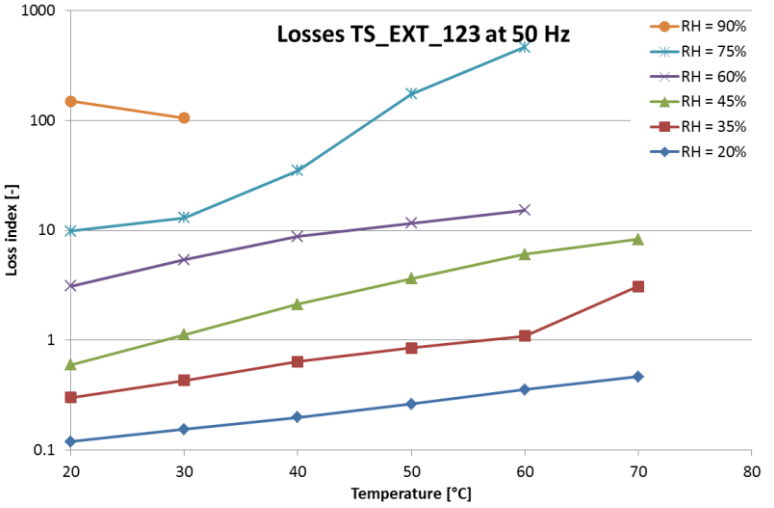

Figure B.11. Loss index of TS_EXT_123 at 50 Hz as a function of temperature.

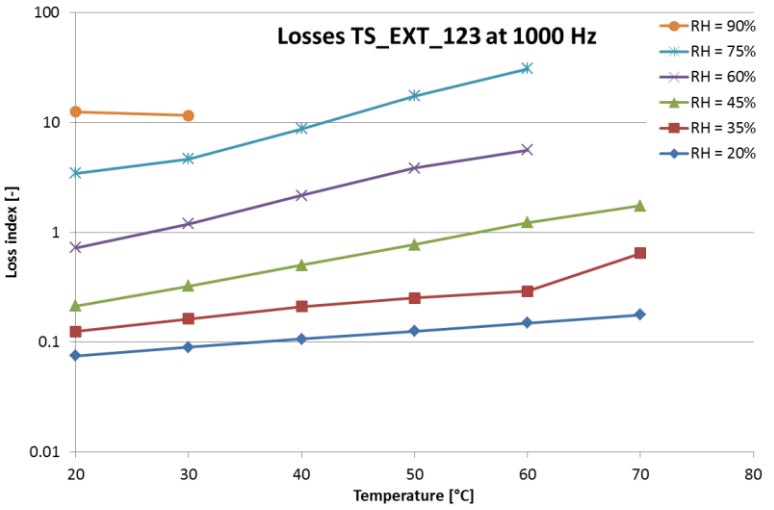

Figure B.12. Loss index of TS_EXT_123 at 1000 Hz as a function of temperature.

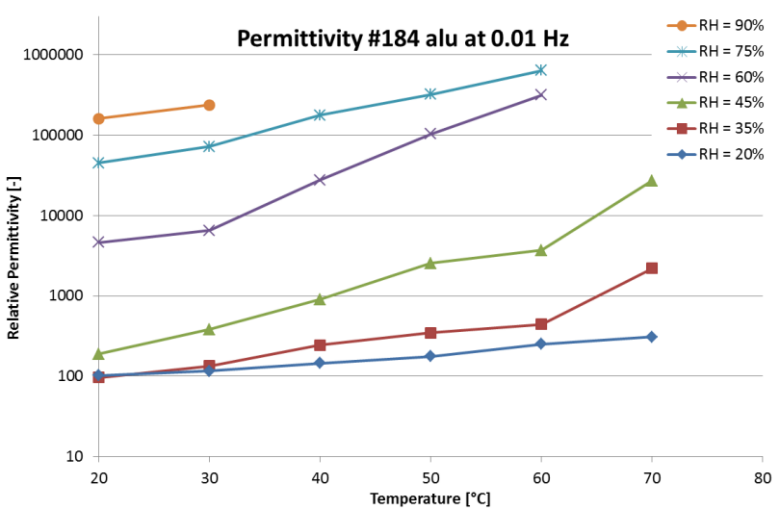

Figure B.13. Relative permittivity of #184 alu at 0.01 Hz as a function of temperature.

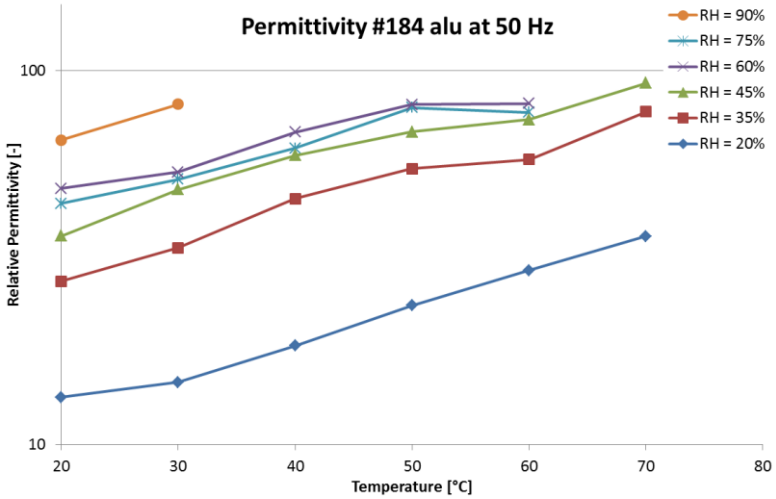

Figure B.14. Relative permittivity of #184 alu at 50 Hz as a function of temperature.

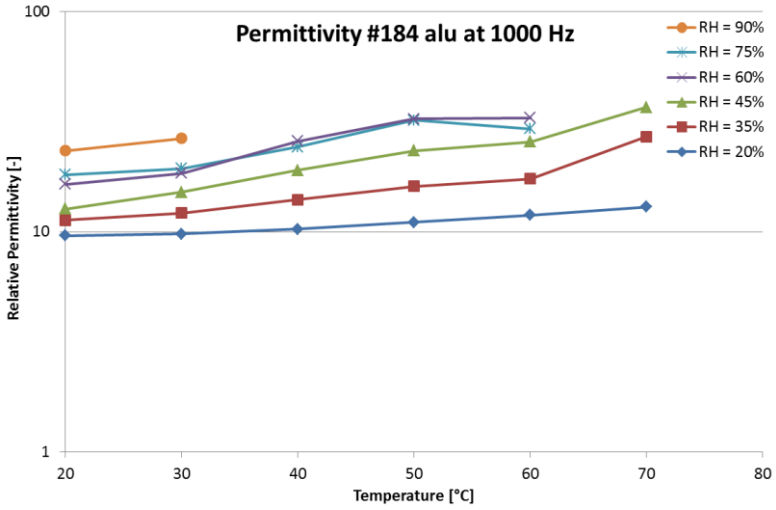

Figure B.15. Relative permittivity of #184 alu at 1000 Hz as a function of temperature.

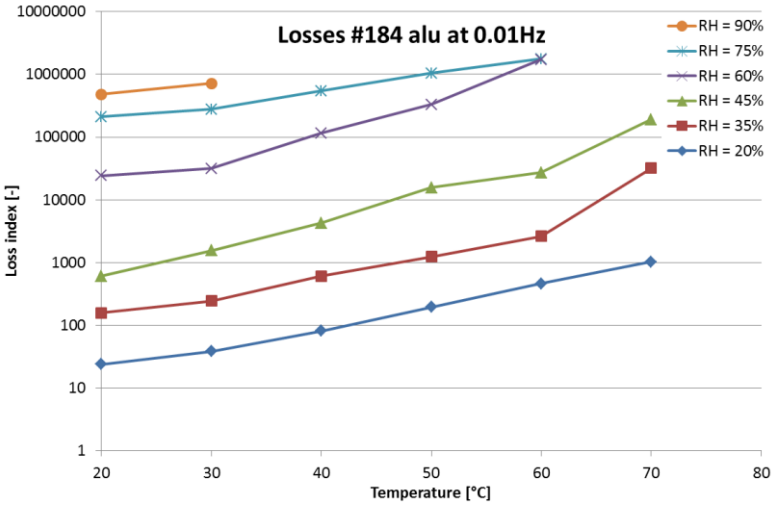

Figure B.16. Loss index of #184 alu at 0.01 Hz as a function of temperature.

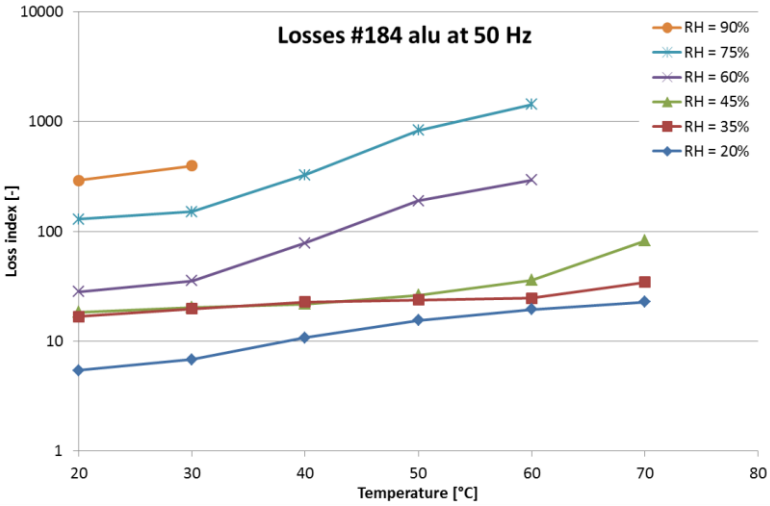

Figure B.17. Loss index of #184 alu at 50 Hz as a function of temperature.

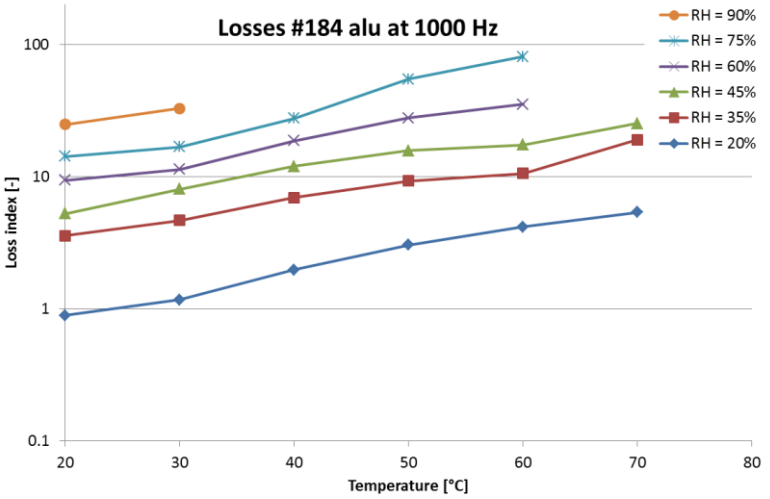

Figure B.18. Loss index of #184 alu at 1000 Hz as a function of temperature.

APPENDIX C – PROPERTIES AT CONSTANT ABSOLUTE HUMIDITY

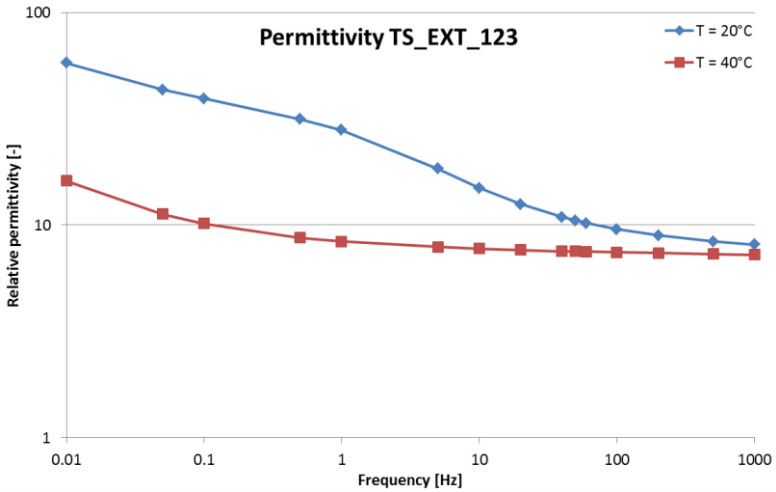

Figure C.1. Relative permittivity of TS_EXT_123 at a constant absolute humidity.

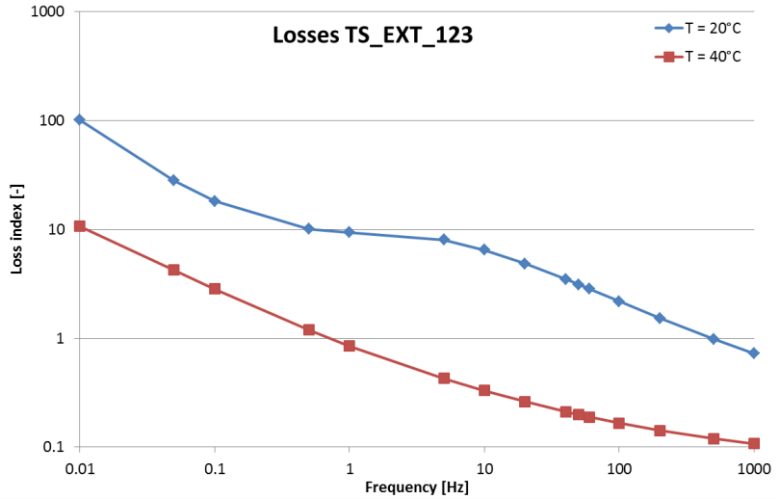

Figure C.2. Loss index of TS_EXT_123 at a constant absolute humidity.

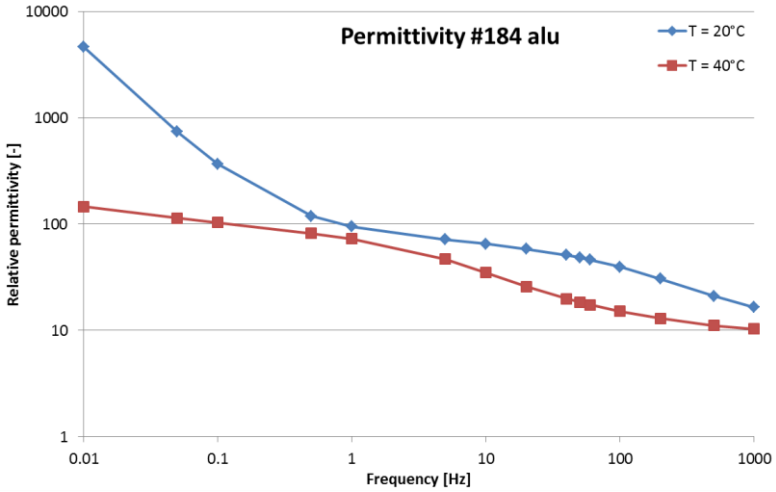

Figure C.3. Relative permittivity of #184 alu at a constant absolute humidity.

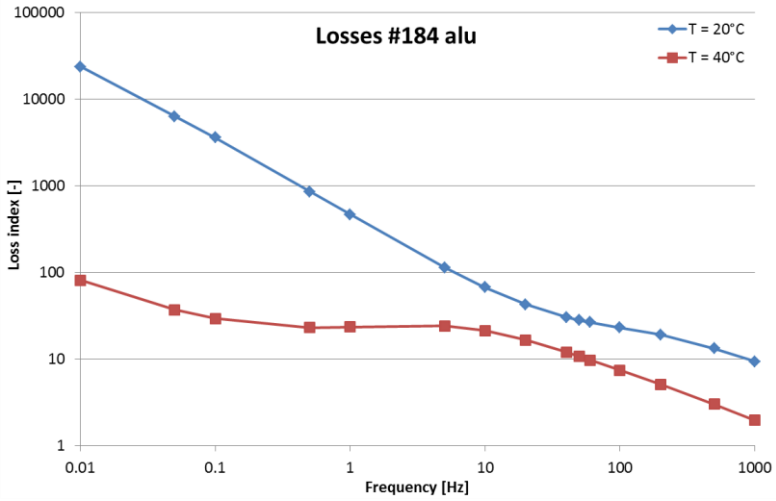

Figure C.4. Loss index of #184 alu at a constant absolute humidity.

APPENDIX D – PHASE COMPOSITION

In the following figures, the code *00-048-0367* is the code for the metastable γ-Al_2O_3. The stable α-Al_2O_3 is coded as *00-010-0173*.

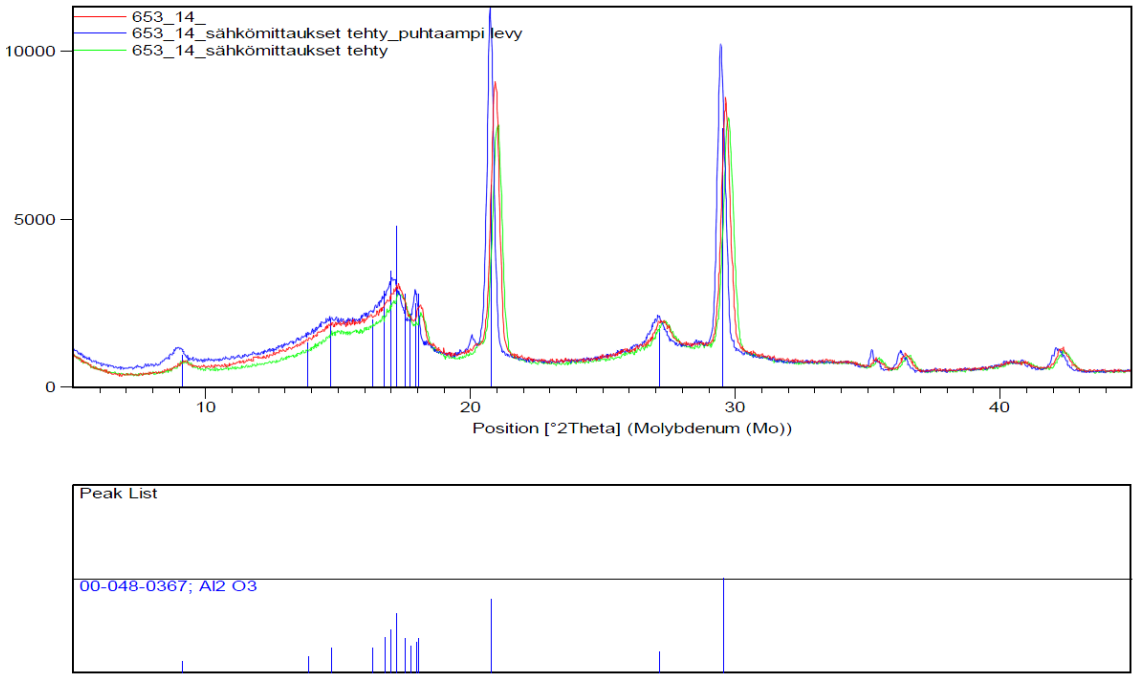

Figure D.1. XRD pattern of HVOF sprayed sample before and after measurements.

The red curves in Figures D.1, D.2 and D.3 are the X-ray diffraction (XRD) patterns before the performed measurements. In Figure D.1, the green curve is the XRD pattern of the HVOF sprayed sample, after the measurements below 100°C. The blue curve is the phase composition of the second HVOF sprayed sample, after the measurements at temperatures above 100°C. In Figure D.2, the blue curve is the XRD pattern of the flexicord sprayed sample after the measurements below 100°C. In Figure D.3, the blue curve is the phase composition of the APS sprayed sample after all the performed measurements.

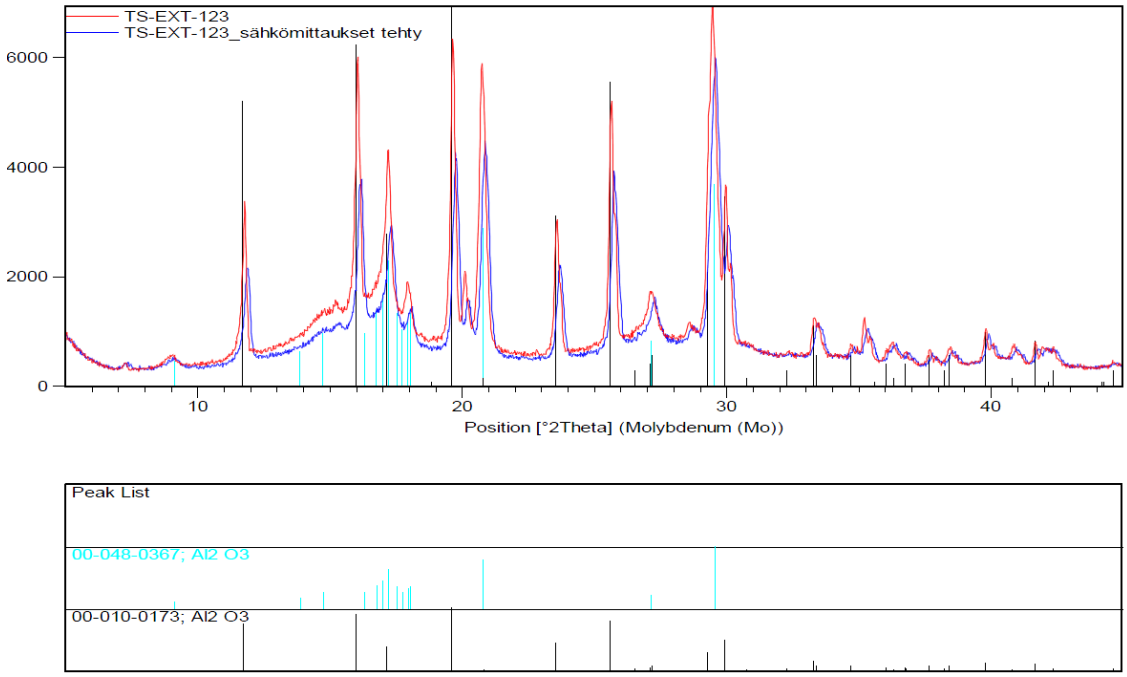

Figure D.2. XRD pattern of flexicord sprayed sample before and after measurements.

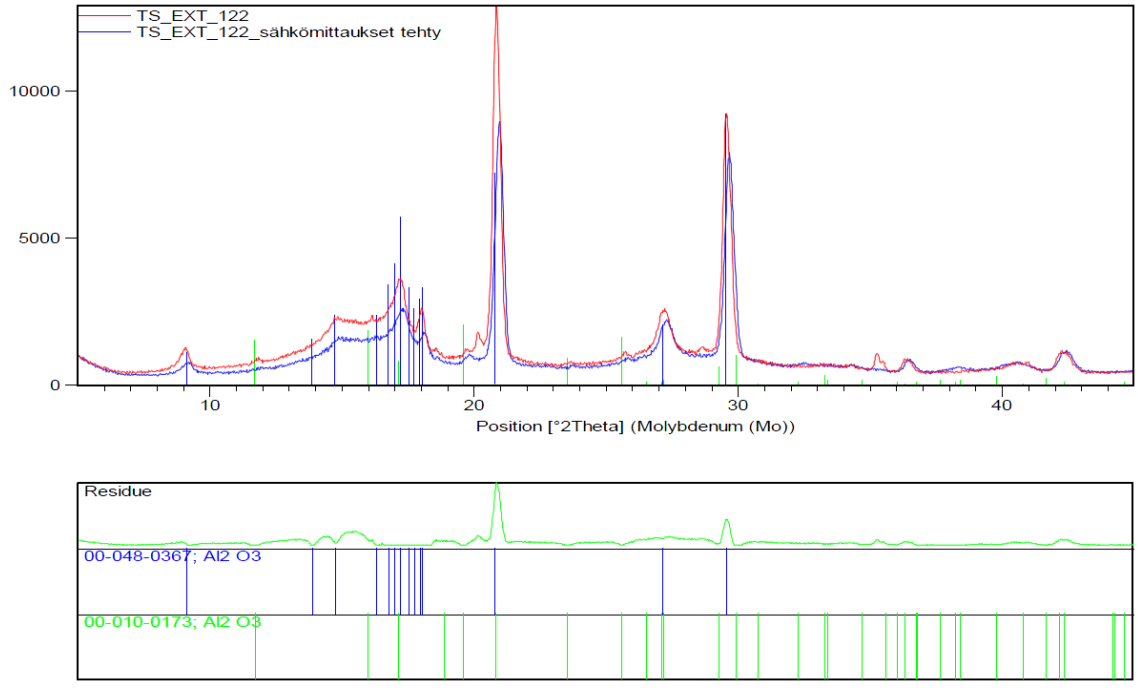

Figure D.3. XRD pattern of plasma sprayed sample before and after measurements.